March 2017

Evaluating the Influence of Breakdown Fouling and Moisture Content on Mechanical and Electromagnetic Properties of Ballasted Railroad Track

Hamed Faghihi Kashani

EVALUATING THE INFLUENCE OF BREAKDOWN FOULING AND MOISTURE CONTENT ON MECHANICAL AND ELECTROMAGNETIC PROPERTIES OF BALLASTED RAILROAD TRACK

A Dissertation Presented

by

HAMED FAGHIHI KASHANI

Submitted to the Graduate School of the
University of Massachusetts Amherst in partial fulfillment
of the requirements for the degree of

DOCTOR OF PHILOSOPHY

February 2017

Department of Civil and Environmental Engineering

EVALUATING THE INFLUENCE OF BREAKDOWN FOULING AND MOISTURE CONTENT ON MECHANICAL AND ELECTROMAGNETIC PROPERTIES OF BALLASTED RAILROAD TRACK

A Dissertation Presented

by

HAMED FAGHIHI KASHANI

Approved as to style and content by:

Carlton L. Ho, Chair

Ching S. Chang, Member

William P. Clement, Member

James P. Hyslip, Member

Richard N. Palmer, Department Head
Civil and Environmental Engineering Department

DEDICATION

To my parents and loving wife.

ACKNOWLEDGEMENTS

I would like to thank my advisor, Carlton L. Ho, for his many years of thoughtful, patient guidance and support. Thanks are also due to introducing me to James P. Hyslip. Together their friendship and selfless contribution to my professional development have been invaluable and will forever be appreciated. I would also like to extend my gratitude to the other members of my committee, Ching S. Chang and William P. Clement for their helpful comments and suggestions on all stages of this project.

I want to thank Federal Railroad Administration (FRA) for funding this research and providing expenses for laboratory set ups and materials. Thanks to William Morehead for manufacturing and sending the box apparatus for the dynamic tests. Also thanks to Charles P. Oden for his help in the first phase of this project.

I wish to express my appreciation to all the individuals who volunteered their participation in this project. Again a special thanks to James P. Hyslip and his wife, Kimberly Hyslip, for supporting me during all section of my PhD research.

A special thank you to all those whose support and friendship helped me to stay focused on this project and who have provided me with the encouragement to continue when the going got tough.

ABSTRACT

EVALUATING THE INFLUENCE OF BREAKDOWN FOULING AND MOISTURE CONTENT ON MECHANICAL AND ELECTROMAGNETIC PROPERTIES OF BALLASTED RAILROAD TRACK

FEBRUARY 2017

HAMED FAGHIHI KASHANI

B. A., AZAD UNIVERSITY, KARAJ, IRAN, 2005

M.A., IKIU UNIVERSITY, QAZVIN, IRAN, 2008

Ph.D., UNIVERSITY OF MASSACHUSETTS AMHERST, 2017

Directed by: Professor Carlton L. Ho

A complete study was performed to develop correlations between electromagnetic and mechanical properties of ballast. These correlations can be used to predict the deformation properties of ballast and also its dynamic behavior under heavy axle load in different fouling and moisture conditions by GPR survey. By developing this technique and performing similar tests on different types of ballast and fouling materials, a criterion can be developed to detect the railroad high risk areas and predict the engineering properties of ballast by GPR surveys. This study was performed on granite ballast and breakdown fouling and has three phases: performing GPR survey on full-scale laboratory models with different amount of fouling and water content; performing box test with equivalent dynamic Heavy Axle Load (HAL) up to 2,500,000 cycles on the reconstituted samples of first phase; performing CIDC triaxial tests on the reconstituted samples of first phase.

In these phases the effect of water content and fouling percentage on the electromagnetic, dynamic and static properties of ballast was investigated and discussed quantitatively

and qualitatively. In addition, existing correlations between electromagnetic and deformation properties of fouled ballast were studied in both time domain and frequency domain analyses from first and third phases. The results show that there are correlations between electromagnetic and mechanical properties of ballast. Plots for predicting the maximum shear strength and elastic modulus of ballast by measured electromagnetic parameters have been presented.

TABLE OF CONTENTS

Page

LIST OF TABLES

Page

LIST OF FIGURES

Page

LIST OF SYMBOLS AND ABBREVIATIONS

Abbreviation	Meaning
AAR	Association of American Railroad
ASTM	American Society of Testing and Materials
AREMA	American Railway Engineering and Maintenance of way Association
C_c	Curvature Coefficient
CIDC	Consolidated Isotropic Drained Compression
cm	Centimeter
CPT	Cone Penetration Test
C_u	Uniformity Coefficient
DCP	Dynamic Cone Penetration Test
DWT	Discrete Wavelet Transform
E50	Elastic Modulus at 50% of maximum shear strength
EM	Electromagnetic
EWL	Equivalent Wheel Load
F(%)	Fouling Percentage
F_0, F_{15}, F_{30}	0%, 15% and 30% Fouling Samples
FC	Field Capacity Water Content
FFT	Fast Fourier Transform
FI	Fouling Index
FRA	Federal Railroad Administration
GHz	Giga Hertz
GPR	Ground Penetrating Radar
GSD	Grain size Distribution
HAL	High Axle Load
Hz	Hertz
In	Inch
kips	Kilo Pounds
KPa	Kilo Pascal
lb	Pounds

LVDT	Linear Variable Differential Transducer
m	Meter
MASW	Multi-channel Analysis of Surface Wave
MGT	Mega Gross Tons
MHz	Mega Hertz
mm	Millimeter
MPa	Mega Pascal
NaCl	Sodium Chloride
OFP	Optimum Fouling Point
Pcf	Pounds per Cubic Feet
Psi	Pounds per Squared Inch
PVC	Percentage Void Contamination
REA	Rail Equipment Accident
SD	Standard Deviation
TTCI	Transportation Technology Center, Inc
USCS	Unified Soil Classification System
VCI	Void Contaminant Index

CHAPTER 1

INTRODUCTION AND SCOPE OF RESEARCH

1.1 Introduction

Although it may initially appear to be very simple and unimportant, ballast is a very important part of railroad track system because it resists the forces applied to the sleepers, provides large voids for drainage, increases the sleeper bearing area, and absorbs airborne noise (Selig & Waters, 1994, Clark *et al.*, 2001). If voids in the ballast are filled with fine particles, it then becomes fouled and loses most of its functions (Janardhanam & Desai, 1983, Kolisoja, 1997, Indraratna & Salim, 2005). Proper maintenance of the ballast is vital to ensure that the track performs properly.

Ballast fouling materials have many sources such as fouling attributed to the breakdown of ballast, outside contamination by coal, dust from trains carrying coal and due to soil intrusions from the base (Anbazhagan *et al.*, 2011). The most common source of ballast fouling is ballast breakdown, up to 76% (Selig & Waters, 1994), which is produced from train dynamic loading. Increase in ballast fouling will decrease the ballast drainage and consequently decreases the workability of the ballast.

To keep the ballast in good condition and to ensure that the track performs properly, the ballast needs maintenance. Maintaining the ballast before getting highly fouled, which cannot be detected from the surface, costs less than completely fouled ballast, which can be identified from the surface.

There are currently over 232,000 miles of railroad track in the US which need continuous inspection. Researchers have assessed the degree of fouling and moisture

of track substructure by using Non-destructive testing (NDT) methods, such as Ground Penetrating Radar (GPR) surveys, to identify the fouled or moist parts of the track for maintenance (Al-Qadi *et al.*, 2010). Most research has focused on using GPR to locate the moist parts of the ballast, to provide evidence of fouled zone in ballast and need of maintenance for better workability of the track. Because changes in moisture and void ratio (fouled Ballast) in ballast, identified by GPR, also change the Geotechnical deformation properties, this proposed research assesses the qualitative and quantitative correlations between the electrical properties from GPR survey and deformation geotechnical properties of ballast. The changes in electrical properties will be related to changes in water content, dry density, void ratio and grain size distribution. Information collected from this evaluation can also be applied for estimating the loading capacity of railroad tracks.

This document presents detailed objectives and scope of work for the research in this Chapter. Chapter 2 includes a review of the literature relevant to the mechanical and index properties of the railroad ballast, its changes by change in fouling percentage, GPR application in railroad industry from different approaches and methods used to assess the Geotechnical aspects by GPR survey. Chapter 3 evaluates the correlation between geotechnical index and electromagnetic properties of fouled ballasted track with a full scale laboratory model and this Chapter is published in Transportation Research Record (TRR) journal, No. 2545 in 2016. Chapter 4 is a laboratory evaluation of railroad ballast behavior under heavy axle load and high traffic conditions and it is submitted for publication at Transportation Geotechnics journal. Chapter 5 assesses

the effect of water content and fouling on the triaxial test results and evaluates correlations between results in Chapters 3 and 5.

1.2 Objectives and Scope of Research

This study has two objectives. The first objective is to evaluate the effects of changes in dry density, fouling percentage and water content of railroad track ballast on GPR data analyses. The second objective is to evaluate qualitative and quantitative correlations between electromagnetic and mechanical properties in ballasted railroad track.

These objectives were met by performing GPR survey on full-scale laboratory model tracks with different water contents, grain size distribution, dry density and fouling percentages followed by performing large scale dynamic box tests and static CIDC triaxial tests on reconstituted specimens.

The scope of this research is as following:

- Make full scale laboratory models of rail road track with 2 feet height AREMA #4 gradation granite ballast overlaid the 1.5 feet compacted sand (lower permeability based on Selig and Waters suggestion for sub-ballast) as a sub-ballast.
- Conduct multi-channel GPR survey at the top of the sample and at 9 to 15 points on center, left shoulder and right shoulder of the track.
- Change the water content of ballast from dry to field capacity moisture and two points between the extremes, in order to evaluate the effect of moisture on GPR reflected signals.

- Increase ballast-breaking-down fouling material massive percentage to two more points and running the past three steps to assess the effects of fouling material on GPR reflected signals.
- Perform non-level railroad ballast density measurement test (Yoo *et al.*, 1978) on clean and fouled ballast in each model.
- Collect clean and fouled ballast samples from different parts of the samples and performing GSD test.
- Run static triaxial CIDC tests on reconstituted samples with the same index properties of the full-scale laboratory models, in order to measure the static deformation geotechnical properties.
- Run dynamic box test with load equivalent to Heavy Axle Load (HAL) on reconstituted specimens with the same index properties of the full-scale laboratory models to the effect of fouling percentage and water content on dynamic properties.
- Assess applicable methods for predicting the ballast deformation properties by electromagnetic properties of ballast.
- Study the theoretical reasons for ballast dynamic behavior based on deformation properties

CHAPTER 2

LITERATURE REVIEW

Ballast fouling can cause many problems in railroad track such as reduction in resistance to the vertical, lateral and longitudinal forces applied to the ties, decrease in resiliency modulus and energy absorption capacity, reduction in voids which leads to poor drainage and vegetation growth in the rail, increase in noise level, decrease the electrical resistance between rails and increase the rate and magnitude of settlement (Selig & Waters, 1994, Anbazhagan *et al.*, 2011, Fortunato *et al.*, 2010, Indraratna & Salim, 2005)

When fouling increases in ballast it holds water and not only, decreases the workability of the ballast but also, changes the electromagnetic properties of the ballast. In another perspective, the application of Ground Penetrating Radar (GPR) in railroad investigations has developed rapidly in recent years in an effort to examine railroad infrastructures and maintenance needs. GPR is a non-destructive technique that can detect the wave reflections from layers in the substructure with differing electromagnetic properties and can thereby identify track bed anomalies, and determine the degree of track bed deterioration (Gallagher *et al.*, 1999, Jack & Jackson, 1999, Sussmann *et al.*, 2003).

Many empirical studies have been conducted to calibrate GPR as a tool for demonstrating repeatable and quantifiable results in evaluating the railroad track based on both field and model testing. But as there are many uncertainties within the actual rail track, it is difficult to calibrate the GPR data with actual ballast condition.

To evaluate the effects of moisture and fouling percentage on the mechanical and electromagnetic properties of the ballasted track and development of GPR technique in

detecting moisture and fouling, this Chapter mainly provides the following sections with their literature:

- A review of the basic concepts of railroad track.
- Mechanical and electromagnetic properties of clean and fouled ballast.
- The effect of fouling and moisture on mechanical and electromagnetic properties of clean and fouled ballast.
- Principles of GPR and its usage in geotechnical engineering and railroad track.

2.1 Railroad Track Components

Railroad track can be divided in two parts (AREMA, 2010):

a. Track superstructure which includes the rail, tie fastening systems and track materials that are the components of a conventionally constructed track system.
b. Track substructure, the layered granular materials that provide the foundation of the railroad system and transfer the live and dead loads of the track superstructure to the ground. Some of the important railroad track components are defined as follows.

2.1.1 Fastening Systems

The purpose of the fastening system is to keep the rails against the sleepers and resist vertical, lateral, longitudinal, and overturning movements of the rail. Wood sleepers require steel plates under the rail to distribute the rail force over the wood surface while, concrete sleepers have spring fasteners (Selig & Waters, 1994). (Figure 2.1)

2.1.2 Ties

Sleepers or ties have several important functions:

a. Receive the load from the rail and distribute it over the supporting ballast at an acceptable ballast pressure level.
b. Hold the fastening system to maintain the proper track gage, and
c. Restrain the lateral, longitudinal and vertical rail movement by anchoring to the superstructure in the ballast.

The two most common types of sleepers are wood (timber) and pre-stressed/reinforced concrete (Selig & Waters, 1994).

The width, length and spacing of the ties varies in different countries. For wood ties the variation range for width is 190 -260 mm, for length is 2000 – 2743 mm and for spacing is 495 – 760 mm. In Concrete ties these parameters in the same order varies from 203 – 300 mm, 2057 - 2629 mm and 568 - 700 mm, respectively (Selig & Waters, 1994).

2.1.3 Ballast

Ballast is the crushed granular material placed as the top layer of the railroad sub-structure in which the sleepers are embedded. The ballast is an important component of railroad track. It must perform many different jobs such as: reduce the stress applied to the weaker interfaces; resist vertical, lateral, and longitudinal forces applied to the sleepers to maintain track position; and to provide drainage of water from track structure (Selig & Waters, 1994). These are the main tasks of the ballast but it also has some other functions such as; alleviate frost problems by not being frost susceptible and by providing an insulating layer protect the underlying layers; inhibit vegetation growth by providing a cover

layer that is not suitable for vegetation; absorb airborne noise; provide adequate electrical resistance between rails; facilitate redesign/reconstruction of track. (Selig & Waters, 1994).

As is shown in Figure 2.1, ballast may be subdivided to the following layers;

Crib—Material between Sleepers

Shoulder—Material beyond the sleeper ends down to the bottom of the ballast layer

Top Ballast—Upper portion of supporting ballast layer which is distributed by tamping

Bottom Ballast—Lower portion of supporting ballast layer which is not distributed by tamping and which generally is the more fouled portion

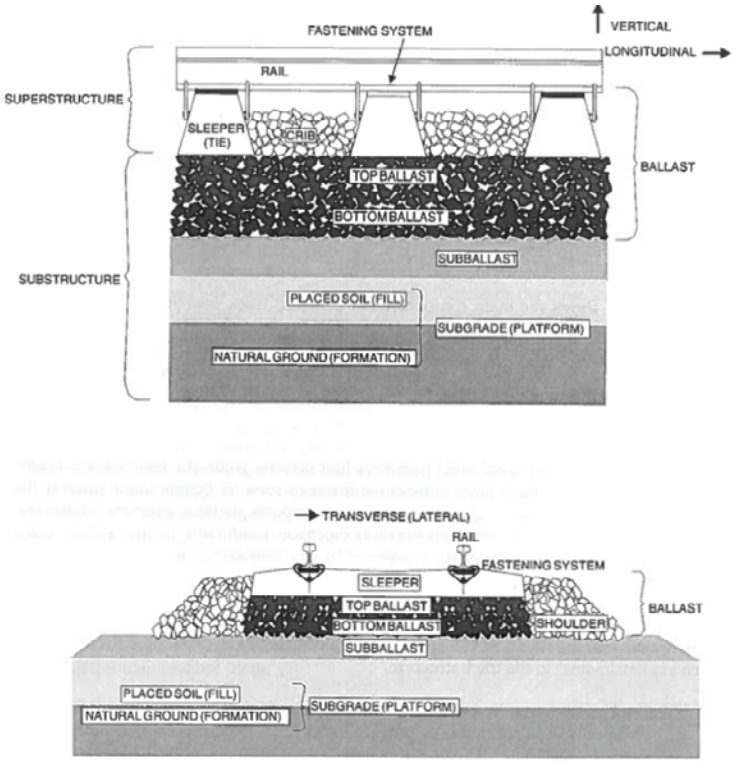

Figure 2.1: Track Structure Components (Selig & Waters, 1994)

2.2 Geotechnical Properties of Ballast Material

Traditionally, angular crushed hard stones and rocks that are uniformly graded, free of dust and dirt, and not prone to cementing action have been considered good ballast materials. Availability and economic considerations have been the prime factors considered in the selection of ballast material. (Selig & Waters, 1994)

The engineering properties of the ballast (e.g. modulus, in-situ density, water content, friction angle, grain size distribution, void ratio, drainage, etc.) are important factors in its performance. The most important properties that are also related to this research program are:

1. Ballast in-situ density
2. Ballast gradation
3. Ballast drainage
4. Ballast elastic modulus (E)
5. Ballast Poisson's ratio
6. Ballast shear strength
7. Ballast friction angle
8. Ballast settlement
9. Ballast resilient modulus

2.2.1 Ballast In-Situ Density

One of the important parameters of in-situ physical state of ballast which is significantly effective on ballast mechanical behavior, is density. Ballast has specific properties such as large voids, large particles and non-cohesive particles. Regarding to the methods

existing for measuring the in-situ density of soils such as rubber balloon method (ASTM D2167-66), sand cone method (ASTM 1556-64), oil-replacement method, as well as the block-sampling and drive-cylinder methods, measuring the in-situ density of ballast is impossible with these methods or need lots of modification. T.S. Yoo et al. in 1978 proposed a suitable method with specific apparatus for in-situ density measurement of ballast that was verified by lab tests and lots of field applications.

Researchers with performing tests in TTCI test-track, reported that the initial dry unit weight of the ballast falls within the range of the values, 16.1 KN/m^3 to 17.6 KN/m^3 (Selig *et al.*, 1981). In addition, it is obvious that the in-situ density of the ballast is significantly related to the gradation, shape and angularity of the particles.

2.2.2 Ballast Gradation

Ballast gradation is the primary factor affecting the stability, safety and drainage of tracks. Typically the size of ballast grains varies in the range of 10-60 mm due to the transportation, handling, placement and compaction of ballast. In accordance with this wide range of size variability and the rail usage of the railroad line, the ballast gradation must provide the two following objectives (Indraratna & Salim, 2005):

a. High shear strength to provide increased stability and
b. Minimum track deformation.

Ballast gradation is determined by washing and mechanical sieving using ASTM C117, C136 and D422.

Selig and Water in 1994 described a number of terms that have been defined for qualitatively describing the shape of gradation curves which can be seen in Figure 2.2. The

terms uniformly graded or poorly graded ($C_u < 4$ in USCS system) means a relatively narrow range of particle sizes, the term broadly graded or well graded ($C_u > 4$ and $1 < C_c < 3$ in USCS system) means a wide range of particle sizes and the term gap graded is the one which has small amount of particles and the fouled ballast is falling within this term.

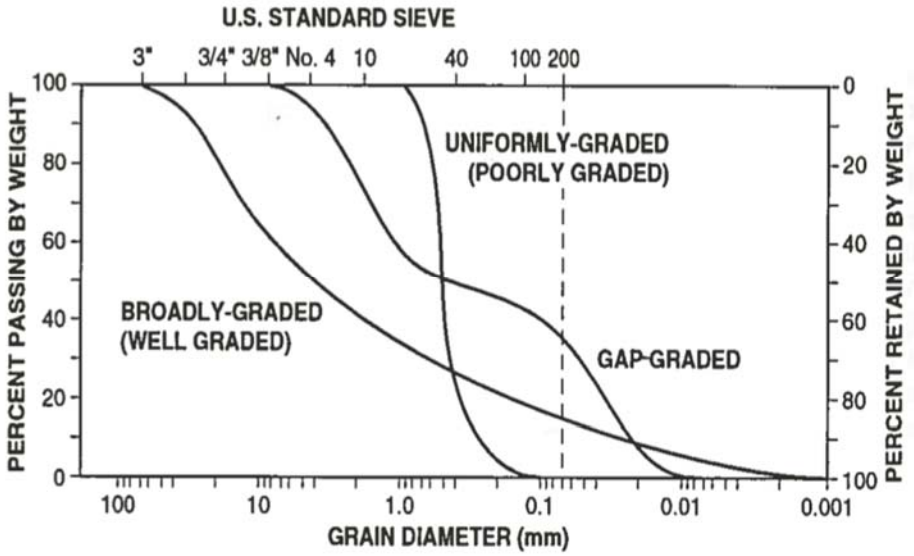

Figure 2.2 ; Definition of Grain Size Distribution (Selig & Waters, 1994)

The gradation is usually shown by the plot of percent finer versus grain size (Figure 2.2, Figure 2.3) and also as a distribution plot with percent by weight of a given size as a function of log of particle size (Figure 2.4)

Many researchers have shown that gradation of the ballast has significant effects on the mechanical properties of ballast, such as increase in plastic strain of the ballast by changing the broadly graded ballast to uniformly graded ballast, increase in friction angle by adding large particles (Klugar, 2014), change in shear strength by change in particles

sizes (Chen, 1948, Holtz & Gibbs, 1956, Koerner, 1970, Leslie, 1963, Marachi *et al.*, 1900) but Selig and Waters in 1994 reported that this effect of particle size on strength is unclear.

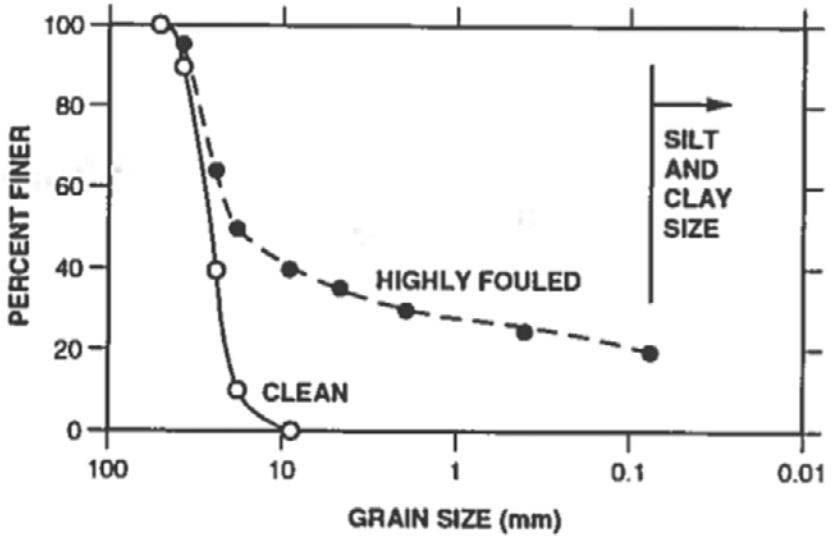

Figure 2.3: Examples of Ballast Gradation Curves (Selig & Waters, 1994)

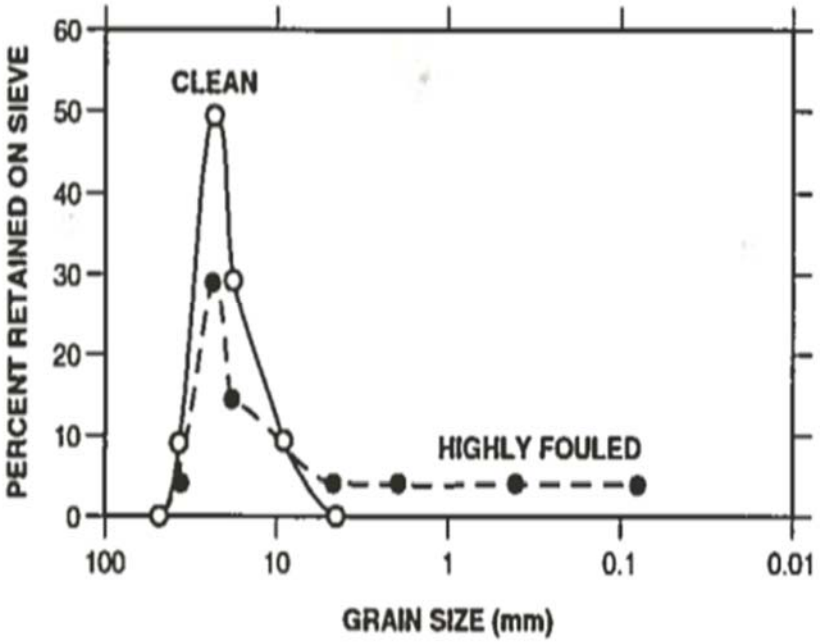

Figure 2.4: Ballast Gradation Presented as a Frequency Distribution Plot (Selig & Waters, 1994)

Table 2.1 shows the American Railway Engineering and Maintenance-of-Way Association (AREMA) recommended ballast Gradation using in United States of America (AREMA 2010).

Table 2.1: The Recommended Ballast Gradation (AREMA, 2010)

Size No. (See Note 1)	Nominal Size Square Opening	Percent Passing									
		3″	2½″	2″	1½″	1″	¾″	½″	d″	No.4	No. 8
24	2½″- ¾″	100	90-100		25-60		0-10	0-5	–	–	–
25	2½″ - d″	100	80-100	60-85	50-70	25-50	–	5-20	0-10	0-3	–
3	2″ - 1″	–	100	95-100	35-70	0-15	–	0-5	–	–	–
4A	2″ - ¾″	–	100	90-100	60-90	10-35	0-10	–	0-3	–	–
4	1½″ - ¾″	–	–	100	90-100	20-55	0-15	–	0-5	–	–
5	1″ - d″	–	–	–	100	90-100	40-75	15-35	0-15	0-5	–
57	1″ - No. 4	–	–	–	100	95-100	–	25-60	–	0-10	0-5
Note 1: Gradation Numbers 24, 25, 3, 4A and 4 are main line ballast materials. Gradation Numbers 5 and 57 are yard ballast materials.											

2.2.3 Ballast Drainage

There are three sources of water that entering the track substructure: precipitation (rain and snow), surface flow and subsurface seepage (Figure 2.5). Because the ballast is exposed, precipitation is the most important source of water entering the track substructure.

Excess water in the track substructure can increase the track maintenance costs because of (Selig & Waters, 1994):

- Increasing the ballast plastic deformation because of pore water pressure increase after dynamic loading
- Decreasing in stiffness and decreasing in strength
- Loss of strength because of moisture increase
- Slurry formation from ballast action
- Hydraulic pumping of fine materials in lower ballast

- Volume change from swelling
- Frost heave/thaw softening
- Ballast degradation from slurry abrasion, chemical action and freezing water
- Sleeper attrition from slurry abrasion

The above items show the importance of ballast drainage in railroad systems. Also fouling particles fill the voids in ballast and will significantly affect the ballast drainage. Table 2.2 is the hydraulic conductivity values for ballast reported by (Parsons, 1990).

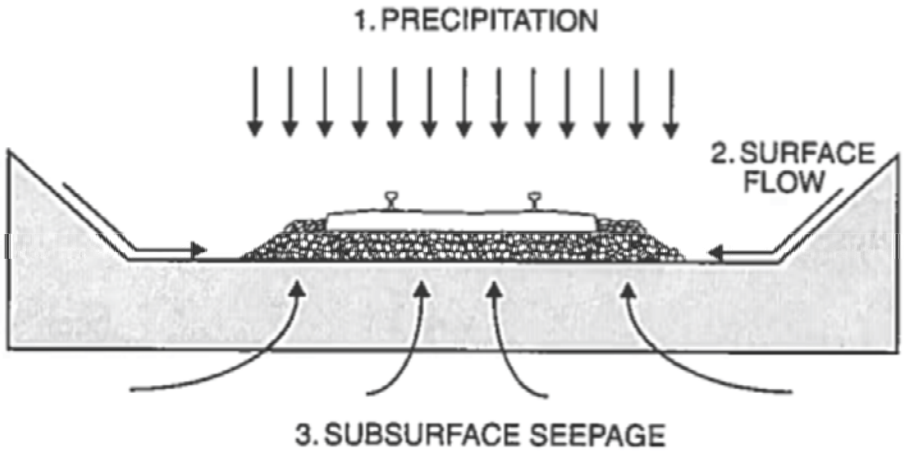

Figure 2.5: Sources of Water Entering Track Substructure (Selig & Waters, 1994)

In the past researchers have attempted to model the hydraulic conductivity of granular soils (Costa, 2006, Courcelles *et al.*, 2010, Yin, 2009) which work well for some types of granular materials, such as silt and sand, but they do not work well for coarse-grained aggregates with inter-connected pore structure such as fouled ballast (Tennakoon *et al.*, 2012).

Table 2.2: Hydraulic Conductivity Values for Ballast (Parsons, 1990)

Fouling Category	Fouling Index	Hydraulic Conductivity, k_h	
		(in./sec)	(mm/sec)
Clean	< 1	1 - 2	25 - 50
Moderately Clean	1 - 9	0.1 - 1	2.5 - 25
Moderately Fouled	10 - 19	0.06 - 0.1	1.5 - 2.5
Fouled	20 - 39	0.0002 - 0.06	0.005 - 1.5
Highly Fouled	> 39	< 0.0002	< 0.005

Based on the assumption of uniform distribution of fine particles in the granular material voids, (Koltermann & Gorelick, 1995)presented the following equation for hydraulic conductivity (k) of a mixture of granular and fine-grained soil;

$$k = \frac{{d_{fp}}^2 {\phi_{fp}}^3}{180(1-\phi_{fp})^2} \quad \text{Eq. (2.1)}$$

which ϕ_{fp} is the composite porosity of the mixture and d_{fp} is the representative grain diameter.

Tennakoon et al. in 2012 proposed the following equation by eliminating the assumption of uniform distribution of fine particles in the granular material voids and specifically for coal-fouled ballast (Tennakoon *et al.*, 2012):

$$k = \frac{k_b \times k_f}{k_f + ({}^{VCI}/_{100}) \times (k_b - k_f)} \quad \text{Eq. (2.2)}$$

where VCI is the void contamination ratio, discussed later in section 2.5, k_b and k_f are the hydraulic conductivities of clean and fouled ballast layers, respectively. It was also reported that the hydraulic conductivity calculated from this equation has a good agreement with the conducted experimental results.

2.2.4 Ballast Elastic Modulus (E)

Railroad track modulus which is an important parameter for measuring the vertical stiffness of the rail foundation (track), typically varies between less than 13.7 MPa (2000 lb/in./in.) as a poor performer to higher than 27.5 MPa (4000 lb/in./in.) as a good performer (Narayanan *et al.*, 2004). Values more than this range, which has been determined up to 137 Mpa (20000 lb/in./in.), can cause failure including ballast degradation or tie cracking due to severe dynamic load environment encountered (Redden *et al.*, 2002)

Some researchers by conducting a bunch of triaxial tests on ballast reported that coarser particles indicate a considerably greater axial strain upon initial loading, consequently resulting in a smaller initial deformation modulus (Indraratna *et al.*, 2013).

2.2.5 Ballast Poisson's Ratio

Poisson's ratio is defined as the ratio of lateral strain to axial strain of a material under stress. For soils, lateral strain is not constant over a specimen's entire height, so Poisson's ratio is calculated from axial strain and volumetric strain with the equation:

$$\varepsilon_{vol} = (1 + \varepsilon_a)^{1-2\nu} + 1 \qquad \text{Eq. (2.3)}$$

which when reworked becomes:

$$\nu = 0.5 \times \left(1 - \frac{ln(1+\varepsilon_{vol})}{ln(1+\varepsilon_a)}\right) \qquad \text{Eq. (2.4)}$$

At small strains, Poisson's ratio can be estimated as:

$$\nu = \frac{\varepsilon_a - \varepsilon_{vol}}{2 \times \varepsilon_a} \qquad \text{Eq. (2.5)}$$

with compressive axial strain and contractive volumetric strain positive. If a material experiences contractive volumetric strain equal to its compressive axial strain, it will have a

Poisson's ratio equal to zero. If a material experiences no volumetric strain under load, it is an incompressible material and will have a Poisson's equal to 0.5. If a material contracts under compressive strain and experiences volumetric strain greater than zero but less than the axial strain, it will have a Poisson's ratio between zero and 0.5. If a material experiences contractive volumetric strain greater than the contractive axial strain, it will have a Poisson's ratio less than zero. If a material experiences dilative volumetric strain (in this case a negative volumetric strain) under compressive axial strain, its Poisson's ratio will be greater than 0.5. This last tendency is impossible for isotropic, linear elastic materials, but can be characteristic of soils, particularly dense granular soils.

Indraratna et al. in 1998 by conducting large scale triaxial tests on ballast reported that coarser particles has smaller Poisson's ratio and smaller deformation modulus (Indraratna *et al.*, 1998)(Figure 2.6).

$\nu = 0.4$ can be considered as a typical Poisson's ratio for fouled ballast which were measured from old railways in France (Selig & Waters, 1994).

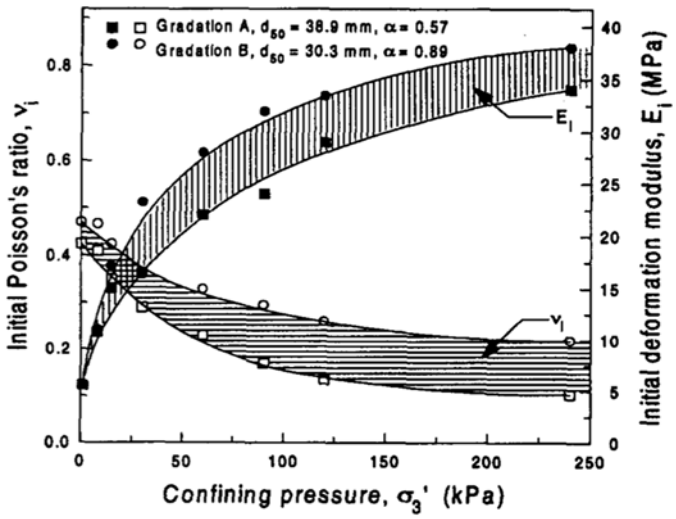

Figure 2.6: The Changes of Poisson's Ratio and Modulus vs. Confining Pressure in Ballast (Indraratna *et al.*, 1998)

2.2.6 Ballast Shear Strength

As previously mentioned, ballast is the selected crushed granular material placed as the top layer of the railroad substructure in which the sleepers are embedded and needs to have adequate load-bearing capacity for 25 – 30 ton axle trains which leads to a vertical stress of 120 to 140 kPa (Gräbe & Clayton, 2009, Jain & Keshav, 1999, Li & Selig, 1998). The strength of different crushed stones that have been using in railroad systems have been studied by different researchers. Although the strength of the parent rock is not usually tested nor required by most ballast specifications (Indraratna & Salim, 2005), a higher parent rock strength is affected by the selection criteria, which includes petrological examination. It should also be noted that the strength of rocks can be indirectly evaluated by performing, Aggregate crushing value, Los Angeles Abrasion value (LAA) and Wet attrition value.

There are also other parameters that are effective in the shear strength of ballast, such as particle angularity, particle surface roughness, quantity of flaky particles, particle size range, particles shape and etc. (Selig & Waters, 1994).

Although the effect of particle size on the shear strength of ballast is challenging and unclear, as discussed in section 2.2.2, Kolbuszewski and Fredrick in 1963 presented that the angle of shearing resistance increases with large particle sizes and Indrartna et al. (1998) reported that the internal friction decreases with increase in the maximum particle size and this can cause a significant reduction in the shear strength and load carrying ability of the track (Indraratna *et al.*, 1998, Kolbuszewski & Frederick, 1963). As Raymond mentioned in 1985, the particle shape and surface roughness are important and affect the track stability. (Raymond, 1985)

Anbazhagan et al. in 2012 determined that particle shape of the aggregates which can be changed from angular to sub-rounded, has a significant effect on shear strength. (Anbazhagan *et al.*, 2012). This is because of increase in the frictional interlock between grains which leads to shear strength increase. Also the load history has effects on the shear strength and behavior of ballast in a long time (Diyaljee, 1987). As mentioned in Ballast drainage, the water in ballast also affects the strength of the ballast.

The variation of shear strength with increase in normal stress for Basalt from different sources is presented in Figure 2.7. It can be seen that for a typical range of normal stresses studied in railroad track ballast, shear strength varies from low numbers to about 600 kPa which also depends on the unit weight.

Consequently, it can be seen from the above explanation that many parameters influence the shear strength of ballast. And also, the fouling material is affecting the strength of the ballast by changing the void ratio and grain size distribution.

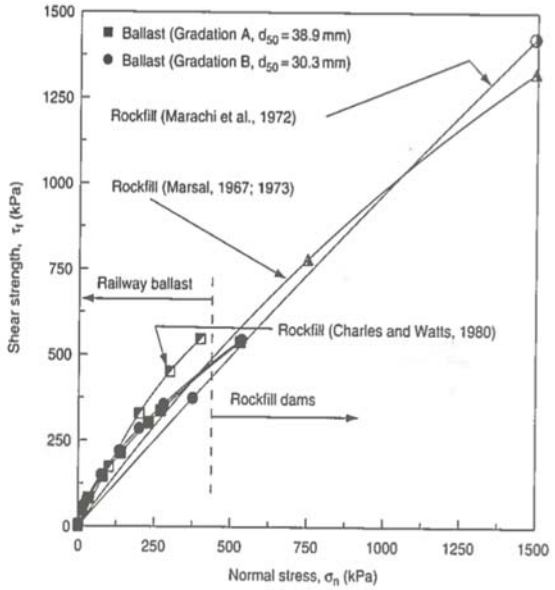

Figure 2.7: Variation of Shear Strength with Normal Stress for Ballast (Indraratna *et al.*, 2013)

2.2.6.1 Tests for Measuring Shear Strength of Ballast

2.2.6.1.1 Large-Scale Triaxial Testing

The strength and degradation behavior of ballast under loading can be investigated using large scale cylindrical triaxial apparatus. Triaxial Apparatus can be used to conduct shearing tests on Ballast with various confining pressures. The cylinder diameters that have been used for running this test on Ballast depends on the maximum size of the aggregates and are 6, 10 and 12 inches with the ratio of height to diameter of 2 (ASTM D7181). This test can be performed statically and dynamically.

2.2.6.1.2 Direct Shear Test

The test device is a square box with side dimensions of usually 12 in. and a specimen height of 203 mm (8 in.). It has a total 102 mm (4-in.) travel of the bottom which is a 152-mm (6-in.) high component, large enough for ballast testing purposes to record peak shear stresses and friction angle (Dombrow *et al.*, 2009).

2.2.7 Ballast Friction Angle (ϕ_{fb})

For the basic friction angle (ϕ_{fb}) for ballast, Indraratna and Salim in 2005 suggested (Eq. 2.6**)** by assuming that the energy consumption due to particle breakage is zero and the friction angle includes particle breakage but excludes the effect of dilation under loading:

$$\frac{q}{p'} = \frac{\left(1-\frac{d\varepsilon_v}{d\varepsilon_1}\right)tan^2\left(45^\circ+\frac{\varphi_{fb}}{2}\right)-1}{\frac{2}{3}+\frac{1}{3}\left(1-\frac{d\varepsilon_v}{d\varepsilon_1}\right)tan^2(45^\circ+\frac{\varphi_{fb}}{2})} \qquad \text{Eq. (2.6)}$$

where q/p' is the deviator stress ratio, $d_{\varepsilon v}$ is the volumetric strain increment, $d_{\varepsilon 1}$ is the major principal strain increment and ϕ_{fb} is the friction angle of particles.

By using laboratory experimental results of deviator stress ration at failure and the values of strain increments, the friction angle of aggregates can be measured.

In addition, they mentioned to the peak friction angle of ballast ϕ_p which it can be calculated from the triaxial test results and peak principal stress ratio. Figure 2.8 presents the different studied friction angles in ballast and the effect of confining pressure, dilatancy and particle breakage on the basic and peak friction angle of ballast. Figure 2.8 also presents that with increasing the confining pressure, the peak friction angle decreases (Charles & Watts, 1980, Indraratna *et al.*, 1998, Marsal, 1967).

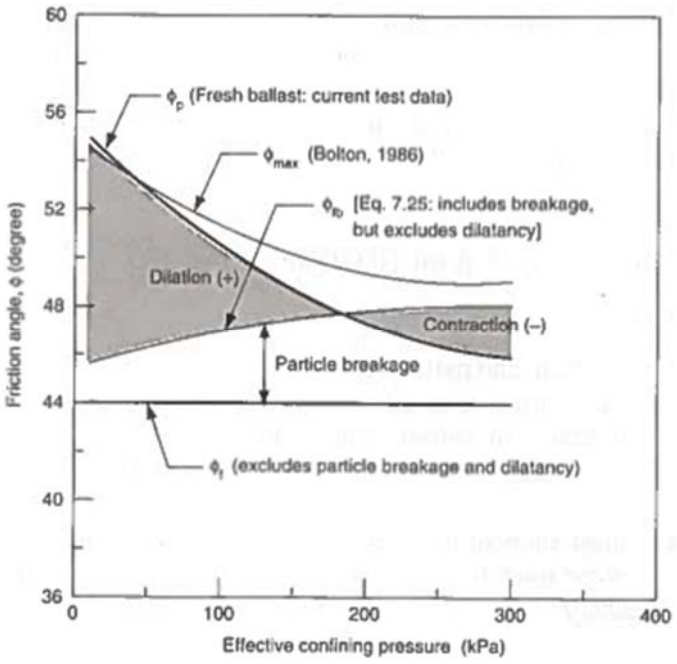

Figure 2.8: Changes of Different Studied Friction Angles in Ballast with the Confining Pressure (Indraratna & Salim, 2005)

2.2.8 Ballast Settlement

The settlement of Ballast can be both elastic (same as compaction) and plastic due to the breakage of ballast particles (Anbazhagan *et al.*, 2012). In most tracks, ballast is the

main source of both average and differential settlement between surfacing operations. Usually, the short term settlement is related to the ballast and long term settlements is subgrade related. Necessary condition for ballast to be the main source of settlement are:

1. Existence of filter/separation layer between the coarse ballast and fine subgrade,
2. A strong subgrade or subballast/subgrade combination, and
3. Good drainage of water entering from the surface (Selig & Waters, 1994).

The repeated load will increase the settlement over time or in the other words, the cumulative strain increases as the number of cycles increases. (Figure 2.9)

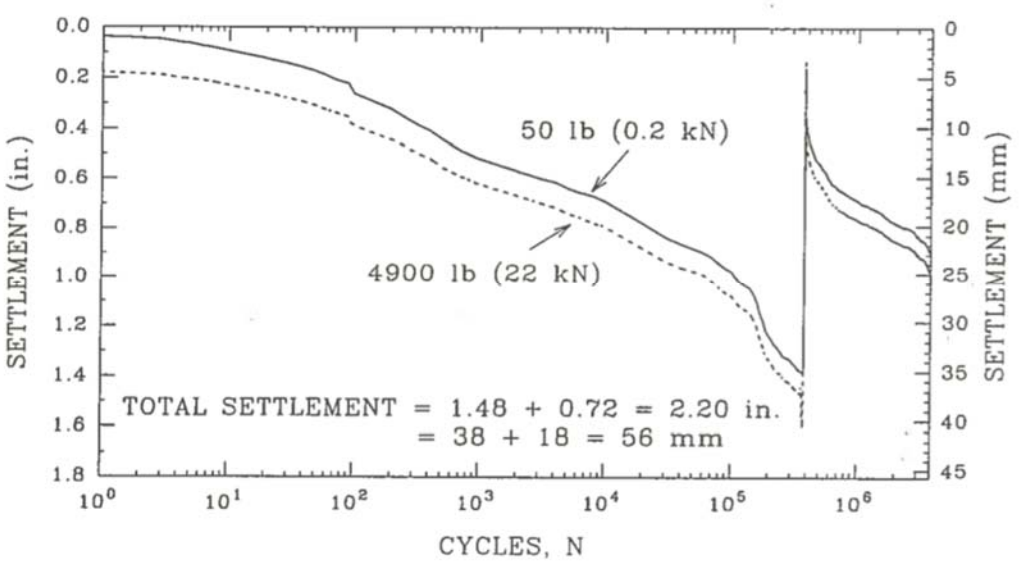

Figure 2.9: The Changes of Ballast Settlement vs. Number of Loading Cycles (Selig & Waters, 1994)

2.2.9 Resilient Modulus

The behavior of granular materials under repeated loading condition is nonlinear and stress-state dependent (Figure 2.10). While repeated loading is taking place, any additional cycle contributes another increment of plastic or permanent strain and the magnitude

of these plastic strain increments decreases with the number of cycles. The resilient Modulus (E_r) of material is the ratio of deviator of repeated stress to strain. (Selig & Waters, 1994)

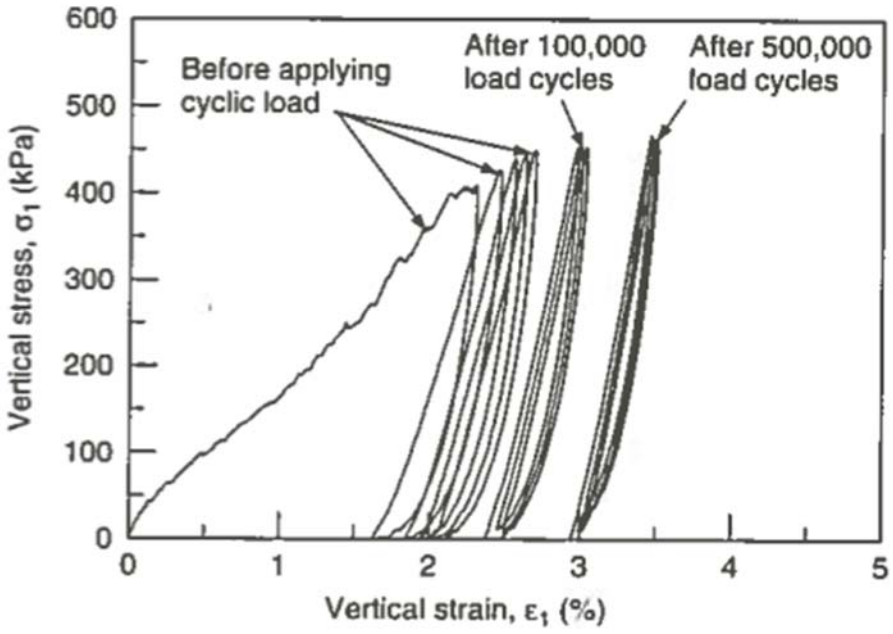

Figure 2.10: Stress-Strain Plots in Repeated Load Test in Various Stages of Cyclic Loading (Indraratna & Salim, 2005)

In granular materials researchers have reported different number of cycles for reaching the constant values for resilient modulus in granular materials between few hundreds to several thousands (Kalcheff & Hicks, 1973, Morgan, 1966). The magnitude of the resilient modulus is very stress-state dependent and there are still lots of uncertainties about the effect of grain size on the plastic deformation and consequently resilient modulus (Indraratna *et al.*, 1998, Janardhanam & Desai, 1983, Raymond & Diyaljee, 1979).

Some researchers reported a linear relationship between resilient modulus and confining stress. They defined the following commonly used equations which represents only unloading cyclic test (Hicks & Monismith, 1971, Pell & Brown, 1972):

$$E_r = K_1(\theta')^{K_2} \quad \text{Eq. (2.7)}$$

$$E_r = K_3 + K_4\,\theta' \quad \text{Eq. (2.8)}$$

where K_1, K_2, K_3 and K_4 are the soil constants from lab tests and θ' is the bulk effective stress in the loaded state and can be calculate by the following equation:

$$\theta' = \sigma_1' + \sigma_2' + \sigma_3' = 3\sigma_3' + (\sigma_1 - \sigma_3)_{max} \quad \text{Eq. (2.9)}$$

There are other relationships for resilient behavior of railroad ballast, such as the following equation, which is based on load-unload tests (Stewart 1982):

$$E_r = \frac{2(q_c - q_e)}{\varepsilon_{rc} - \varepsilon_{re}} \quad \text{Eq. (2.10)}$$

where ε_{re}, ε_{rc}, q_e and q_c are resilient extension strain, resilient compression strain, shear stress in extension (psi) and shear stress in compression (psi):

$$\varepsilon_{rc} = [0.00116\, q_c(\sigma_3')^{-1.15}]^{\eta} \quad \text{Eq. (2.11)}$$

$$\varepsilon_{re} = 0.0039\, q_c(\sigma_3')^{-1.52} \quad \text{Eq. (2.12)}$$

and η is equal to:

$$\eta = 0.78\,(\sigma_3')^{0.088} \quad \text{Eq. (2.13)}$$

where σ_3' is constant confining pressure for cyclic test (psi).

The increase in the slope of the hysteresis loop of the cyclic loading during the initial stages of loading (cycles 1-5) (Figure 2.10) indicates that resilient modulus of ballast increases with increase in repetition load (Indraratna & Salim, 2005).

In accordance with the significant effect of confining pressure on the resilient modulus of Ballast and higher breaking index in high confining pressure, Indraratna et al. in 2005 suggested a range of approximately 45 to 60 kPa for optimum confining pressure with minimal breakage.(Indraratna *et al.*, 2005)

2.3 Electromagnetic Properties of Railroad Track Ballast

In order to better understand GPR results obtained in railroad surveys and site investigation, the electromagnetic properties of ballast need to be evaluated. The first point for any discussion about the nature of materials under the excitation of EM waves is Maxwell's equations. These vector equations describe the spatially and temporally varying coupled electric and magnetic fields. These equations are for heterogeneous, isotropic, linear and stationary media (Balanis, 1989):

$$\nabla \times E = -\partial B/\partial t \qquad \text{Eq. (2.14)}$$

$$\nabla \times H = \frac{\partial D}{\partial t} + J \qquad \text{Eq. (2.15)}$$

$$\nabla . D = \rho \qquad \text{Eq. (2.16)}$$

$$\nabla . B = 0 \qquad \text{Eq. (2.17)}$$

where E is the electric field strength vector (in volts per meter,V/m), H is the magnetic field strength vector (in amperes per meter, A/m), D is the electric flux density vector (in Coulombs per meter squared, C/m^2), B is the magnetic flux density vector (in Tesla, T), J is the current density vector (in amperes per meter squared, A/m^2), ρ is the change of density (in coulombs per meter cubed, C/m^3), ∇ is the del vector operator, × is the cross product and • is the dot product.

The EM properties of Earth materials can be characterized by magnetic permeability, electrical conductivity and dielectric permittivity. The following constitutive relations define these material properties as following:

$$D = \varepsilon E \quad \text{Eq. (2.18)}$$

where ε is the permittivity of the material (in Farads per meter, F/m)

$$J = \sigma E \quad \text{Eq. (2.19)}$$

where σ is the conductivity of the material (in Siemens per meter, S/m)

$$B = \mu H \quad \text{Eq. (2.20)}$$

where μ is the permeability of the material (in Henrys per meter, H/m)

In general, if there is any free charge available, then under the influence of the applied EM field, these will flow through the material and because all of the subsurface materials have some form of free charge, such as electrons and ions, they show some degree of EM attenuation. The response of subsurface materials and other particulate media to an applied electromagnetic field depends on the properties, volume fraction, and spatial distribution of the fluid and solid phases (Santamarina *et al.*, 2001).

Mitchell and Soga in 1976 reported that the flow of electricity through a soil is a composite of (Mitchell & Soga, 1976):

1. Flow through the soil particles alone, which are small, because the solid phase is a poor conductor,
2. Flow through the pore fluid alone, and
3. Flow through both solid and pore fluid.

The total electrical flow also depends on the porosity, tortuosity of flow paths, and conditions at the interfaces between the solid and liquid phases. So, in the following sections the magnetic permeability, electrical conductivity and electrical permittivity will be evaluated in these three phases.

2.3.1 Magnetic Permeability

Moving electric charges generate magnetic fields. Because a matter consists of moving charged particles, it exhibits a magnetic field. Materials are classified as paramagnetic, diamagnetic, or ferromagnetic based on their magnetic permeability. Table 2.3 presents the real relative magnetic permeability of different materials in three different categories of diamagnetic, paramagnetic and ferromagnetic substances.

Magnetic permeability is a function of frequency and the magnetic permeability of mixtures of ferromagnetic inclusions in non-ferromagnetic host material depends on the volume fraction, size and spatial distribution of the inclusions (Santamarina *et al.*, 2001).

As it can be seen in Table 2.3, the magnetic permeability of crushed stone granite which is a type of railroad track ballast, is approximately equal to 1 which is equal to the magnetic permeability of air. Consequently, in most circumstances, the magnetic effect of materials (i.e., diamagnetic, paramagnetic and super paramagnetic phenomena) has little effect on propagating EM waves (Olhoef, 1998). Significant changes in magnetic permeability of railroad ballast track can be because of contaminated or fouled with ferromagnetic materials or ballast composed of crushed stones with iron minerals.

Most soil constituents are either paramagnetic or diamagnetic and consequently, the assumption that magnetic effects are unimportant is justified as long as the soil is iron free and doesn't have ferromagnetic material.

Table 2.3: Real Relative Magnetic Permeability of Selected Materials (Santamarina *et al.*, 2001)

Material	μ'_{rel}
Diamagnetic μ'_{rel} *slightly* < 1	
water	0.99991
gold	0.9999973
silver	0.9999981
copper	0.999990
quartz (SiO_2)	0.999999 – 0.9999988
kaolinite	0.99999995 – 1.0000023
Paramagnetic μ'_{rel} *slightly* > 1	
montmorillonite (2.8% FeO, 3% Fe_2O_3)	1.000026
illite (1.4% FeO, 4.7% Fe_2O_3)	1.000034
shale	1.000005 – 1.0015
granite	1 – 1.004
ochre (hematite)	1.002 – 1.003
Ferromagnetic μ'_{rel} > 1	
anealed nickel	≈ 300 (low H)
iron (commercial)	≈ 550 (may exceed 6000)

Sources: Bozorth (1951); Omar (1975); Carmichael (1989); Schroeder, Pruett and Hurst (1998); the authors (frequency = 2 kHz).

2.3.2 Electrical Conductivity

Electrical conductivity is a measure of charge mobility due to the application of an electric field and it is proportional to ionic concentration and ion mobility. The electrical conductivity in mixtures is sensitive to the spatial distribution of the components. Table 2.4 presents nominal values for selected materials (Santamarina *et al.*, 2001). Because the mobility of ions in minerals typically found in soils is very small, the conductivity of dry soils is significantly lower than the conductivity of electrolytic pore fluids, even at low ionic concentration. In the soil-water mixture the conductivity may be higher or lower than

the conductivity of the fluid phase and this depends on the specific surface of the particles and the ionic concentration of the fluid and which one can overcompensate.

Table 2.4: Electrical Conductivity of Selected Materials (Santamarina *et al.*, 2001)

Material	Electrical conductivity (S/m)
Glass	10^{-12}
Calcite	10^{-14}
Diamond	0.4
Dolomite	2.3×10^{-14}
Granite	2×10^{-12} to 4×10^{-11}
Kaolinite	3.1×10^{-8}
Magnetite	2×10^{4}
Montmorillonite	4.8×10^{-7}
Muscovite	4.6×10^{-13}
Quartz	5×10^{-15}
Oil	10^{-11}
Pure water	10^{-6}
Fresh water	10^{-3}
Seawater	4
Aluminum	3.7×10^{7}
Copper	5.9×10^{7}
Gold	4.5×10^{7}
Iron	10^{7}
Lead	4.8×10^{6}
Nickel	1.4×10^{7}

Sources: Olhoeft (1980, 1981); Keller (1989).

Figure 2.11 shows a conductivity data obtained for a mixture of crushed granite with $Na^{+}Cl^{-}$ electrolytes that can show the increase of mixture conductivity with increasing the fluid conductivity.

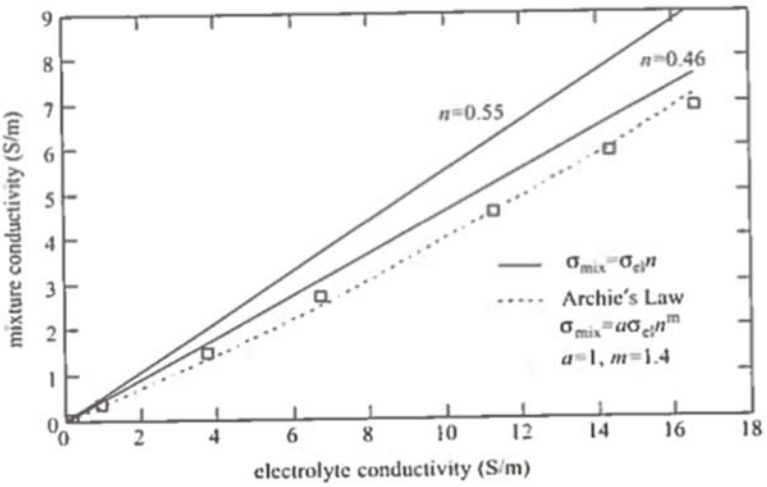

Figure 2.11: Conductivity of Granite-NaCl Electrolyte Mixtures as a Function of Electrolyte Conductivity (Santamarina *et al.*, 2001)

Low specific surface particles contribute negligible surface conduction while high specific surface such as clays have a significant effect on conductivity (Santamarina *et al.*, 2001). Ballast electromagnetic properties as a particulate material, which is composed of crushed stone, will be affected by its different mineralogy, specific surface and also the characterization of the mixed fluid. But from the last two sections it can be derived that evaluating the magnetic permeability and conductivity of ballast-water mixture is so complex and may not be helpful to the railroad industry in practice. Because it is significantly dependent on existence of iron in the stones and ionic concentration of the pore fluid, respectively. Over time, the ballast might be contaminated by many kinds of fluids such as leaked diesel or oil with high ionic concentration or fouled with high specific surface soils such as clays. It also might get replaced by stones with iron. These contaminations and replacements can change the conductivity of the ballast.

From the above explanation we can obviously understand that ballast by itself cannot have a high conductivity unless it gets fouled with clay or contaminated by a pore fluid with high conductivity or high ionic concentration.

2.3.3 Dielectric Permittivity

Dielectric permittivity describes the ability of a material to store and release EM energy in the form of electricity and classically relates to the storage ability of capacitors. It is usually quoted in terms of a non-dimensional, relative permittivity term (ε_r) where (Jol, 2008) defined as following:

ε_r = permittivity of a material (ε)/permittivity of free space or vacuum (ε_0) Eq. (2.21)

Inertial and viscous forces oppose the applied forces imposed by electric and magnetic fields and dipoles inside the medium. This is a good evidence of dependency of electromagnetic properties of materials to frequency therefore permittivity will become a complex quantity with the real component representing the 'instantaneous' energy storage-release mechanism and the imaginary component representing the energy dissipation (Jol, 2008, Santamarina *et al.*, 2001). In order to study both phase and amplitude response, the complex material parameters have been defined. The complex permittivity reflects the interplay between porosity, volumetric water content, pore fluid characteristics, specific surface, mineralogy and fabric. The relevance of each parameter varies with frequency. Table 2.5 shows values of the real relative permittivity and electrical conductivity of some common materials (Conyers & Goodman, 1997, Daniels, 2005, Jol, 2008, Santamarina *et al.*, 2001).

Table 2.5: Typical Values of Relative Permittivity (Real Component) and Static Conductitvity for Common Subsurface Materials (Jol, 2008)

Material	Static conductivity, σ_s (mS/m)	Relative permittivity, ε_{ave}
Air	0	1
Clay – dry	1–100	2–20
Clay – wet	100–1000	15–40
Concrete – dry	1–10	4–10
Concrete – wet	10–100	10–20
Freshwater	0.1–10	78 (25 °C)–88
Freshwater ice	1–0.000001	3
Seawater	4000	81–88
Seawater ice	10–100	4–8
Permafrost	0.1–10	2–8
Granite – dry	0.001–0.00001	5–8
Granite – fractured and wet	1–10	5–15
Limestone – dry	0.001–0.0000001	4–8
Limestone – wet	10–100	6–15
Sandstone – dry	0.001–0.0000001	4–7
Sandstone – wet	0.01–0.001	5–15
Shale – saturated	10–100	6–9
Sand – dry	0.0001–1	3–6
Sand – wet	0.1–10	10–30
Sand – coastal, dry	0.01–1	5–10
Soil – sandy, dry	0.1–100	4–6
Soil – sandy, wet	10–100	15–30
Soil – loamy, dry	0.1–1	4–6
Soil – loamy, wet	10–100	10–20
Soil – clayey, dry	0.1–100	4–6
Soil – clayey, wet	100–1000	10–15
Soil – average	5	16

Santamarina in 2001, also mentioned that spectral features in permittivity measurements reflect internal spatial scales and the spectrum of electromagnetic parameters helps identify the internal structure of the medium which is a proof for using GPR to evaluate sub-ground layers.(Santamarina *et al.*, 2001)

Santamrina also reported that the complex relative permittivity of minerals is relatively low compared to water. Furthermore, the relative permittivity of dry soils (less than 10) is lower than the relative permittivity of the parent rock due to porosity and this indicates that permittivity is a good parameter to evaluate voids in a medium. As an example, Figure 2.12 shows the relative permittivity for dry shale and dry kaolinite (Santamarina *et al.*, 2001).

By adding water, the permittivity of soil-water mixture will change and its value depends on the type of soil, including its specific surface area, the characteristics of the fluid, the volumetric fluid content and the frequency of the applied electric field. In railroad surveys usually the dielectric permittivity measurements are recorded as a function of time during each load increment.

From the experiments, the dielectric constant for the different types of ballast, was found using the following equation (Daniels, 1996):

$$\varepsilon_r = (\frac{ct}{2d})^2 \qquad \text{Eq. (2.22)}$$

where c is the velocity of light (3×10^8 m/s); ε_r is the dielectric constant of a material; t is the time taken for electromagnetic wave to travel distance; and d (s) is the depth of material layer (m). This low loss equation is accurate for materials with low attenuation such as ballast.

In accordance with section 2.3 of this study, electromagnetic properties of subsurface materials can indicate the underground situation. GPR can measure these parameters and has been used in a wide range of applications in research and practice in the world. With regards to traffic infrastructure, GPR application in railway surveys have had the fastest growth in recent years which started in Finland in mid-1980 with some not encouraging results and widely developed around the world (Jol, 2008). In the next section the principles of GPR and its usage in Railroad track will be explained.

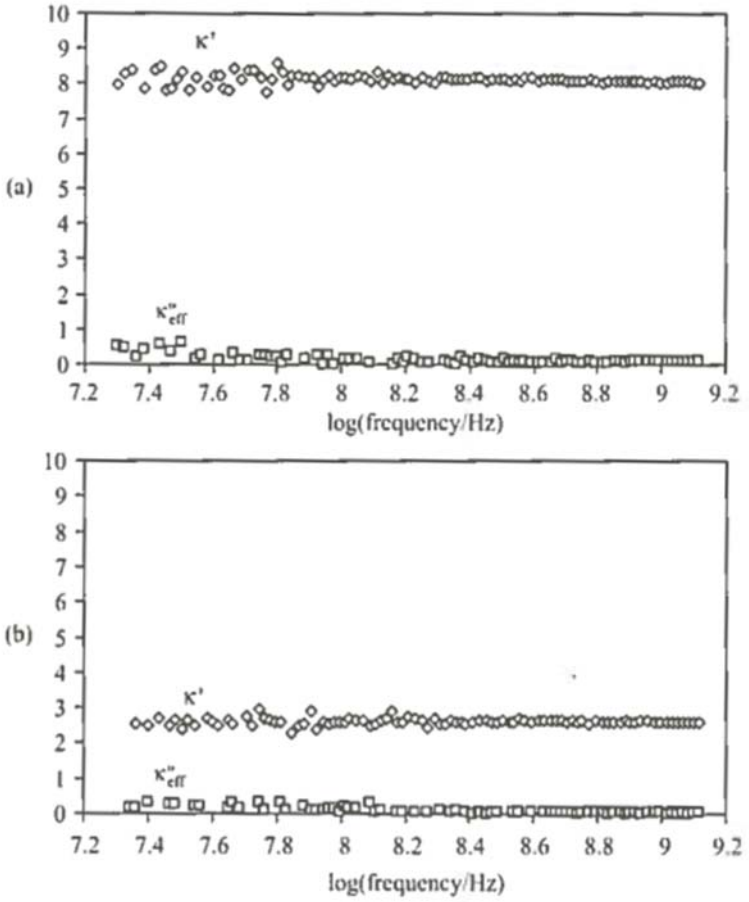

Figure 2.12: Relative Permittivity Spectra for Solids: (a) A Shale and (b) Kaolinite (Santamarina *et al.*, 2001)

2.4 Principles of Ground Penetrating Radar (GPR)

In general, the radar technique involves the pulsing of radar waves into soil and/or construction materials (Colla *et al.*, 1998). Radar is used to obtain object information by measuring the characteristics (arrival time and amplitude) of the electromagnetic (EM) fields scattered by the object. The Ground Penetrating Radar (GPR) method is based on sending short EM waves into the ground using a transmitting antenna. A receiver antenna records the transmitted signal from interfaces between the materials and scattering from

inhomogeneities having different EM properties within the materials. The amount of energy transmitted or reflected at an interface is quantified by the interface reflection and transmission coefficients (Uzarski & McNeil, 1994). (Figure 2.13)

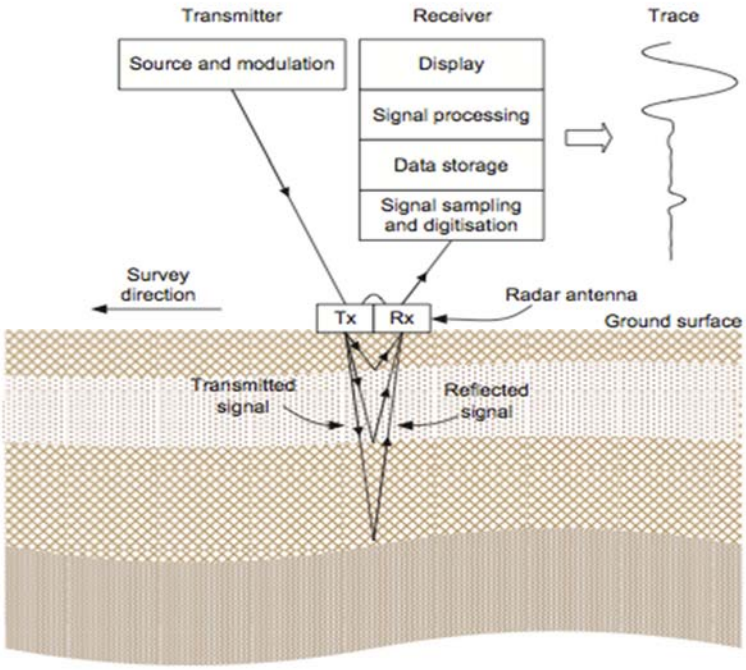

Figure 2.13: GPR System Components and GPR Work Process (Reynolds, 2011)

The propagation of the signal is affected by the electromagnetic properties of the material, discussed in section 2.3, so that by analyzing amplitude changes and the time for the pulse to travel through the ground, information about the layer thicknesses and properties of the materials can be obtained.

The time taken for a wave to traverse from one interface, reflect off a second interface, and travel back to the first interface is known as the round-trip, or two-way travel time for a wave within the medium bounded by the two interfaces. This is computed using the following equation (Daniels, 1996):

$$t = \frac{2d}{v} \qquad \text{Eq. (2.23)}$$

where t is the round-trip travel time, v is the propagation velocity of the wave and d is the distance between the two interfaces. Calculation of the round-trip travel time in each layer is necessary for computing the total reflected wave at the source.

The velocity of an electromagnetic wave in a dielectric medium is computed using the following equation (Daniels, 1996):

$$v = \frac{c}{\sqrt{\varepsilon_r}} \qquad \text{Eq. (2.24)}$$

where v is the velocity of propagation, c is the speed of light (3×10^8 meters per second), and ε_r is the dielectric constant of the medium. The value of v varies depending upon the composition and water content of the ballast and the sub-ballast layers, and generally falls within the range $[1.2 – 2.0] \times 10^8$ meters per second. In comparison, the velocity of electromagnetic wave propagation is 3.33×10^7 meters per second in pure water. In the most cases the dielectric constant is unknown and we use the propagation velocity to calculate the dielectric constant. If the antenna offset can be changed, there are two common methods to measure the propagation velocity:

a) Common Mid-Point (CMP): Both antennas are moved apart with the same increment and on either side of the midpoint of the profile.
b) Wide Angle (WA): One antenna stays stationary and the other moves along the profile direction (Tillard, 1995) (Figure 2.14).

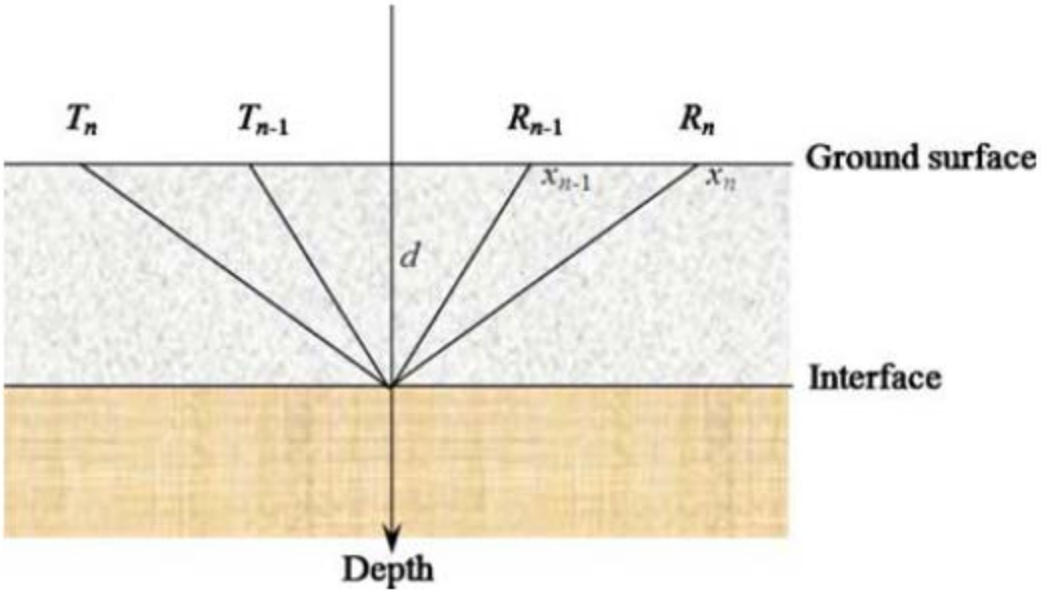

Figure 2.14: Common Mid-Point Measurement (Su *et al.*, 2010)

If the antenna offset cannot be changed, the measurement can be determined using multi-offset method with multiple pair antennas or one transmitter and multiple receivers (Figure 2.15).

The raw GPR data need to be processed to be ready for subsurface evaluation. Typically, this initial data processing includes, trace editing, filtering or data correction and introduce minimal operator bias into the data. (Jol, 2008).

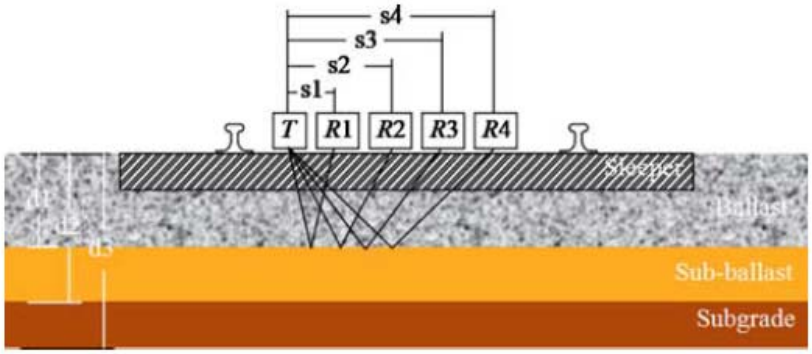

Figure 2.15: A Radar with Multi-Offset Antenna (Su *et al.*, 2010)

2.4.1 GPR with Impulse Radar Technique

There are different categories of GPR, which are beyond the scope of this study. The GPR systems that are being used for railroad substructure purposes are based on the impulse radar technique. In these systems a pulse is sent to an antenna, which produces an electromagnetic (EM) wave. A time domain pulse is transmitted and the reflected energy is received as a function of time. The result is a waveform that indicates the amplitude of energy scattered from sub-surface objects versus time. In practice, in order to evaluate the railroad substructure condition, the GPR is mounted to a vehicle and data were recorded while the vehicle is moving. A continuous presentation of amplitudes profiles (traces) for all surveying points will form a radargram.

Figure 2.16 shows a radargram and amplitude profile (waveform trace) captured by 800 MHz antenna. The interfaces between different layers are clearly visible on the radargram. The amplitude profile shows a significant increase in amplitude of the reflected signal. This change can be detected at the interface related to the difference in relative permittivity of the materials (Su *et al.*, 2010).

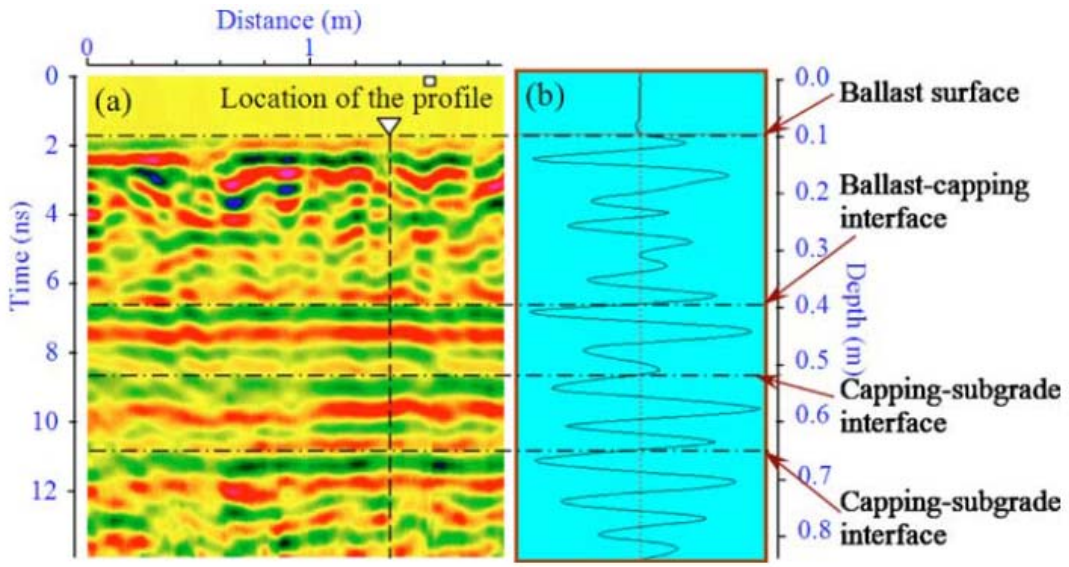

Figure 2.16: (a) Radargram and (b) Amplitude Profile for 800 MHz (Su *et al.*, 2010)

The brightness and darkness of the radargram texture is related to the reflection coefficient. The reflection coefficient depends on the velocity propagation of the electromagnetic waves in an inhomogeneity region. For example, in a two subsurface layer, assume an electromagnetic wave traveling in Region 1 and perpendicularly incident at an interface with Region 2. The reflection coefficient for the reflected wave in Region 1 is given by:

$$\Gamma = \frac{v_2 - v_1}{v_2 + v_1} \qquad \text{Eq. (2.25)}$$

where v_1 is the velocity of propagation in Region 1 and v_2 is the velocity of propagation in Region 2. The transmission coefficient for the transmitted wave in Region 2 is given by:

$$T = \frac{2v_2}{v_1 + v_2} \qquad \text{Eq. (2.26)}$$

Thus, if the material dielectric constants on each side of the interface are substantially different, the wave propagation velocities will also be substantially different. In such a case,

the reflection coefficient will be high, and the image will appear brighter at the corresponding depth. On the other hand, if the dielectric constants on both sides of the interface are closer to each other, the reflection coefficient will be small, and the image will look darker. The above is also true when inhomogeneities are present in layers considered to be uniform, such as the ballast and the sub-ballast. If the inhomogeneities are widely distributed, the image will appear speckled within the layer. On the other hand, if the layer is relatively homogeneous, the image will appear dark since there will be no dielectric discontinuities within the layer to cause myriad reflections.

2.4.2 GPR Antenna Frequency

The antenna frequency should be determined based on the requirements for both resolution and depth penetration (Daniels, 1996). High frequency antennas have a higher resolution and penetrate to a shallower depth than low frequency antennas with lower resolution. Because high frequency antennas can monitor ballast condition by providing strong reflection from the voids and have higher resolution radargram texture. However, this strong reflection from voids weakens the reflections from the interfaces. On the other hand, the lower frequency waves have weaker reflections from the voids and can strongly be reflected by the existing interfaces.

As an example, Figure 2.17 shows a part of radargram from a GPR survey on ballast with 500 MHz, 800MHZ, 1.6 GHz and 2.3 GHz (Anbazhagan *et al.*, 2011). This figure shows that by increasing the antenna frequency the resolution increases and the evaluated depth decreases. Clark in 2001 suggested 500 MHz antenna as an appropriate and effective

commercial antenna for railroad track subsurface evaluation and confirmed it with experimental results (Clark *et al.*, 2001).

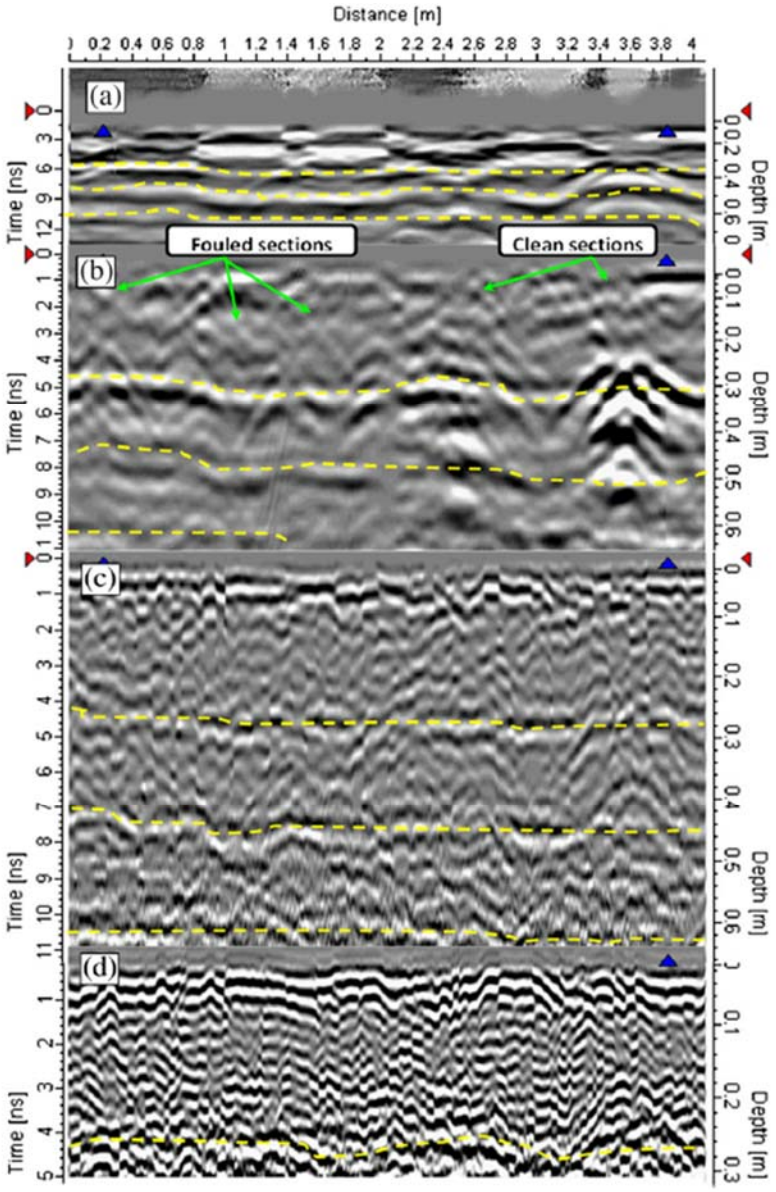

Figure 2.17: Comparison between Processed GPR Data from Different Antennas; A, B, C, and shows Processed Signal with Respect to Antenna Frequency of 500 MHz with, 800 MHz, 1.6 GHz And 2.3 GHz (Anbazhagan *et al.*, 2011)

The range resolution for a radar system in a medium of dielectric constant ε_r is approximately given by (Skolnik, 1980):

$$\Delta R \cong \frac{c\tau}{2\sqrt{\varepsilon_r}} \qquad \text{Eq. (2.27)}$$

where c is the speed of light and τ is the transmitted pulse width. The range resolution, ΔR, is the minimum distance that a pulse of duration τ can resolve.

The operating frequency of the GPR is simply the reciprocal of the pulse width; for example, a 400-MHz GPR system has a pulse width of 2.5 ns. It should be noted that for pulsed GPR systems, the transmitted pulse is a single bipolar pulse. In GPR work, the pulse width must be chosen so that ΔR is less than the thickness of the thinnest layer of interest. In other words, for closely spaced subsurface layers, a short pulse length (high frequency) must be used. The consequence of using a higher frequency, however, is a decrease in the depth of signal penetration as natural media have higher signal loss at higher frequencies. Choosing the correct pulse frequency becomes very important, with desired range resolution and depth of penetration being the dominant factors. It should be noted that antenna size also increases with decreasing frequency (Narayanan *et al.*, 2004).

2.4.3 GPR Antenna Deployment

The two basic categories of antennas are air-coupled and ground-coupled (Smith, 1995). Antennas that are air-coupled, are designed to be used suspended above the ground surface, with an air gap. Ground-coupled antennas are designed to be in direct contact with the ground surface. Air-coupled antennas are particularly well suited to railroad applications since they are suspended above the ground and thereby allow high speed measurement and clearance for turnouts, grade-crossings, wayside detection devices, trash, etc.

2.4.4 Multi-Channel GPR

Because the amount of the information transmitted in a unit of time is proportional to the radar's bandwidth, increasing the system's capacity requires expanding its band of frequencies (Taylor, 2000) and also, the quality of GPR data that can be obtained is strongly correlated to the frequency of the antenna which was discussed in section 2.4.2. Therefore the GPR with different frequencies were tested to evaluate the ballast condition to simultaneously image the ballast, the sub-ballast and the subgrade layers (Anbazhagan *et al.*, 2011, Narayanan *et al.*, 2004).

2.5 Fouled Ballast

In general, ballast contamination because of the filling of voids due to ballast breakdown and infiltration of other materials from the ballast surface or base is called ballast fouling. Fouling particles are particles smaller than 9.5 mm (Selig & Waters, 1994), which fill the ballast voids and leads to poor ballast performance (Indraratna & Salim, 2005, Janardhanam & Desai, 1983, Kolisoja, 1997).

Fouling materials have different sources which can be divided into five categories (Selig & Waters, 1994);

1. Ballast break down
2. Infiltration from ballast
3. Sleeper (Tie) wear
4. Infiltration from underlying granular layers
5. Subgrade infiltration

The subcategories are shown in Table 2.6.

Figures 2.18, 2.19 and 2.20 show the schematic section fouled with different sources explained above. The evaluation on the variety of sources in different railroads around the world shows that fouling source categories have different portion in contaminating the ballast in different places (Collingwood, 1988, Selig & Waters, 1994, Selig & Russo, 1991, Tung, 1989).

The results show that in North America the average percent distribution by weight of the fouling components for each of the categories (showed in Table 2.6) are as Figure 2.21.

Table 2.6: Source of Ballast Fouling (Selig & Waters, 1994)

I. Ballast breakdown a) Handling (related to IIA) 1) At quarry 2) During transporting 3) From dumping b) Thermal stress from heating (desert) c) Freezing of water in particles d) Chemical weathering (including acid rain) e) Tamping damage f) Traffic damage 1) Repeated load 2) Vibration 3) Hydraulic action of slurry g) From compaction machines
II. Infiltration from ballast surface a) Delivered with ballast b) Dropped from trains c) Wind blown d) Water borne e) Splashing from adjacent wet spots f) Meteoric dirt
III. Sleeper (tie) wear
IV. Infiltration from underlying granular layers a) Old track bed breakdown b) Subballast particle migration from inadequate gradation
V. Subgrade infiltration

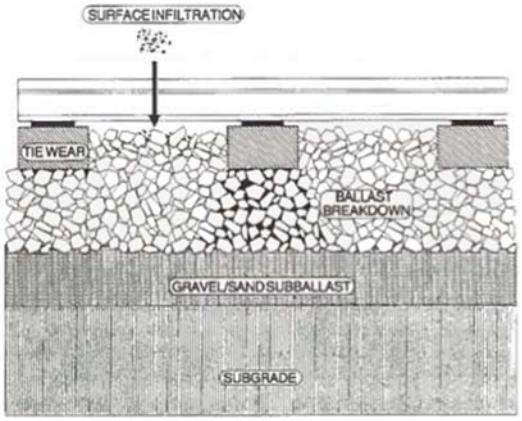

Figure 2.18: Ballast Breakdown, Sleeper Wear, and Subsurface Infiltration Causing Ballast Fouling (Selig & Waters, 1994)

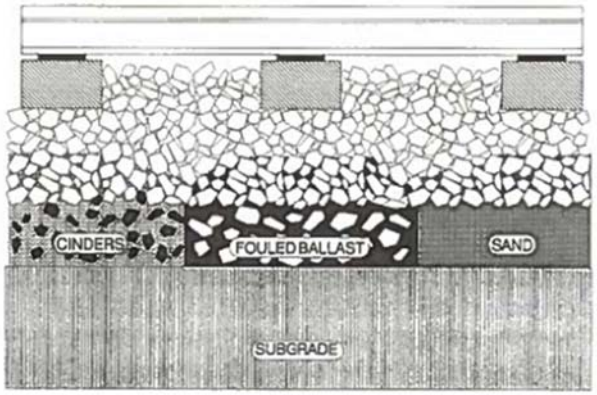

Figure 2.19: Underlying Layer Infiltration Causing Fouling (Selig & Waters, 1994)

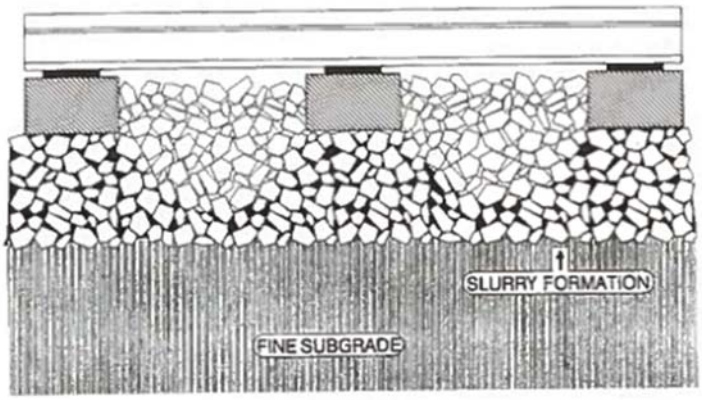

Figure 2.20: Subgrade Infiltration Causing Ballast Fouling (Selig & Waters, 1994)

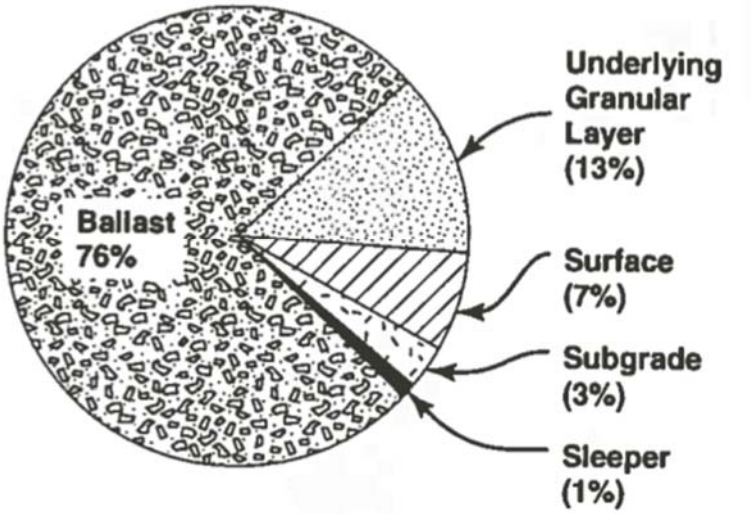

Figure 2.21: Sources of Ballast Fouling (Selig & Waters, 1994)

2.5.1 Quantification of Ballast Fouling

Quantification of ballast fouling is an important problem in geotechnical engineering of railroad track. There have been different methods developed in order to distinguish between different types of fouling materials.

2.5.1.1 Fouling Index

Selig and Waters in 1994 proposed Fouling Index (FI) as a term to quantitatively measure the fouling particles in the ballast. This evaluation was based on the clay pumping and infiltration of the materials as well as the other sources of fouling such as breakdown particles and the other objects delivered from the ballast, dropped from trains, wind or water blown. The Fouling Index can be calculated by the following equation;

$$FI = P_4 + P_{200} \qquad \text{Eq. (2.28)}$$

where P_4 is the percent of material passing 4.75 mm (No. 4 Sieve) and, P_{200} is the percent of material passing the 0.075 mm (No. 200 Sieve). They also defined different categories of fouling based on the Fouling Index (FI) (Table 2.7).

Ionescu, 2004 proposed a different ballast fouling index given as below:

$$FI = \frac{D_{90}}{D_{10}} \quad \text{Eq. (2.29)}$$

where D_{90} and D_{10} are grain diameter for the 90% and 10% passing by weight, respectively.

Table 2.7: Fouling Index (Selig & Waters, 1994)

Fouling Category	Fouling Index
Clean	< 1
Moderately Clean	1 - 10
Moderately Fouled	10 - 20
Fouled	20 - 40
Highly Fouled	> 40

2.5.1.2 Percentage of Fouling (% Fouling)

The percentage of fouling was also developed by Selig and Water in 1994 which is the ratio of dry weight of material passing 9.5 mm sieve (3/8" sieve) to the dry weight of the total sample.

2.5.1.3 Percentage Void Contamination (PVC)

Because of this importance that FI and percentage of fouling cannot show the relative density of the fouling material and ballast, and do not represent the volume and quantity of fouling materials in the ballast Feldman and Nissan in 2002 developed Percentage Void Contamination (PVC) (Feldman & Nissen, 2002):

$$PVC = \frac{V_2}{V_1} \times 100 \quad \text{Eq. (2.30)}$$

where V_1 is the initial volume of voids in the clean ballast and V_2 is the bulk volume of contamination in the ballast.

2.5.1.4 Relative Ballast Fouling Ratio (R_{b-f})

This parameter was proposed by Anbazhagan et al. (2010) and defined as the ratio of the dry weight of fouling particles (passing sieve 3/8") to the dry weight of ballast (retaining 3/8" sieve). It can be calculated by using the following equation (Anbazhagan *et al.*, 2010):

$$R_{b-f} = \frac{M_f \times \frac{G_{s-b}}{G_{s-f}}}{M_b} \times 100 \qquad \text{Eq. (2.31)}$$

Where M_f and G_{s-f} are the mass and the specific gravity of ballast fouling (fines), M_b and G_{s-b} are the mass and specific gravity of ballast.

2.5.1.5 Void Contaminant Index (VCI)

The bulk volume of fouling material needs to be determined based on the specimen compacted at standard proctor energy level to calculate PVC. Tennekon et al. in 2012 proposed VCI to capture the role of different fouling materials as a modification of the PVC (Tennakoon *et al.*, 2012):

$$VCI = \frac{V'_f}{V_{vb}} \times 100 = \frac{(1+e_f)}{e_b} \times \frac{G_{sb}}{G_{sf}} \times \frac{M_f}{M_b} \times 100 \qquad \text{Eq. (2.32)}$$

where V'_f is actual volume of fouling material within the ballast voids, V_{vb} is the initial voids volume of clean ballast, e_b void ratio of clean ballast, e_f void ratio of fouling material, G_{sb} specific gravity of clean ballast, G_{sf} specific gravity of fouling material, M_b dry mass of clean ballast, and M_f dry mass of fouling material.

As mentioned previously, the fouling particles fill the voids and prevent the drainage of the ballast. In order to evaluate the effects of fouling materials and the trapped water (by fouling) on the performance of the ballast under loading and on the GPR surveying results, the next two sections will review the conducted researches on these important parameters.

2.5.2 Fouling and Moisture Content Effects on Ballast Geotechnical Properties

In general, ballast fouling can cause many problems in railroad track such as reduction in resistance to the vertical, lateral and longitudinal forces applied to the ties to retain the track in its required position, decrease in resiliency modulus and energy absorption capacity, reduction in voids which leads the track to poor drainage and vegetation growth in the rail, increase in noise level and decreasing the electrical resistance between rails increasing the rate and magnitude of settlement. The severity of these effects is significantly related to the type and amount of fouling material and the water content of the fouled ballast (Anbazhagan *et al.*, 2011, Fortunato *et al.*, 2010, Indraratna & Salim, 2005, Selig & Waters, 1994).

Some of the researches on the effects of fouling material and water content on ballast performance have been briefly explained in the following paragraphs:

Based on the obtained samples taken from wide variety of track sites in North America, Selig and Waters in 1994 presented Figure 2.22 which represents gradation ranging from clean to highly fouled.

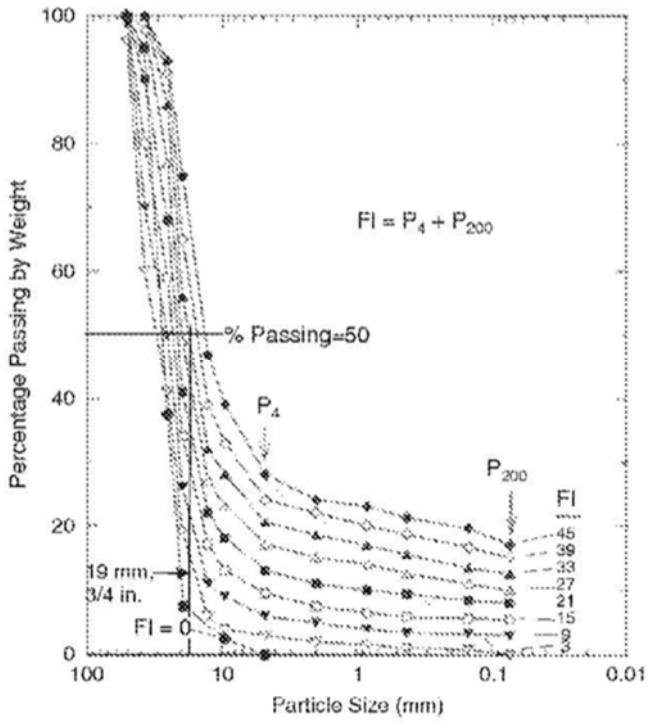

Figure 2.22: Influence of Fouling on Ballast Gradation Curve (Selig & Waters, 1994)

Figure 2.23 presents that with increasing the confining pressure, the peak friction angle of fresh and recycled ballast decreases and in a constant confining pressure a fouled (recycled ballast) has much lower peak friction angle than fresh ballast. These results reveal that the peak friction angles of fresh and recycled ballast decrease from 69° to 46° and 54° to 43°, respectively, as the effective confining pressure increases from 10 to 300kPa (Charles & Watts, 1980, Indraratna *et al.*, 1998, Marachi *et al.*, 1900, Marsal, 1967).

Han & Selig in 1997 and Indraratna et al. in 1998 by performing a series of loading tests on fouled ballast reported that ballast settlement typically increases by the increase of fouling material amount and most of these differential settlements are related to the local crushing at inter-particle contacts (Han & Selig, 1997, Indraratna *et al.*, 1998).

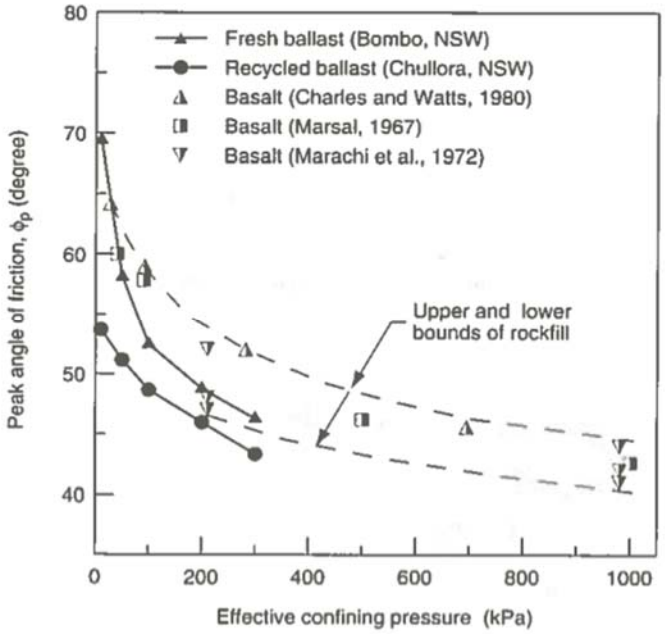

Figure 2.23: Variation of Peak Friction Angle of Fresh and Recycled Ballast with Effective Confining Pressure (Indraratna & Salim, 2005)

Budiono et al. in 2004, Huang et al. 2009 and Giannakos in 2010 showed that fine fouling material particles adversely affect the strength, stiffness and life cycle of the track (Budiono *et al.*, 2004, Giannakos, 2010, Huang *et al.*, 2009).

Indrartna and Salim in 2005, by performing experimental tests reported that fresh ballast has a higher elastic modulus than recycled ballast (fouled ballast) (Figure 2.24) due to the higher angularity and better friction interlocking.

Indraratna and Salim in 2005, Fortunato et al. in 2010 and Vitnam Trinh et al. in 2012 evaluated the behavior of fresh and fouled ballast under representative cyclic loading in dry and wet states by conducting triaxial apparatus. They reported that not only the ballast settlement increases by increase in the number of loading cycle but also, in a constant number of cycles fouling material and water will significantly increase the plastic settlement of ballast under loading (Figure 2.25). Furtunato et al. in 2010 also stressed that the

resilient modulus decreases by water content increase and in wet condition is less effective to the fouling index changes (Fortunato *et al.*, 2010, Indraratna & Salim, 2005, Trinh *et al.*, 2012).

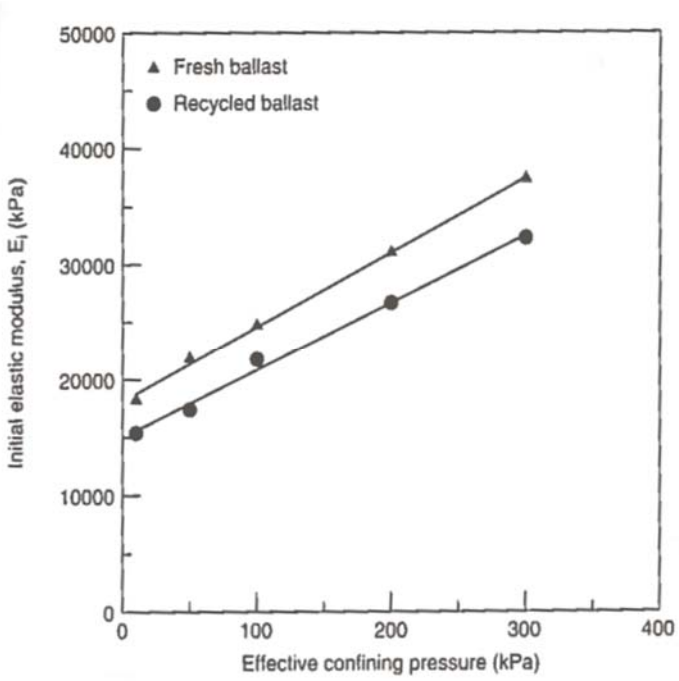

Figure 2.24: Initial Deformation Modulus of Fresh and Recycled Ballast at Various Confining Pressures (Indraratna & Salim, 2005)

Huang et al. in 2009, by performing direct shear tests on clean and fouled ballast with different fouling materials such as coal dust, clay and mineral filler assessed the effects of fouling and moisture on the shear strength of the soil. They reported that the highest shear strength values are from the clean ballast and shear strength decreases by increasing fouling material. This can also be related to the type of fouling material and moisture content (Huang *et al.*, 2009).

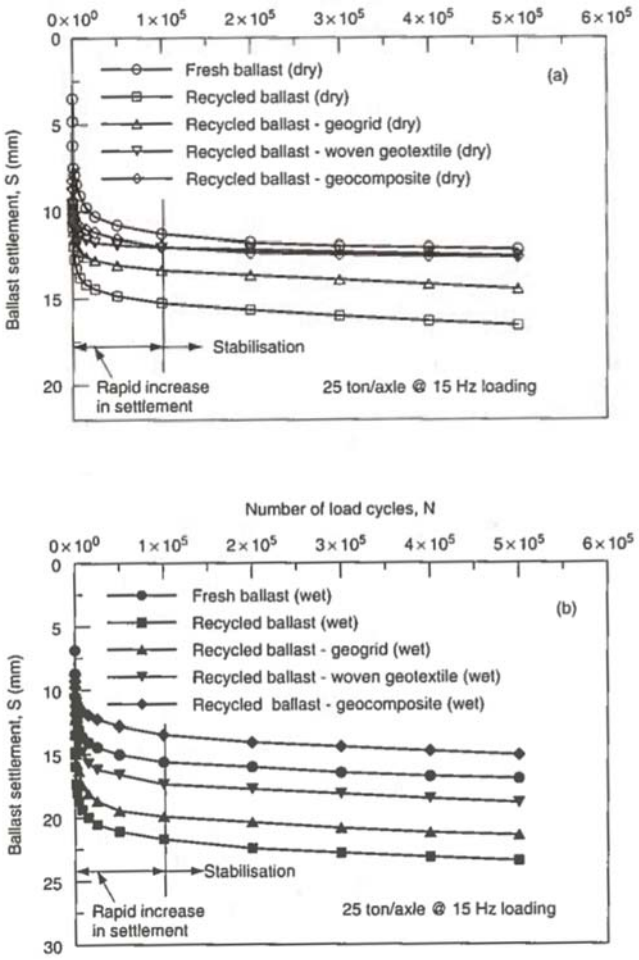

Figure 2.25: Settlement Response of Fresh and Recycled Ballast Under Cyclic Loading, (a) in Dry Conditions, and (b) in Wet Conditions

In 2010 Konstantinos Giannakos presented an equation to relate the fouling percentage to the ballast hardness derived from the analysis of the laboratory test result. He reported that in a constant loading cycles the breakdown fouling particles increase by decrease in the hardness of ballast (Giannakos, 2010).

Indraratna et al. in 2013 conducted many triaxial tests on the clay-fouled ballast. These tests indicated that an increase in fouling material will decrease the shear strength.

This is dependent upon VCI, which at high normal stress (σ_n = 200 kPa) remaining relatively unaffected, independently of VCI (Indraratna *et al.*, 2013).

Indraratna et al. in 2011 mentioned that fine particles change the pore matrix of the ballast assembly and reduces the particles interlock. In addition, by conducting multi-channel analysis of surface wave (MASW) on ballast fouled by clayey sand and coal, they reported that shear modulus initially provide extra stiffness to the ballast and when the ballast gets highly fouled, the particles will lose their direct contact due to lubrication effects and cyclic loading and the shear modulus decreases, consequently (Indraratna *et al.*, 2011).(Figure 2.26)

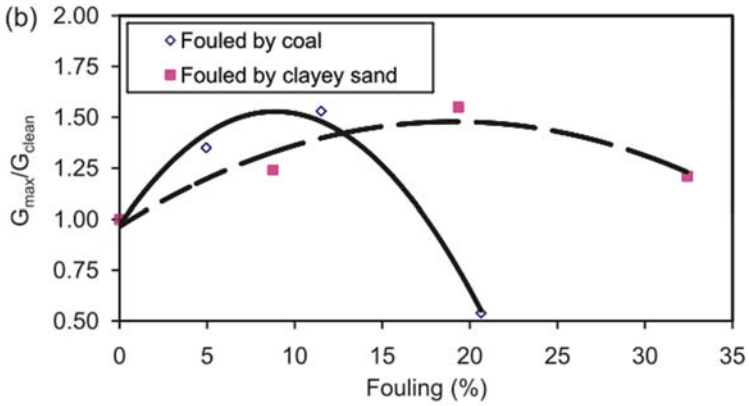

Figure 2.26: The Relationship between Normalized Shear Modulus and Fouling Percent (Indraratna *et al.*, 2011)

Tennakoon et al. in 2012 by conducting experimental tests and numerical modeling proposed a new parameter, Void Contaminant Index (VCI), and reported that overall hydraulic conductivity decreases with the increase in VCI and the critical conditions in the perspective of track maintenance would occur when VCI exceeded 50% (the fouling material is clayey fine sand in this study)(Tennakoon *et al.*, 2012) (Figure 2.27).

Anbaazhagan et al. 2010, measured the permeability of clayey sand fouled ballast and coal fouled ballast from experimental studies and reported that permeability is decreasing by increase in fouling particles. And permeability can be related to shear wave velocity with common percentage of fouling on x axis (Anbazhagan *et al.*, 2010).

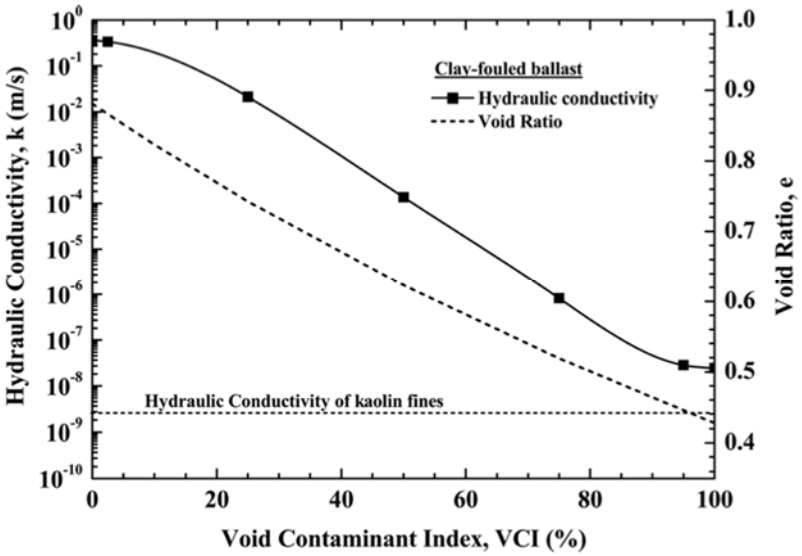

Figure 2.27: Variation Hydraulic Conductivity with Void Contaminant Index for Uniform Clay Fouled Ballast (Tennakoon *et al.*, 2012)

2.5.3 Fouling and Moisture Content Effects on Electromagnetic Properties of Ballast

In order to identify the condition of ballast Halabe et al. in 1993, developed an equation in order to calculate the dielectric permittivity of a mixture by having the dielectric permittivity of each component (Halabe *et al.*, 1993):

$$\sqrt{\varepsilon_t} = \sum_{i=1}^{n} \frac{A_i}{100} \sqrt{\varepsilon_{A,i}} \qquad \text{Eq. (2.33)}$$

in which, ε_t is the relative dielectric permittivity of the mixture, $\varepsilon_{A,i}$ is the relative dielectric permittivity of component i and A_i is the volumetric percentage of mixture component i. This equation indicates that the dielectric permittivity is directly related to the volumetric

percentage of the mixture occupied by its components. Adding or eliminating any components of a mixture will affect the electromagnetic properties of the mixture.

Studies on electromagnetic properties of clean and fouled ballast indicate that increase in permittivity associated with increase in ballast fouling and this behavior is highly related to the moisture content of the ballast (Clark *et al.*, 2001, Sussmann *et al.*, 2003).

Considerable information can be obtained by studying the amplitude and arrival times of the GPR signal reflections. For example, very high amplitude reflections may indicate presence of high water content or sudden increase in arrival times can infer the presence of ballast pockets (Hyslip *et al.*, 2005)

Table 2.8 shows the dielectric permittivity and wave propagation velocity in air, water and ballast in some different conditions. The dielectric constant and velocity of wave propagation of a clean ballast in comparison with spent ballast is lower and higher respectively because, the clean ballast has more air voids than the fouled ballast. The dielectric constant of air is 1 (velocity of 3×10^8 m/s), which as a result allows the electromagnetic wave to propagate through it at a higher speed compared with the fouled ballast with less air voids (Clark *et al.*, 2001).

It can be seen in Table 2.8 that the dielectric permittivity of wet ballast is higher than dry ballast due to the fact that the speed of electromagnetic shear wave through water is very slow (0.33×10^8 m/s) compared to that of the ballast or air. Thus with the wet ballast the characteristics of the water will predominate, since the water will be replacing the air in the voids. This table also shows that adding volumetrically, 5% water to fouled ballast will increase the dielectric value up to 45%. The increase of the dielectric value in fouled ballast is higher than clean ballast because the fouled ballast has a higher capacity for water

retention due to the high fines content. This can also be confirmed with the linear relationship reported between bulk ballast dielectric constant and moisture content (Leng & Al-Qadi, 2010, Sussmann *et al.*, 2002).

Table 2.8: The Dielectric Constant and Velocity of Air, Water and Ballast in Different Conditions (Clark *et al.*, 2001)

Material	ε_r	Velocity (m/s)
Air	1	3.00×10^8
Water	81	0.33×10^8
Dry clean ballast	3.0	1.73×10^8
Wet clean ballast (5% water[a])	3.5	1.60×10^8
Saturated clean ballast	26.9	0.48×10^8
Dry spent ballast	4.3	1.45×10^8
Wet spent ballast (5% water[a])	7.8	1.07×10^8
Saturated spent ballast	38.5	0.58×10^8

[a] 5% water by volume added.

Clark et al (2001) by conducting a quick GPR survey after saturation and before complete drain in the clean and fouled ballast, reported that relative difference between the saturated spent and clean ballast on a radar plot is 4.5 ns, which is a significant and detectable change (Clark *et al.*, 2001).

2.6 GPR from Geotechnical Engineering Approach

Performing GPR surveys with different frequency antennas in places with different geologies represent that interpretation of GPR profiles can provide significant geotechnological information about soils, thickness of unconsolidated deposits, depth of bedrock,

permafrost distribution, relative abundance of ice and their spatial extension in different deposits (i.e. Aeolian and Fluvial deposits). (Jol, 2008, Pilon *et al.*, 1992).

Saarenketo and Scullion (1996) explored the relationship between the dielectric properties of base course aggregates used in subgrade construction. This study observed the existence of a very high correlation between the dielectric properties and the strength and deformation characteristics of all types of soils and aggregates. This clearly establishes the basis for a possible relationship between GPR data and deformation characteristics of the railroad ballast. They evaluated this relationship in different soils by conducting "bucket test" with the help of Dynamic Cone Penetration test (DCP) for Engineering properties and dielectric tube probe for electrical properties (Saarenketo & Scullion, 1996).

Several researchers have used GPR to scan the subsurface and evaluate the old infrastructures or buried structures or study potential places for landslides by highly changes in electrical properties of soil as the result of moisture or different material (Bednarczyk, 2008, Benedetto *et al.*, 2012, Coutinho & Mayne, 2012, Whiteley & Siggins, 2000).

P. Cosenza et al. 2006, K. Marschall et al. 2007 and F.M. Fernandes et al. 2008 compared the GPR surveys on different soils, mostly fine grain soils, with Cone Penetration test (CPT) to evaluate the stratigraphy of the sub-layers and water content and develop a qualitative correlation between electrical properties and engineering properties in different fields. The reports show satisfying results in stratigraphy but because of inhomogeneity in natural soil, generalizing a correlation was impossible (Cosenza *et al.*, 2006, Fernandes *et al.*, 2008, Marschall *et al.*, 2007).

2.7 GPR from Railroad Track Approach

GPR signals can detect the wave reflections from the layer's substructure and can be used to identify track bed anomalies and determine the degree of track bed deterioration (Gallagher *et al.*, 1999, Jack & Jackson, 1999, Sussmann *et al.*, 2003).

Saarenketo and Scullion (1996) reported dielectric constant values for aggregates with different coefficient modulus. These analyses provide quantitative basis for postulating the relationship between the GPR and track engineering properties (Saarenketo & Scullion, 1996).

Despite the ability that GPR has on detecting the ballast status, there are still lots of uncertainties within the actual rail track and it is difficult to calibrate the GPR data with actual ground conditions (Anbazhagan *et al.*, 2012).

2.7.1 Model Track Studies

Performing GPR survey on a railroad track model with a defined condition such as the amount and type of fouling material, the depth of the layers, water content, density and grain size distribution is a reliable method to study the effects of different parameters on the GPR reflected waves.

Clark et al. in 2001, by conducting GPR surveys on six different ballasts (dry, 5% wet and saturated ballast of clean and fouled ballast) in a brick tank reported different dielectric permittivity and signal velocities (Table 2.8). Their collected data indicate that the dielectric constant of clean ballast was lower than fouled ballast and that for wet ballast is higher than dry ballast (Clark *et al.*, 2001).

In 2010 Li-Jun Su et al. used GPR survey on the model track with different amount and type of fouling materials to find a correlation for identifying the fouling degree to which ballast has become fouled (Su *et al.*, 2010).

Anbazhagan et al. in 2011 used a multi-channel GPR with four different frequencies (500 MHz, 800MHz, 1.6 GHz and 2.3 GHz) on a large scale model track with coal, clayey sand and ballast breakdown and with different fouling material R_{bf} s and thicknesses; they reported some correlations between the optimum fouling point (OFP) and shear strength for clay and coal fouled ballast (Anbazhagan *et al.*, 2011).

2.7.2 Field Track Studies

For improving the GPR data collection and processing, researchers from around the world are conducting field tests to better understand the effect of different properties of the subsurface layers on the GPR signal profile. GPR not only provides continuous vertical profile of the ballast and the subgrade, but also identify moist subgrade sections which shows brighter reflections in comparison with dry sections.

The field studies show that many valuable track substructure condition such as subsurface water pockets, saturated soil condition, thickness of the ballast layer, ballast deterioration and the subsoil penetration into the ballast layer can be detected by using GPR (Gallagher *et al.*, 1999, Hugenschmidt, 2000, Roberts *et al.*, 2006, Selig, 2002, Silvast *et al.*, 2010).

The field measurements on various tracks indicate that GPR is also effective in identifying subsurface water content, density, trapped water and fouling condition within

the ballast (Hyslip *et al.*, 2003, Narayanan *et al.*, 2001, Roberts *et al.*, 2006) (Figures 2.28 and 2.29)

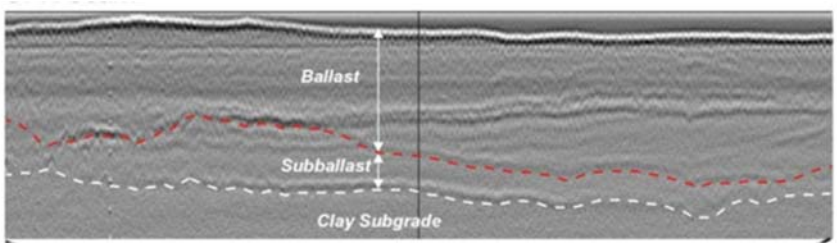

Figure 2.28: A Radargram that Indicates the Subsurface Layers for a Track Section (Hyslip *et al.*, 2003)

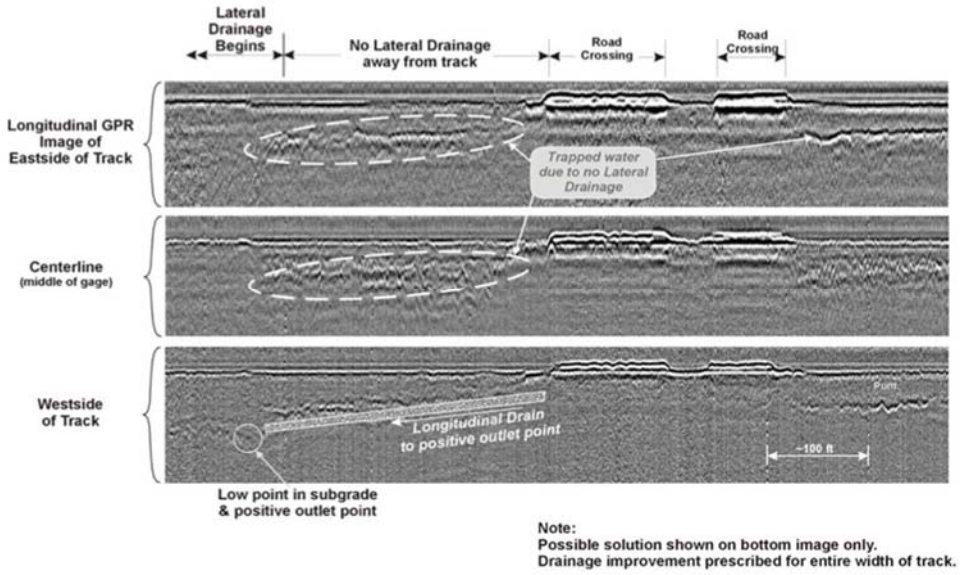

Figure 2.29: A Radargram that Indicates the Trapped Water in Ballast Section (Hyslip *et al.*, 2003)

In-situ tests such as DCP and CPT tests have been used to evaluate the stiffness and stratigraphy of the subballast and subgrade layers in addition to the GPR survey for the problematic parts of the track. The results have had a good agreement with the detected interfaces by GPR survey (Roberts *et al.*, 2006, Sussmann Jr, 1999).

In 2004, Narayanan et al. developed a multivariate linear regression model to predict the track modulus with an accuracy of approximately 3.4 MPa using 100 and 400 MHz frequency pulsed GPR system. This general linear model for multiple regression is a promising approach to modeling the track modulus using GPR data and track modulus measurements at a variety of locations at the Transportation Technology Center, Inc. (TTCI) (Narayanan *et al.*, 2004).

The new development of frequency analysis of the GPR signal produces continuous information concerning the ballast fouling. This method overcomes the limitation of the techniques using a preset threshold to estimate the ballast condition. GPR fouling indices derived by time-frequency technique and frequency spectrum from field surveying match the results of ground truth trenches, drilling data and ballast gradation analysis (Al-Qadi *et al.*, 2010, Silvast *et al.*, 2010).

Shangguan et al. in 2012, by conducting both laboratory and field GPR collecting data, proposed a new approach, Discrete Wavelet Transform (DWT). In this approach Standard Deviation (SD) values of the wavelet coefficients were calculated to quantify the scattering intensity and were capable of indicating the fouling level of the ballast. This approach was validated by field GPR data and ground truth measurements (Shangguan *et al.*, 2012).

2.8 Summary

A review of the literature has shown that fouling and moisture content have significant effects on deformation and index geotechnical properties of the ballast. In addition, ballast is an important part of the railroad track which must perform different functions.

An increase in fouling percentage and moisture content will decrease the workability of the ballast and takes the ballast to the high risk situation and safety problems. In another perspective, the review also reveals the significant effects of moisture content and fouling percentages on the electromagnetic properties of the ballast, which can be detected by GPR technique.

Existence of a high correlation between the dielectric properties and the strength and deformation characteristics of all types of soils and aggregates from past research (Saarenketo & Scullion, 1996) clearly establishes the basis for a possible relationship between GPR data and deformation and index characteristics of the railroad ballast.

Although the most fouled ballasts in North America are because of ballast breakdown (Selig & Waters, 1994), most of the past research is based on coal and clay fouling materials.

In accordance with the above explanation, a complete and comprehensive geotechnical testing program followed by GPR surveying is needed on ballast with different breakdown fouling percentages and water contents. More study is required to investigate how geotechnical and electromagnetic properties change as the result of fouling and moisture content change and evaluate any existing correlation between geotechnical and electromagnetic properties of ballast.

CHAPTER 3

EVALUATING THE CORRELATION BETWEEN GEOTECHNICAL INDEX AND ELECTROMAGNETIC PROPERTIES OF FOULED BALLASTED TRACK BY FULL SCALE LABORATORY MODEL[1]

3.1 Abstract

To determine the correlation between water content or fouling of a railroad track and Ground Penetrating Radar (GPR) signals, a full-scale railway track model was designed and constructed at the University of Massachusetts Amherst. To simulate a track section, the model consisted of rails and ties placed on a ballast layer overlain on a sub-ballast layer. The model was constructed three times with three different fouling percentages. Each model was tested with water content conditions of dry, field capacity and two points between these extremes. 450 MHz and 2 GHz frequency antennas were used to evaluate the different conditions. The design and construction of the full-scale track in addition to the GPR data analysis and interpretation are presented in this paper. The results show that the dielectric permittivity and frequency spectrum can be used as an indicator of fouling percentage and water content in a track. In addition, a linear correlation is observed between the fouling percentage and water content under field capacity conditions.

Keywords: GPR, Fouling, Ballast, Moisture, Full Scale Laboratory Model

---

[1] This paper is published in *Transportation Research Record*, No. 2545, 2016, pp. 66-78. DOI: http://dx.doi.org/10.3141/2545-08

3.2 Introduction

Railroads are an important means of moving passengers and freight over the world. To ensure safety and timely delivery, a railroad track must be inspected and maintained regularly. Common track damage is caused by infiltration of fines into the ballast layer due to progressive crushing and breakdown of granular particles. This can result from dynamic loading causing breakdown fouled ballast. This problem leads to a gradual deterioration of the track due to problems such as reduction in track hydraulic permeability, shear strength, stiffness and resilient modulus. Also, ballast fouling can lead to an increase in vegetation growth and an increase in rate and magnitude of plastic settlement. (Anbazhagan *et al.*, 2011, Fortunato *et al.*, 2010, Han & Selig, 1997, Indraratna & Salim, 2005, Selig & Waters, 1994).

The detection of fouled ballast before being visible from the surface would improve track inspection and reduce the track maintenance costs. Therefore, using GPR as a Non-Destructive Test (NDT) method has been increasing to monitor track conditions. By studying the GPR reflections from different layers of substructure with different electrical properties, track bed anomalies and inhomogeneities are detectable (Gallagher *et al.*, 1999, Jack & Jackson, 1999, Sussmann *et al.*, 2003). The field measurements on various tracks indicate that GPR is also effective in identifying subsurface water content, density, trapped water and fouling condition within a ballast layer (Clark *et al.*, 2001, Narayanan *et al.*, 2001, Hyslip *et al.*, 2003, Roberts *et al.*, 2006).

New developments in frequency analysis of GPR signals have overcome the limitations of time domain analysis for prediction of substructure condition (Al-Qadi *et al.*, 2010, Silvast *et al.*, 2010). Despite these abilities of GPR to detect ballast conditions, there are

uncertainties within the actual rail track and it is difficult to calibrate GPR data with actual ground condition (Anbazhagan *et al.*, 2012).

Recently, studies have been conducted to validate the substructure properties from GPR signal analysis with ground-truth trenches in field or large scale models (Al-Qadi *et al.*, 2010, Su *et al.*, 2010, Anbazhagan *et al.*, 2011, Kashani *et al.*, 2015). Most of these studies have the following limitations: (a) model studies mostly focus on clayey sand and coal dust as the fouling material; (b) all model studies have rectangular ballast cross-sections; (c) less attention has been paid to the evaluation of geotechnical index properties such as density by GPR signal analysis; (d) there is not much assessment to correlate moisture content and fouling percentage, or to study them separately with careful control on boundary conditions; (e) in field studies it is difficult to establish meaningful correlations by GPR due to many unknowns in the track condition. (Hyslip *et al.*, 2003, Sussmann *et al.*, 2003, Fortunato *et al.*, 2010).

In this study, a full scale model track with a trapezoidal ballast cross-section is designed and built with three different breakdown fouling percentages, each with four different moisture conditions. Careful control of mass and volume was important to verify the effect of density on GPR signal reflections. Both frequency and time domain analysis have been conducted on GPR signals at different locations. The design and construction of the model track with geophysical and geotechnical results are presented and discussed in this paper.

3.3 Design and Construction of the Model Track

3.3.1 Model Description

A full scale railroad model track has been built at the University of Massachusetts Amherst. The model consists of sub-structure and super-structure components of railroad track such as sub-ballast, ballast, timber ties and rails. The box is not designed for carrying load, so all connections are built to have the fewest possible metal components to limit noise in the radar signal. The box contains the sub-ballast with dimensions of 17.5 ft. (5.3m) × 17.5 ft. (5.3 m) × 1.5 ft. (0.5 m). It is made of a layer of 3⁄4 in. (19 mm) plywood supported by 2 in. (51 mm) × 4 in. (102 mm) pine lumber and diagonal bracing with the same lumber at 18 in. (0.5 m) intervals. The box was sealed with two layers of 6 mil plastic sheet for water proofing. In addition, four pairs of wooden triangle templates fixed on the box corners were designed to control the consistency of section geometry in all models.

3.3.2 Ballasted Track

After waterproofing, the box was filled with uniformly layered, clean and well graded sand up to 1.5 ft. (0.5m) above the bottom as a sub-ballast layer. A ballast layer with trapezoidal cross-section and 2 ft. (0.6 m) thickness was built on the sub-ballast layer. A 6 mil plastic sheet between the ballast and sub-ballast was used to retain the moisture in the sub-ballast layer and highlight the interface. Figure 3.1 shows a schematic plan and cross-section of the model track. The ballast layer was compacted in five lifts: three 4 in. (102 mm) lifts on the sub-ballast layer; one 5 in. (127 mm) lift; and one 7 in. (178 mm) lift on the top. The ties were embedded in the last 7 in. lift.

In this study, Connecticut granite crushed stone was used as ballast and its stone dust was used as breakdown fouling material. The stone dust was non-plastic fouling material based on ASTM D2488-06 standard (American Society for Testing and Materials.).The ballast gradation meets the American Railway Engineering and Maintenance-of-Way Association (AREMA) #4 ballast (*AREMA. Manual of Railway Engineering*, 2006). In order to have a uniform distribution of fouling in the ballast for fouled models, the ballast sub-layers were divided into two or three sub-sub-layers and stone dust was added followed by compaction after founding each sub-sub-layer. After the completion of the fourth layer the timber ties were installed with 19.5 in. (0.5 m) center to center intervals (Selig & Waters, 1994). Figure 3.2 shows some images of the model construction process.

Three models with nominal fouling percentages (by dry weight) of 0%, 15% and 30% were constructed for this study. Grain Size Distribution (GSD) tests were performed on the random samples from the models in accordance with ASTM D6913-04 standard (ASTM, 2007) to verify the gradation of the ballast with AREMA #4 ballast (*AREMA. Manual of Railway Engineering*, 2006) and the actual fouling percentage in each model.

The geometry and clean ballast weight were unchanged in all models, so that any changes in dry density and void ratio could be related to the fouling percentage changes. The in-situ dry density measurements were performed at different locations and depths in accordance with the non-level ballast density method suggested by Yoo et al. in 1978 (Yoo *et al.*, 1978) and after the completion of GPR surveys in each model. Table 3.1 presents the results from GSD and dry density tests on different models.

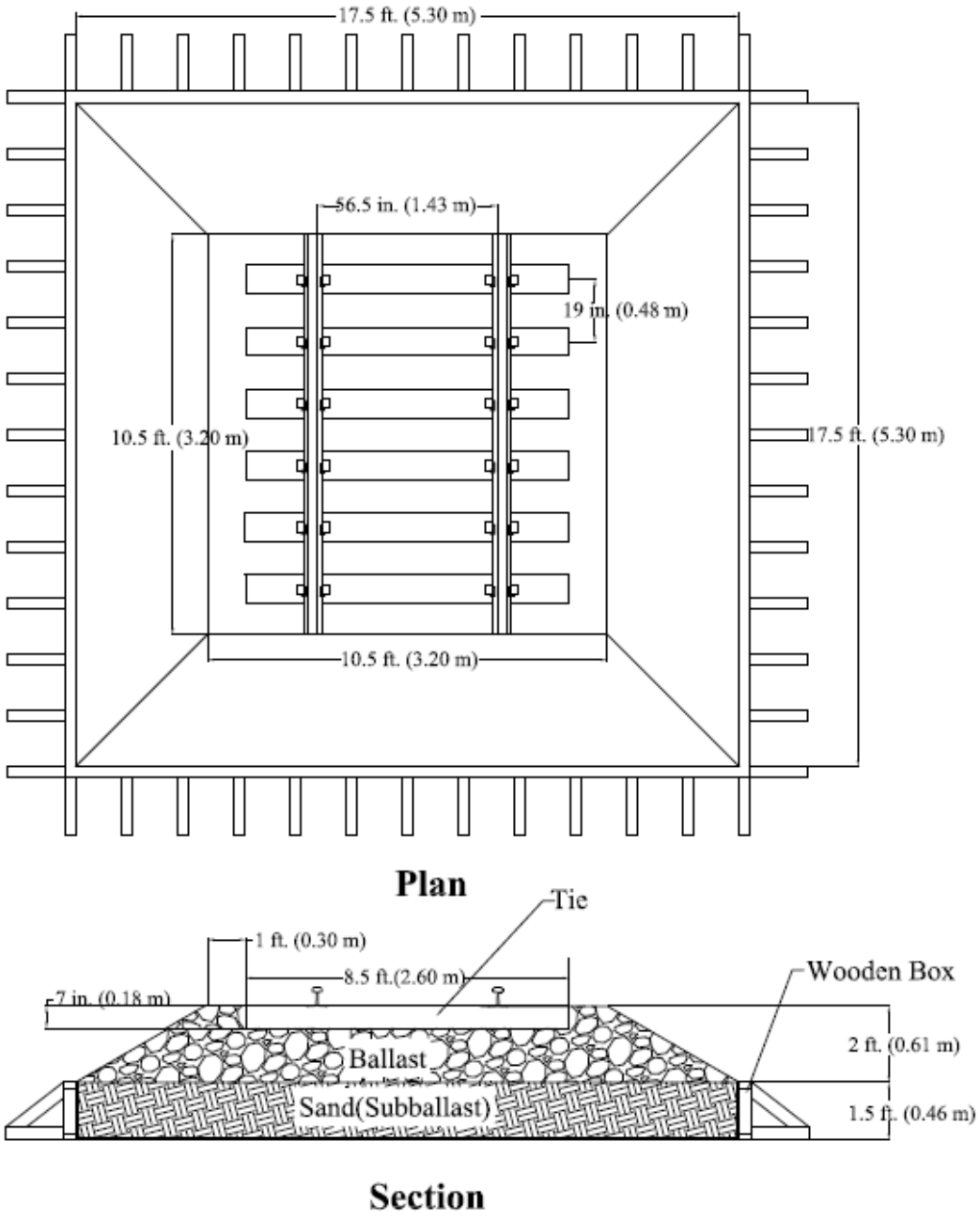

Figure 3.1: Typical Plan and Cross-Section of a Full-Scale Model

Figure 3.2: Full-Scale Model Construction Process.

3.3.3 Water content of the Models

Each model at different water contents was investigated using GPR to evaluate the effect of water content at a constant fouling percentage on GPR reflected signals. Each model had water contents of natural humidity (dry), field capacity and two points between these end points. Field capacity is defined as the moisture content held in ballast after excess water has drained away. In order to measure the approximate field capacity, three reconstituted models were made with the same grain size distribution of the ballast for each model. The reconstituted models were inundated in water and allowed to drain with the water content sampling followed immediately. These water contents were used for predicting the field capacity water content of different models. The water content measurements

in this study were all performed based on ASTM D2216-05 standard (American Society for Testing and Materials.).

Table 3.1: The Grain Size Distribution (GSD) Test Results, Density Test Results, Targeted and Average Measured Water Contents of the Models

Parameters		Model 1	Model 2	Model 3
Fouling (%)		1.3	14.9	27.1
Testing Sample Weight (kg)		129	171	192
Gs		2.75	2.75	2.75
E		0.74	0.42	0.31
e values Standard Deviation (%)		0.10	0.04	0.05
e values Standard Error (%)		0.04	0.02	0.02
D_{10}(mm)		16.7	1.2	0.2
D_{30}(mm)		21.2	19.5	13.0
D_{50}(mm)		24.0	22.7	21.0
D_{60}(mm)		25.2	24.2	23.0
Cu		1.5	20.2	100.0
Cc		1.1	13.1	31.9
Dry density (kg/m^3)		1555	1921	2117
Dry Density Standard Deviation (kg/m^3)		58.8	35.1	64.5
Dry Density Standard Error (kg/m^3)		26.0	13.0	26.0
Targeted Water Content from reconstituted sample (%)	Dry	0.0	0.0	0.0
	w_1	0.3	1.1	1.6
	w_2	0.5	2.1	3.2
	Field Capacity	0.8	3.2	4.8
Measured Water Content from Model Track (%)	Dry	0.1	0.3	0.6
	w_1	0.5	1.6	3.5
	w_2	0.5	2.1	4.0
	Field Capacity	0.6	3.4	4.6

NOTE: 1lb = 0.454 kg, 1 in. = 25.4 mm, 1 kg/m^3 = 0.062 pcf

Migration of fouling particles during drainage of the reconstituted models was an issue in collecting water content samples with uniform fouling percentages. In order to overcome this issue, the water content samples were sieved with 3/8 in. sieve after oven drying to determine the fouling percentage (by dry weight) for each sample. Figure 3.4 shows water content values versus fouling percentages for 15% and 30% Fouling models. This plot was used to find the approximate field capacity corresponding to the amount of fouling percentage in each model.

After determining the approximate field capacity, water contents of one third and two thirds between dry and field capacity conditions were selected as moderate moistures (w_1, w_2). The models were wetted to the moderate water contents and field capacity, respectively followed by GPR sampling of dry condition.

The amount of water added to the samples was controlled by monitoring the flow rate. After each wetting step, the model was covered and sealed with plastic sheets for 16 hours to achieve moisture equilibrium. The actual water content at different depths and locations of each model was measured after the completion of GPR sampling. The targeted water contents and measured water contents for all models are presented in Table 3.1.

3.4 Ground Penetrating Radar (GPR) Data

GPR data were collected using a ground coupled system with 450 MHz and 2 GHz frequency antennas. The GPR sampling was performed at defined lines illustrated in Figure 3.1. The device was placed far enough from the adjacent rail to reduce interference. The data were collected at 9 to 15 points in cribs and on shoulders for each model and at each water content. To evaluate the data and study their correlations with geotechnical index

properties, only fundamental filters such as band passing were applied to the raw data. The propagation velocity in ballast layer was calculated by the travel time to known depth of the ballast for each model

In this study, each trace at each location was evaluated. The sampling rate for 450 MHz and 2 GHz antennas was 125 and 26 picoseconds per sample, respectively. Each 450 MHz GPR scan had 1024 samples and each 2 GHz scan had 512 samples.

3.5 Model Verification

In order to verify the validity of the results obtained from the current study, we compared some of our measurements with measurements in literature. These measurements include dielectric permittivity, in-situ density and grain size distribution. Figure 3.3 compares the gradation of a clean mixed ballast used in this study with the minimum and maximum gradation range of AREMA # 4 ballast (*AREMA. Manual of Railway Engineering*, 2006). Table 3.2 presents the measured dry density values of Model 1 of this study at different locations and depths compared with field measured dry densities of clean granite ballasted track by Selig in 1989. In addition, Table 3.3 shows the average dielectric permittivity in different conditions of this study and the estimated dielectric permittivities by Sussman in 1999 (Sussmann Jr, 1999). This verification shows a good agreement between the results from this study and other studies and validates the full-scale model for simulating a real track with the same index properties.

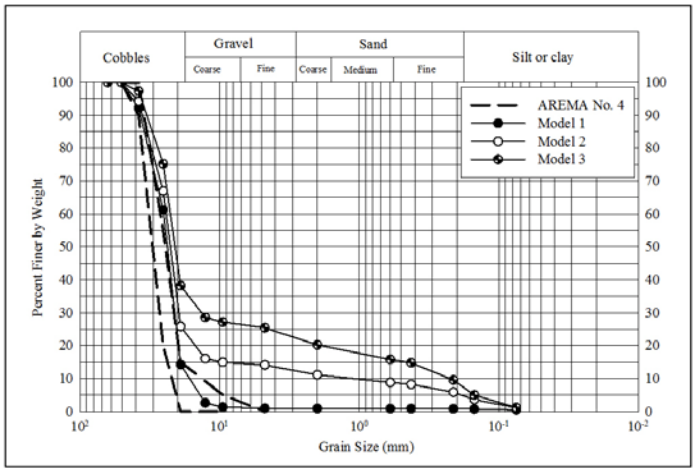

Figure 3.3: The Grain Size Distribution (GSD) Plot of Full-Scale Models. AREMA No. 4 Ballast (*AREMA. Manual of Railway Engineering*, 2006).

Table 3.2: Full Scale Models Dry Density Verification

Clean Ballast Density (Model 1) (pcf)	Field Measurements on Granite Ballast (Selig, 1989) (pcf)
97.9	107.4
99.3	104.8
90.6	94.1
98.6	99.2
99.0	101.3
108.9	101.0
Mean = 99	Mean = 101.3

Table 3.3: Full Scale Models Dielectric Permittivity Verification

Material	Average Dielectric Permittivity Model (1, 2 & 3)	Estimated Dielectric Permittivity (Sussmann Jr, 1999)
Clean Dry	3.1	3.6
Clean Moist	3.8	4
Fouled Moist	5.5	5.2

3.6 Results and Discussion

3.6.1 Correlation between Ballast Breakdown Fouling and Excess Water

Excess water in track substructure can increase the track maintenance and costs because of an increase in ballast deformation, decrease in strength, frost heaving or thaw softening, etc. (Selig & Waters, 1994). One of the main reasons for excess water in track substructure is ballast fouling that fills the voids and decreases the ballast's hydraulic conductivity. To evaluate the relationship between the fouling percentage of ballast and field capacity, all field capacity samples were sieved by 3/8 in. sieve after oven drying. These samples include samples collected from full scale and reconstituted fouled models (model 2 and 3). Figure 3.4 shows the changes of the field capacity versus fouling percentage. The scatter covers a wide range of fouling percentages from clean ballast with less than 5% fouling to highly fouled ballast with more than 45% fouling. Based on measurements in North America, most highly fouled ballast locations at different sites had fouling percentages between 30 to 58% (Han & Selig, 1997). Therefore, Figure 3.4 can be used to predict the approximate field capacity corresponding to breakdown fouling percentage in ballast.

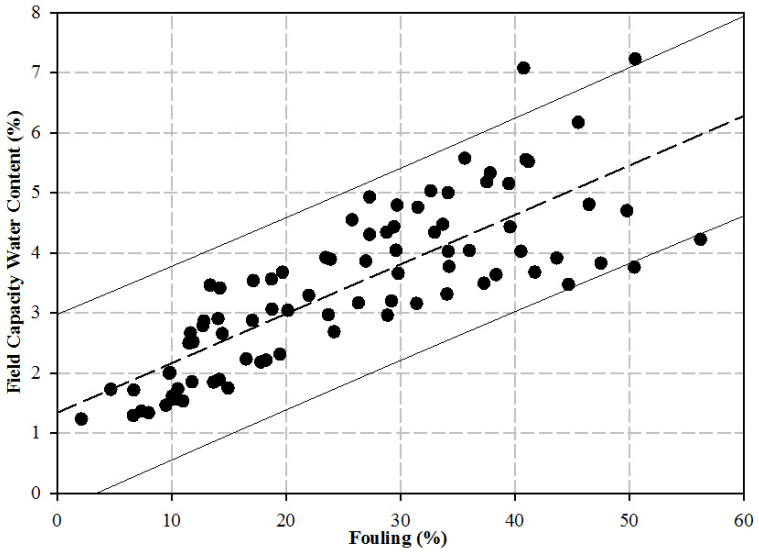

Figure 3.4: The Field Capacity Water Content (w%) vs. Fouling (%) (by Dry Weight), from Samples in Different Locations of the Full Scale and Reconstituted Models. The Band Highlights the Trend.

3.6.2 The Effect of Density and Water Content on GPR Wave Propagation in Ballast

Electromagnetic wave properties such as dielectric permittivity (ε) and propagation velocity (v) in a mixture depends on the percentage of the mixture components and their electromagnetic properties (Halabe *et al.*, 1993). Because clean ballast has more air filled voids than fouled ballast, its dielectric constant is lower and its velocity of wave propagation is higher than fouled ballast (Clark *et al.*, 2001).

As a review, Eq. (3.1) is the calculation of time taken for a wave to travel a round trip from one interface to the second interface (Daniels, 1996).

$$t = \frac{2d}{v} \qquad \text{Eq. (3.1)}$$

where t is the round-trip travel time, d is the distance between the two interfaces and v is the velocity of the electromagnetic wave in a dielectric medium. Propagation velocity can

be computed using the following equation which has been rewritten based on Maxwell's equations:

$$v = \frac{c}{\sqrt{\varepsilon_r}} \quad \text{Eq. (3.2)}$$

where c is the speed of light (3×10^8 m/s), and ε_r is the relative dielectric permittivity of the medium.

The velocity and relative dielectric permittivity can be calculated from the known ballast thickness and the travel time measured from the GPR traces. Obviously, fouling in fouled ballast models holds the moisture easily and becomes more difficult to distinguish moisture from fouling in GPR signal studies. Therefore, the dielectric permittivity and propagation velocity of each trace at each location were evaluated in different models to study the effects of water content and fouling separately.

Figure 3.5 depicts the average Hilbert envelope from different locations of Model 2 with different water contents. The delay between two peaks is the two-way travel time of signal in ballast layer. Figure 3.5 shows that traveling times increase with increasing water content in a constant density. Figure 3.6 shows the changes of dielectric permittivity and wave propagation velocity for all collected data in all models versus water content. Comparing dry samples (water content < 1%) in different models shows that fouling itself is not changing the permittivity and propagation velocity significantly. But water held by fouling has a significant effect on electromagnetic properties. In dry conditions, a 26% increase in fouling changes the average of velocity and dielectric permittivity about 12% and 24%, respectively. In studied models with constant fouling, 3 to 4% increase in water content changes the average of velocity about 22 to 26% and dielectric permittivity about 75 to 90%.

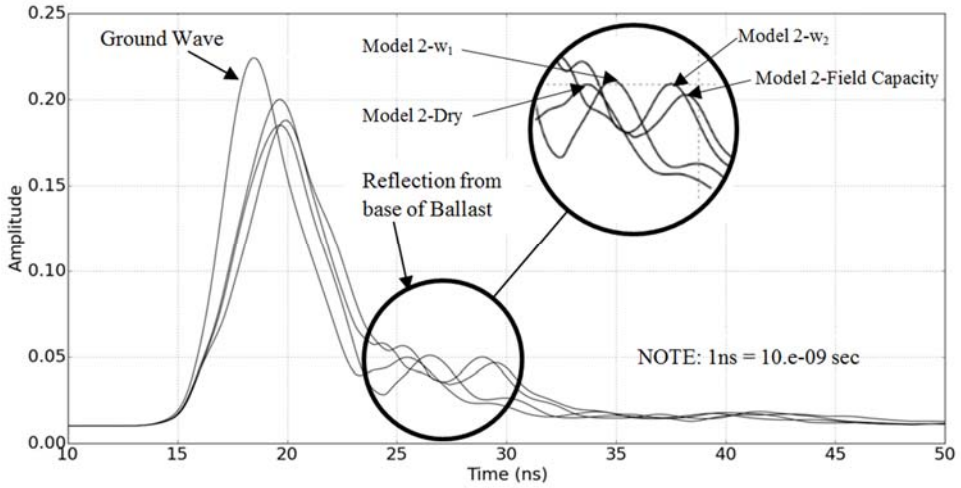

Figure 3.5: The Effect of Moisture on the Hilbert Envelope (450 MHz antenna, Model 2)

3.6.3 The Effect of Density and Water Content on Frequency Spectrum Analysis

In studies conducted by Clark et al. in 2004, Silvast et al. in 2006 and Al-Qadi et al. in 2010, frequency analysis was used to evaluate the fouling condition and ballast thickness (Al-Qadi *et al.*, 2010, Clark *et al.*, 2004, Silvast *et al.*, 2006). The presence of fouling particles increases the attenuation of the high frequency electromagnetic waves. Therefore, evaluating the frequency spectrum to study the attenuated energy may provide valuable information.

Studying the frequency spectrum of traces using 2 GHz antenna at one location clearly showed that the area under the frequency spectrum decreases with an increase in water content, keeping the fouling percentage constant. The changes of normalized area for all collected data by 2 GHz antenna is shown in Figure 3.7(a). The trend demonstrates that the average of normalized areas decreases clearly by an increase in water content, although there is scatter for different locations in each model. A 4.5% increase in the average water content decreases the average of normalized area by 27%.

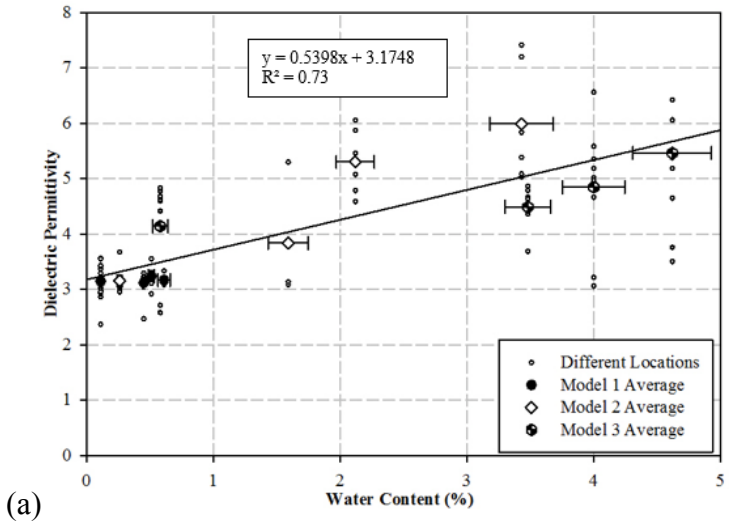

(a)

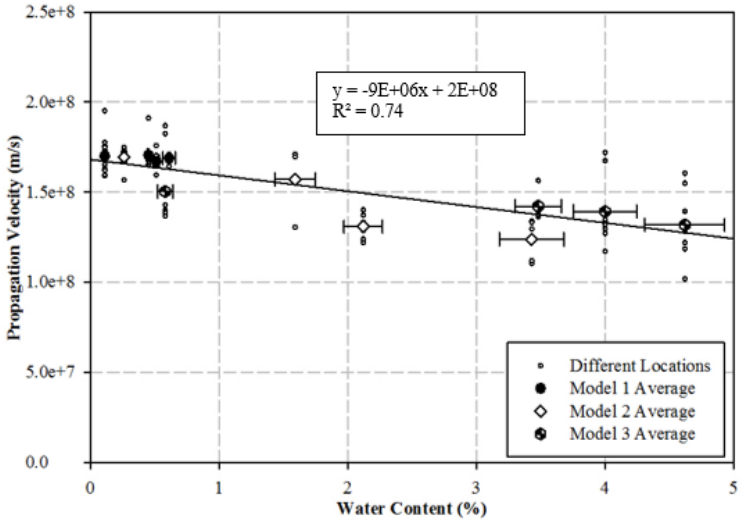

(b)

Figure 3.6: (a)The dieletric permittivity vs. water content (w%) in all models (2 GHz antenna). (b) The signal propagation velocity vs. water content (w%) in all models (2 GHz antenna). Error bars represent the standard error regarding to water content results. The small circles represent the dependent variable in different locations for average water content and the bold larger markers are the average of smaller markers.

Comparing the attenuated signal energy of dry samples (water content < 1%) at different densities in Figure 3.7(b) also illustrates that the effect of density on the spectrum's area is significantly more than time domain analysis. Therefore, studying frequency

spectrum can be a better technique for distinguishing fouled and clean ballast in dry conditions. Figure 3.7(b) also shows that a decrease in energy attenuation from clean ballast to medium fouled ballast is much more significant than medium fouled ballast to highly fouled ballast. In dry conditions, the normalized area under frequency spectrum reduces with an 22% per 23% increase in density from Model 1 to 2, while this change is not detectable in the time domain parameters for the same density change.

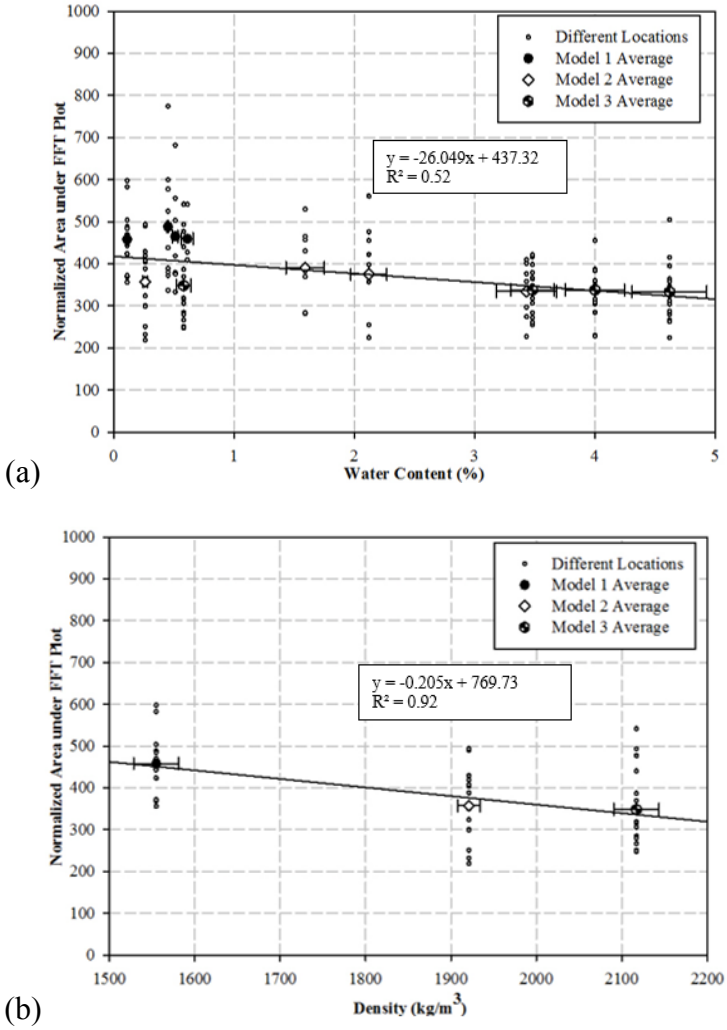

Figure 3.7: (a)The normalized area under Fast Fourier Transform (FFT) plot vs. water content (w%) in all models (2 GHz antenna). (b)The normalized area under FFT plot vs. dry density (2 GHz antenna). Error bars represent the standard error regarding to inde-

pendent variables. The small circles represent the normalized area under frequency spectrum in different locations for average independent variables and the bold larger markers are the average of smaller markers.

It has been observed that GPR traces from ballast with different fouling percentages have different magnitude of frequency spectra (Shao *et al.*, 2011). In order to evaluate these changes in reflected GPR waves by changes in water content and density Figure 3.8 has been presented.

Figure 3.8 demonstrates that the average peaks of Fast Fourier Transform (FFT) magnitude in the models for 2 GHz frequency antenna are decreasing slightly by an increase in water content and density. Although there are some fluctuations in the dry conditions (water content < 1%) and clean ballast, the regression shows a promising trend.

According to Figure 3.8(a), as the average water content increases about 4.5%, the average peak of FFT magnitude decreases about 45%. While Figure 3.8(b) shows a decrease of 49% in the average peak of FFT magnitude as the result of 36% increase in dry density. Therefore, the effect of water in ballast, held by fouling, on the peak of FFT magnitude is more significant than only fouling particles in dry condition.

3.6.4 The Effect of Density and Water Content on Time Domain Analysis

Ballast under different fouling conditions generates different electromagnetic (EM) scattering patterns (Al-Qadi *et al.*, 2008). Evaluating the volume scattering of radar waves specifically in high frequency signals such as 2 GHz is a method to predict the air voids volume (Zhang *et al.*, 2004) and other replaced materials in voids such as water or fine particles in fouled ballast. In order to study the effect of water content and density on the volume scattering of radar waves, each EM signal at each location in different models was

assessed. Due to the random volume scattering that is experienced by 2 GHz radar waves, there is no expectation of coherent arrivals from location to location. Therefore, the volume scattering of scattered signals from all locations of each model in dry condition was compared. Also as explained in the previous sections, the changes in density is mostly related to the fouling in the studied models.

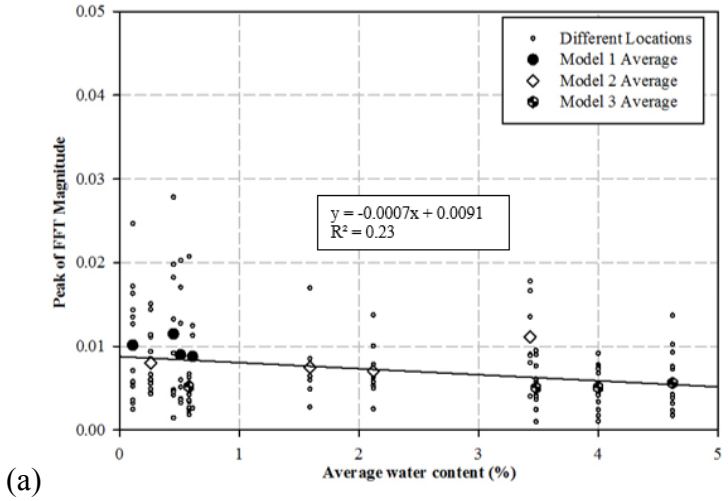

(a)

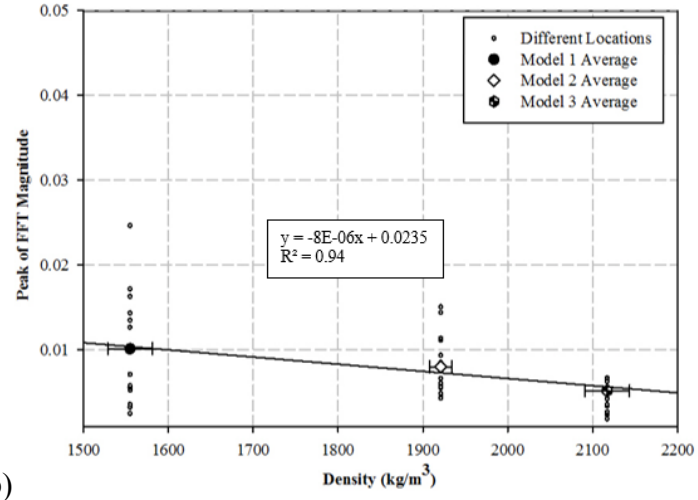

(b)

Figure 3.8: (a) The peak magnitude of FFT vs. average water content (%) (2 GHz antenna). The error bars are not included because the plot is vs. average water content. (b) The peak magnitude of FFT vs. dry density (2 GHz antenna). Error bars represent the standard error regarding to dry density results. The small circles represent the peak magnitude of the frequency spectrum in different locations for average independent variables and the bold larger markers are the average of smaller markers.

This is as the result of unchanged geometry and same amount of clean ballast in the models. Based on this assumption, any changes in volume scattering amplitude is related to the density changes and this behavior is due to the reduced void size and void contrast in higher density models with higher fouling percentages.

To quantify the changes of volume scattering versus dry density, two approaches have been used. These approaches include the area under the squared amplitude and the amplitude Standard Deviation (SD) for each trace. The reduction of volume scattering in the models can be numerically validated by Figure 3.9. This study shows that by 36% increase in dry density as the result of 26% increase in breakdown fouling, the average of the squared amplitude area and the Standard Deviation (SD) amplitude of the traces are decreasing around 52% and 54%, respectively.

As explained in the previous sections, highly fouled ballast results in undrained excess water in the track. Therefore, studying the effect of water content on traces without considering the fouling amount is not applicable. Figure 3.10 shows the effect of water content held by fouling on the area under the squared amplitude and the amplitude Standard Deviation (SD) of GPR traces. It is clear from these figures that the area under the squared amplitude and the SD of traces decrease with water content increase as the results of fouling increase. Quantitatively, the average area under the squared amplitude and the amplitude Standard Deviation (SD) of traces decrease about 74% and 53%, respectively with 4.5% increase in moisture held by more breakdown fouling material.

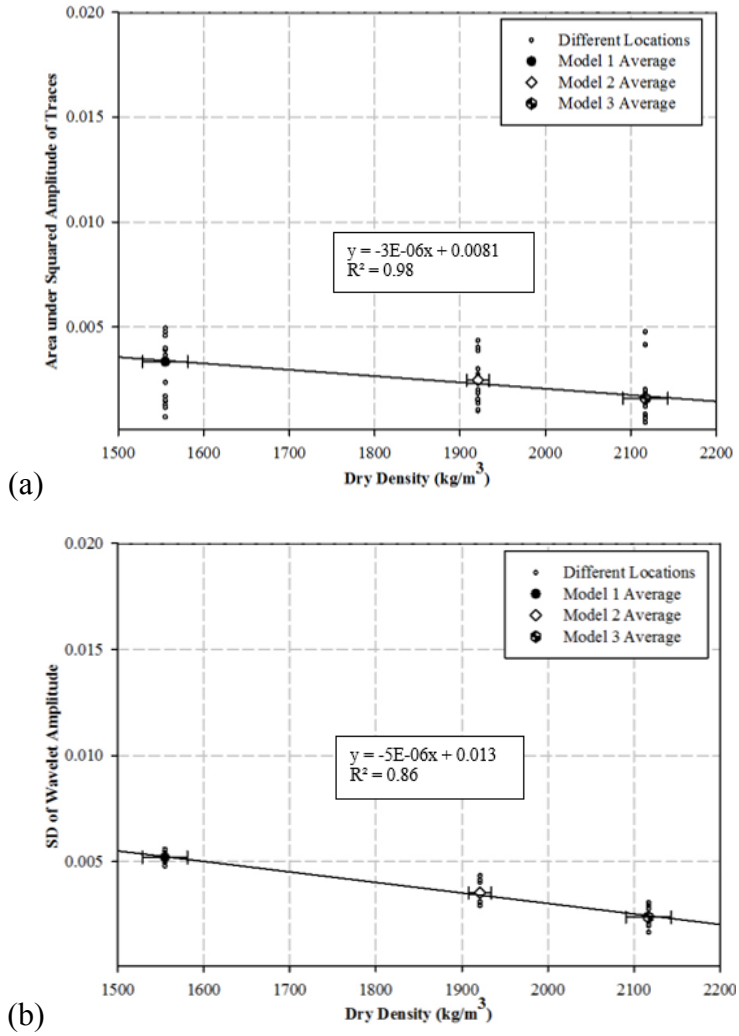

Figure 3.9: (a) Area under squared amplitude of traces vs. dry density (2 GHz antenna). (b) The standard deviations (SD) of traces amplitude vs. dry density (2GHz antenna). Error bars represent the standard error regarding to dry density results. The small circles represent the dependent variables in different locations for average dry density and the bold larger markers are the average of smaller markers.

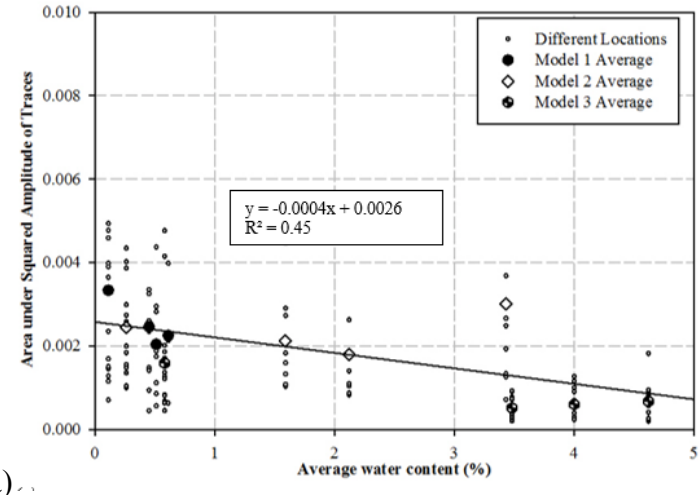

(a)

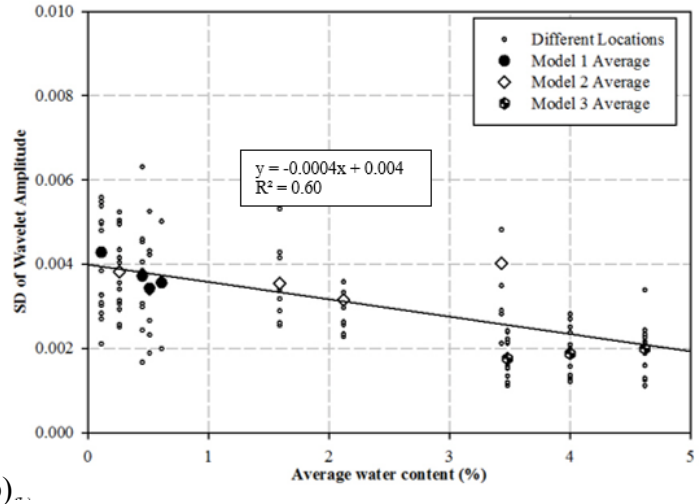

(b)

Figure 3.10: (a) The area under squared amplitude of traces vs. average water content (w%) in all models. (b) The standard deviation (SD) of traces amplitude vs. average water content (w%) in all models. The error bars are not included because the plot is vs. average water content. The small circles represent the dependent variables in different locations for average water contents and the bold larger markers are the average of smaller markers.

3.7 Conclusion

GPR and geotechnical index tests were acquired on full scale ballasted track models with different breakdown fouling percentages and water contents. Based on the data analysis, the effects of water content and density changes in the frequency and time analysis of

GPR reflected waves were discussed and evaluated qualitatively and quantitatively. Also a correlation has been suggested in this study for estimating the field capacity moisture based on breakdown fouling percentages.

Ground coupled antenna with 450 MHz and 2 GHz frequencies were used in this study. The data were collected at different locations in cribs and shoulders of the test area. Data analysis was conducted on individual traces from each location. The 450 MHz antenna was used mostly for verifying the results, layer thicknesses and measuring the dielectric permittivity. The 2 GHz antenna was used mostly for evaluating the effect of moisture and density on scattering patterns and frequency analysis in the ballast layer. Based on this study the following conclusions can be drawn:

- The techniques for building a ballast model with all substructure and superstructure features and with trapezoidal cross-section of ballast layer have been created and tested.
- The design technique in correlating the changes in density only due to the fouling percentages for the models has also been created, tested and refined.
- An increase in breakdown fouling will increase the field capacity water content. This behavior is a linear behavior. Based on experiments in this study a plot has been presented for estimating field capacity water content based on fouling percentages.
- Under dry condition, density (in the range of 1500 to 2100 kg/m^3) does not significantly affect the dielectric constant and wave propagation velocity.

- Excess water trapped in ballast because of voids filled by breakdown fouling significantly affects the wave propagation velocity and dielectric constant.
- Comparing the attenuated signal energy of dry samples shows that the effect of density on the frequency spectrum analysis is significantly more evident than on time domain analysis.
- The normalized area under the frequency spectrum decreases with an increase in water content and density and this results from increased energy attenuation by moisture and fouling in the voids.
- Moisture and density will also affect the magnitude of the frequency spectrum amplitude. This study shows that a few percentage points increase in water content has more effect on peak magnitude than about 36% change in density in dry condition.
- Different methods have been evaluated to quantify the changes in wave scattering amplitude from changes in water content and density. These methods used the Standard Deviation of wave amplitude and area trapped by scattered wavelets. Both methods are showing a promising trend by changes in density and moisture.

CHAPTER 4

LABORATORY EVALUATION OF RAILROAD BALLAST BEHAVIOR UNDER HEAVY AXLE LOAD AND HIGH TRAFFIC CONDITIONS[2]

4.1 Abstract

Repeated loading of railroad traffic over a period of time results in both elastic deformation and plastic settlement of the track foundation materials. The degree of ballast fouling and moisture condition, affect the rate and magnitude of this degradation. In addition, defects from wheels or track super structure components such as rails can also expedite this degradation with increasing the repeated load impaction. Accumulation of traffic and increase in deformation of the track, leads the track to a point where maintenance is required. Therefore, studying the effects of these parameters and simulating the fouled ballast in different moisture condition stages under different loads can help the railroad industry to better understand the risk factors and maintenance needs of the track at different conditions.

In this study, a railroad ballast box test with new dimensions has been used to simulate the gradual degradation of fouled ballast at different moisture conditions under heavy axle loading and high traffic conditions. The tests were conducted on clean, moderately fouled and highly fouled ballast up to 2,500,000 cycles of repeated loading from dry to saturated conditions. The risk factor of traffic increase in saturated conditions simulating heavy rainfall conditions has also been evaluated. The final results have been compared with the

[2] This paper is submitted for publication at Transportation Geotechnics Journal, ELSEVIER.

computer model suggested by Selig and Alva-Hurtado in 1982 and different measured settlements in the field. The box test results present comparable results with field measurements and computer modeling. The paper also concludes discussions about the effects of various factors on the rate and magnitude of the plastic and elastic settlement qualitatively and quantitatively.

Keywords: Fouled Ballast, Moisture, Settlement, Heavy Axle Load, High Traffic Conditions

4.2 Introduction

Under good track conditions, where there is a filter layer between the ballast and subgrade and also a strong subgrade or subballast/subgrade combination, ballast is the main source of settlement (Selig & Waters, 1994). Ballast becomes fouled by the contamination due to abrasion of ballast under repeated loading or infiltration of other materials. The most common source of ballast fouling is abrasion fouling, also known as breakdown fouling, contributes to 76% of the ballast fouling (Selig & Waters, 1994, Selig & Russo, 1991). Fouling also holds the water entering from the surface by filling the voids over time. Fouling and moisture degrades the ballast over time with repeated traffic loading and causes geometric deformation. The geometric deformation produces vibration, decreases the ride quality and may also cause safety problems: Regarding to the Rail Equipment Accident (REA) databases recorded by Federal Railroad Administration (FRA) from 2001 to 2010 and analysis performed at the University of Illinois Urbana-Champaign, track geometry problems cause 7.3%, 7.2% and 3.6% of the freight train derailments in main, siding and

yard types of track, respectively. This represents the second highest cause of freight train derailment in the main lines (Liu *et al.*, 2012).

To keep the geometry in good condition, track maintenance such as undercutting, surfacing or renewal of fouled ballast is performed. Maintenance work is often performed by railroad inspectors who usually don't have defined criteria for critical fouling and moisture conditions.

By conducting experimental tests, Freeme and Servas (1985) qualitatively reported that high amount of fine particles and moisture in granular materials under repeated loading can drastically change the rate and magnitude of settlement (Freeme & Servas, 1985). Many numerical and experimental studies have been performed to evaluate the resilient and permanent deformation behavior of ballast under repeated loading and effective parameters (Brown, 1974, Gräbe & Clayton, 2009, Han & Selig, 1997, Huang & Tutumluer, 2011, Indraratna, 2007, Shenton, 1975, Mishra *et al.*, 2013, Norman & Selig, 1983, Qian *et al.*, 2015, Selig, 1982, Stewart, 1982, Selig, 1981, Yoo, 1979). But there are still challenges in quantifying the geotechnical ballast properties that might change the settlement rate and magnitude significantly and cause safety issues. Quantifying these parameters will help the railroad industry to recognize the critical points of moisture and fouling for better prioritizing sections need maintenance. This will decrease accidents caused by track settlements.

In summary, most of the past research has evaluated the ballast in small scale tests with loads equivalent to passenger train loads, other types of fouling and low numbers of cycles (up to 1×10^6). In this research the box tests with modified dimensions have been conducted on clean and breakdown fouled ballast. While the traffic was increasing, water

was added to simulate the gradual degradation of non-tamped ballast in heavy axle load (HAL) conditions up to 2,500,000 cycles of load. The design and construction of the box test set up, methodology and the results evaluating effects of different geotechnical properties on ballast settlement will be discussed and presented.

4.3 Design and Construction of the Ballast Box Test

To simulate the behavior of ballast under dynamic loading, ballast box test has been used since its development at the University of Massachusetts in 1983 (Norman & Selig, 1983). The box tests were conducted on ballast for better understanding of ballast field performance under dynamic loading. Tests have had comparable results with the measurements in the field. Recent numerical analyses have shown that there are some issues such as significant reduction of ballast strength capacity, increase in plastic deformation, rotational instability of the tie and punching shear at the depth of the sample in the old box test that affected the results. These problems are mostly because of shear stress concentrations as the result of inappropriate boundary conditions. As the result of finite element modelling, a 50% increase in the box dimensions was suggested to eliminate the shear stress concentrations (Bennett *et al.*, 2011). In this study a box apparatus with new dimensions and draining system was constructed at the University of Massachusetts, Amherst to overcome the problems mentioned above. Figure 4.1 shows a cross-section of the box set up.

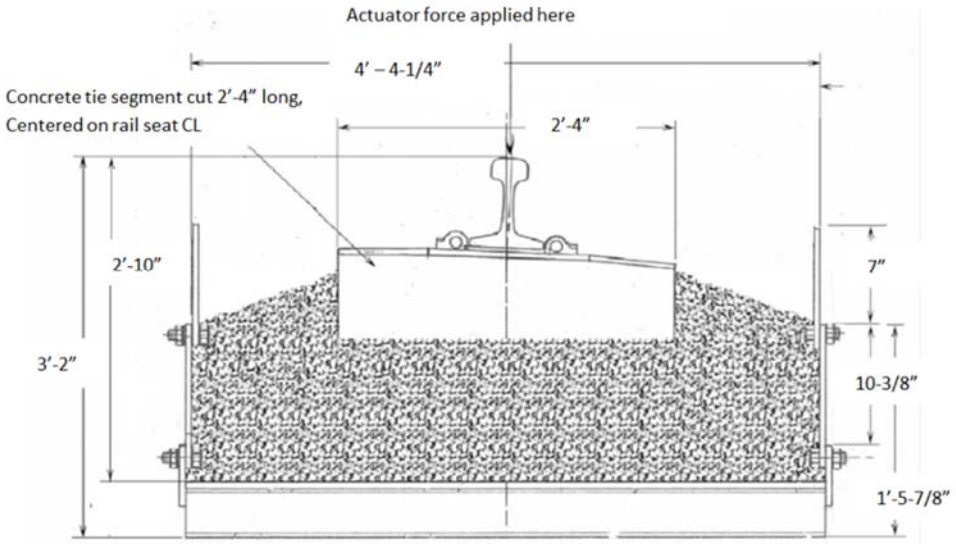

Figure 4.1. Schematic Section of the Modified Box Apparatus

The modified box test apparatus was made with the dimensions of 52 in. (132 cm) long, 33 in. (84 cm) wide and 20.5 in. (52 cm) deep to modify the old box apparatus dimensions of 24 in. (61 cm) long, 12 in. (30.d cm) wide and 19 in. (48 cm) deep.

The walls of the box consisted of fix and removable sections for facilitating the testing process. The walls were bolted to a 52 in. (132 cm) × 33 in. (84 cm) × ½" in. (12.7 mm) steel plate welded on three longitudinal steel I beams. A drain line at one end of the bottom of the box was attached to a water pump for water inflow and discharge. The box was placed in a self-reacting load frame and loaded by using an MTS servo controlled hydraulic system with a 500 kN (110 kip) capacity actuator. To transfer the load from the actuator to the substructure, a 27.5 in. concrete tie including fastening components and rail was used. This tie length was selected to have a symmetrical distance to the walls. A linear variable differential transducer (LVDT) was held by a frame attached to the box in order to record the differential settlement between the box and the tie and also eliminate any error records in the settlement measurements from the box movement. The tests were conducted

under the assumption of negligible tie tilting toward the middle of the tie. Figure 4.2 shows images of the load frame and the box test set up.

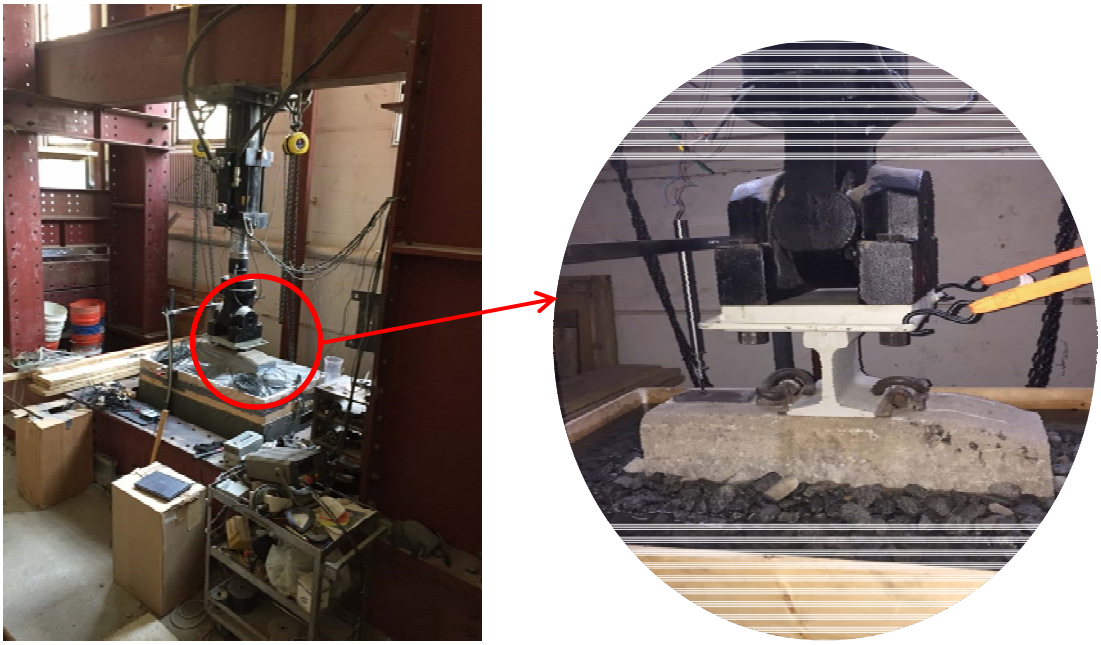

Figure 4.2. The Ballast Box Test Setup at the University of Massachusetts, Amherst

4.4 Methodology

Railroad track elastically deforms under each application of a wheel load. Also it settles because of plastic deformation in the ballast, subballast and subgrade through accumulation of many cycles of loading. The elastic deformation measures the track properties such as stiffness. The plastic settlement causes the degradation of the track which deteriorates the track geometry and leads to necessary track maintenance (Selig, 1982). Railroad line traffic relates to the number of load cycles in the measuring amount of time, the magnitude of the axle loads using the line and the number of axles per load cycle by the following equation (Li, 2016):

$$N_b = {}^{10^6}/_{4P_s} \qquad \text{Eq. (4.1)}$$

where N_b is the number of load cycles per Million Gross Tons (MGT) for ballast layer and P_s is the static wheel load in tons.

By using laboratory tests, Freeme and Servas (1985) showed that an increase in the amount of fine particles in substructure granular material under accumulation of repeated loading will increase the amount of deformation (Freeme & Servas, 1985). They also showed that existence of water in substructure material will change the settlement rate of substructure under accumulation of repeated loading (Figure 4.3). Figure 4.3 qualitatively shows that settlement rate over traffic loading is repeatable under the same moisture condition.

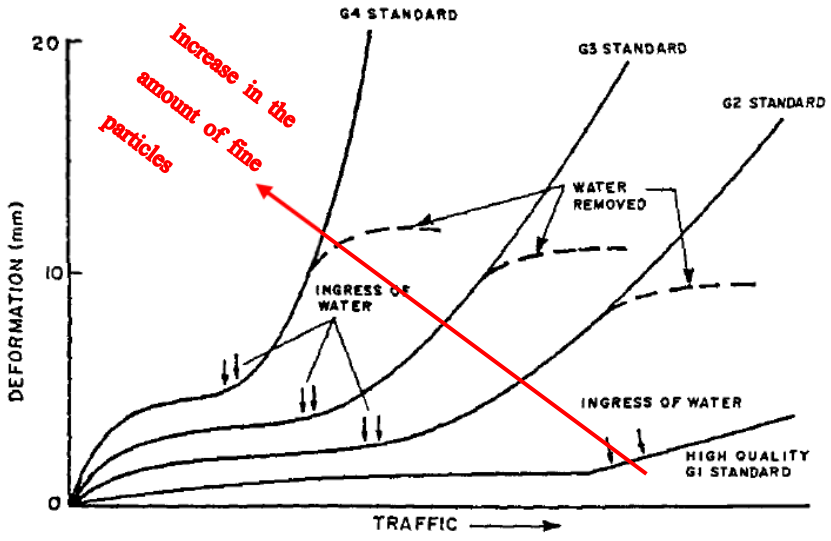

Figure 4.3. Effect of Material Quality on Granular Behavior (Freeme & Servas, 1985)

In this study a large scale laboratory model is used to evaluate the cumulative effect of water content and fouling on the elastic and plastic deformation of ballast by many cy-

cles of traffic loading qualitatively and quantitatively. To simulate the degradation of ballast by increase in traffic loading and also evaluate the effect of water and fouling in the rate of this degradation, clean and fouled ballast were subjected to cyclic loading in the modified box test. Initially, the material with defined fouling content was compacted in the box with densities close to the measured densities in the real track (Selig, 1989) (Table 4.1). To simulate gradual degradation of ballast by increase in amount of water held by breakdown fouling, water was added to the ballast while the amount of cyclic loading was increasing.

To evaluate the effect of water content on the rate and amount of elastic deformation and plastic settlement, cyclic loading was continued until the rate of deformation versus loading cycles became constant. Then, the tests were stepped up to the next water content stage by adding water to the ballast. The water content stages have been discussed in section 3.2.

Defects on the rail or the train wheels can cause sudden impacts on the track that increase the amount of load. Few heavy wheel loads as the result of rail or wheel defects, such as impact from wheel flats, can cause as much track deformation as many trains with smaller loads (Stewart, 1982). Therefore, the effect of load change has been also evaluated in this research. The effect of loading on the rate and amount of elastic deformation and plastic settlement was evaluated only under a saturated condition. The loading stages have been discussed in section 3.3.

4.4.1 Ballast and Fouling

The ballast in this evaluation was Connecticut granite crushed stone meeting American Railway Engineering and Maintenance-of-Way Association (AREMA) #4 gradation (*AREMA. Manual of Railway Engineering*, 2006). The tests were conducted on clean ballast with <5% fouling, moderately fouled ballast with approximately 15% fouling and highly fouled ballast with approximately 30% fouling. Percent fouling is the ratio of fine particles weight passing through a 3/8" sieve to the total weight of the fouled ballast (Selig & Waters, 1994). The breakdown fouling material used in this study consisted of abraded stone dust from the same source. This type of fouling was selected because it typically contributes a large percentage of actual fouling (Selig & Waters, 1994). To ensure the uniformity of ballast density, the tests were prepared with careful control on the mass and volume.

The ballast in the box was compacted in six lifts as three 3 in. (7.6 cm) lifts and three 2.5 in. (6.3 cm) lifts from the bottom to the top. A 27.5 in. (69 cm) long concrete tie was placed on the top of the last layer and was imbedded in 4 in. (10 cm) tapered layer of ballast.

In order to have uniformly distributed fouling in the fouled ballast, each layer was divided into several sub-layers and the computed amount of fouling was added after spreading each sub-layer of clean ballast with compaction followed. In order to look at the effect of fouling in this study, all mixtures had the same amount of clean ballast. The only variable changing the ballast density was the amount of breakdown fouling filling the voids.

To verify the AREMA gradation and amount of fouling in the samples, Grain Size Distribution (GSD) tests were performed in accordance with ASTM D6913-04 (American Society for Testing and Materials.). Measured density and parameters derived from GSD

test are presented in Table 4.1. The GSD plots for the clean and fouled ballasts are presented in Figure 4.4.

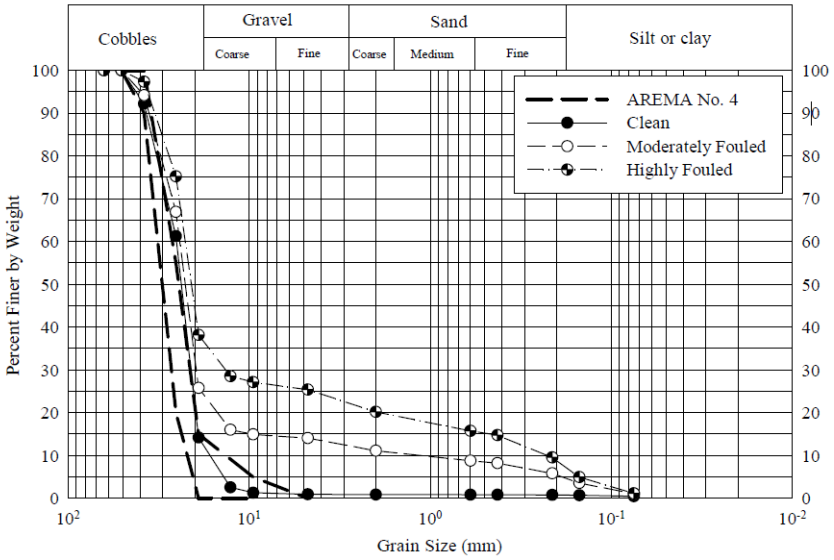

Figure 4.4. Grain Size Distribution Plot

4.4.2 Water Content

In order to evaluate the effects of water content on the ballast settlement rate and magnitude, five different water contents were determined from dry to saturated conditions. Table 4.1 shows the determined and measured water contents in the tests. To determine the amount of water needed to be added to the ballast, reconstituted samples with the same grain size distributions were built at the same room temperature in the lab. The ballast was saturated with water and drained immediately following by water content sampling (Kashani *et al.*, 2016). Dry condition was defined as zero water content and two points of w_1 and w_2 were defined as ⅓ and ⅔ of distance between dry and field capacity as intermediate water contents. The water content sampling for this study and minimum requirement

for mass of test specimen were all performed in accordance with ASTM D2216-05 standard (American Society for Testing and Materials.). The measured water content was the average of five to six samples from each reconstituted sample.

To keep track of the change in water content over cycles, a reconstituted sample was built at the same room temperature for each test during conducting the test. The water was added to the reconstituted sample at the same time that water was added to the main sample in the box. The water content samples were collected at the same time period (number of cycles) that the settlement data were collected. The water content for each testing stage is the average of collected samples at different cycles of that test stage.

For the intermediate water contents, the water was introduced to the box test from the top by measuring water flow rate. The box and reconstituted sample were covered for 16 hours to allow the water to be equilibrate prior to the start of the test. The box and reconstituted samples at intermediate moisture content and field capacity conditions were covered by a polyethylene sheet to minimize the effects of evaporation during the cyclic loading.

For the field capacity water content, the box and reconstituted sample were inundated with water from the bottom for saturation verification. After complete saturation, the samples were drained followed by cyclic loading. For the saturated conditions the box was filled with water and the test started immediately.

Table 4.1: Geotechnical Properties of Clean and Fouled Ballast

Parameters		Clean (F_0)	Moderately Fouled (F_{15})	Highly Fouled (F_{30})
Fouling (%)		1.3	14.9	27.1
D_{10}(mm)		16.7	1.2	0.2
D_{30}(mm)		21.2	19.5	13.0
D_{50}(mm)		24.0	22.7	21.0
D_{60}(mm)		25.2	24.2	23.0
C_u		1.5	20.2	100.0
C_c		1.1	13.1	31.9
Dry Density (kg/m3)		1555	1921	2117
Targeted Water Content from Reconstituted Samples (%)	**Dry**	0.0	0.0	0.0
	w_1	0.3	1.1	1.6
	w_2	0.5	2.1	3.2
	Field Capacity	0.8	3.2	4.8
	Saturated	---	---	---
Measured Water Content (%)	**Dry**	0.1	0.3	0.6
	w_1	---	1.8	1.8
	w_2	---	2.1	3.1
	Field Capacity	0.6	3.4	4.7
	Saturated	---	---	---

Note: Parameters D_{10}, D_{30}, D_{50}, D_{60}, C_u and C_c are the diameters of the grains at 10%, 30%, 50%, 60% sieve passing, Coefficient of uniformity and curvature of tested ballast, respectively.

4.4.3 Loading

As it was discussed in the previous sections, at test stages with different water content amounts the load was constant. The constant load selected for these tests was 78.75 kip (39.4 tons) static axle load based on the Association of American Railroads (AAR) Manual recommendations for wheels and axles (AAR Manual, 2013). The selected wheel diameter was 38 inches (96.5 cm) and the cyclic load frequency was 1 Hz. To prevent impact of the load, the seating load of 0.2 kips (0.1 tons) was used.

The dynamic factor was calculated using the AREMA suggested equation:

$$P_d = P_s(1 + 0.33(V/D)) \quad \text{Eq. (4.2)}$$

where P_d is the dynamic wheel load, P_s is the static wheel load, V is the maximum train speed assumed 60 mph and D is the wheel diameter equal to 38 inches (96.5 cm). The

dynamic factor is (1 + 0.33(V/D)) which for this study is 1.52 and results in dynamic wheel load of approximately 60 kips (26.8 tons).

To calculate the Equivalent Wheel Load (EWL) according to the concrete tie segment and fastening component properties used in the lab, GEOTRACK model was used. GEOTRACK is a three-dimensional superposition model for determining the response of the track structure using stress-dependent properties of the substructure materials (Chang, 1980). In GEOTRACK model 60 kips (26.8 tons) dynamic load was applied on every other tie in a six tie sequence and the pressure underneath the end of the middle tie, producing the highest stress, was selected. The ties used in the GEOTRACK model were 103.5 inches (262.9 cm) long with 24 inches (61 cm) spacing. The stresses determined from GEOTRACK modeling compared well with under tie stresses from field measurements (McHenry, 2014). Ten thousand cycles of the load in this study is equivalent to 0.8 million gross ton (MGT).

The dynamic wheel load shouldn't exceed more than ten to twenty percent of static load if the rail is well maintained. However, the rail or wheel defects can cause very high loads (Selig & Waters, 1994). In order to simulate the effects of high impact loading of moderately and highly fouled ballast at heavy rainfall conditions, after performing the load equivalent to 60-kip wheel load under saturated conditions and stabilization of the deflection-cycle curve, the load was stepped up to higher loads. The loads were increased by the factors of 25%, 50% and 75%. These applied loads were equivalent to 75, 90, and 105-kip wheel loads. The load increase can also be used to evaluate the safety factor of regular loadings at saturated conditions of moderately and highly fouled ballast. Table 4.2 shows

different stages of the tests at different water contents and different loading conditions in addition to the amount of traffic that each stage of test represents.

Table 4.2: The Traffic MGT at Different Stages of the Box Tests

Moisture Condition	Load (EWL)	Clean	Moderately Fouled (F_{15})	Highly Fouled (F_{30})	Test Stage
Dry	60kips	9 MGT	14 MGT	14 MGT	1
W_1	60kips	---	29 MGT	29 MGT	2
W_2	60kips	---	43 MGT	43 MGT	3
Field Capacity	60kips	25 MGT	74 MGT	74 MGT	4
Saturated	60kips	40 MGT	104 MGT	104 MGT	5
	75kips (25% increase)	---	127 MGT	127 MGT	6
	90kips (50% increase)	---	180 MGT	180 MGT	7
	105kips (75% increase)	---	221 MGT	221 MGT	8

4.5 Results and Discussion

4.5.1 Dynamic Behavior of Fouled and Moist Ballast

Cyclic dynamic wheel loading and unloading from train traffic causes elastic deformation and plastic settlement in the track. Fouling material produced from this dynamic loading will change the behavior of the track under the repeating load. Water held by fouling particles will make the degradation rate even faster.

A typical pattern for cyclic loading in granular materials has been presented in Figure 4.5. This plot shows that the primary loading cycles produce a significant initial plastic settlement and the following cycles will add smaller plastic deformations to the initial settlement. After few cycles, the material deformation becomes mainly elastic, and there is elastic or recoverable strain in every cyclic load. The amount of plastic settlement will reach equilibrium after some amount of loading as a result of the particles not having any

more room to move or the load not being high enough to break more particles. In previous studies, the plastic equilibrium occurs after approximately 10000 cycles (Brown, 1974), which has a good agreement with this study (Figure 4.6).

In this study, the ballast resilient and plastic behavior have been studied by accumulation of many load cycles, and also each cycle has been evaluated under different fouling conditions, different moisture contents and loading stages. The results are discussed in the next sections.

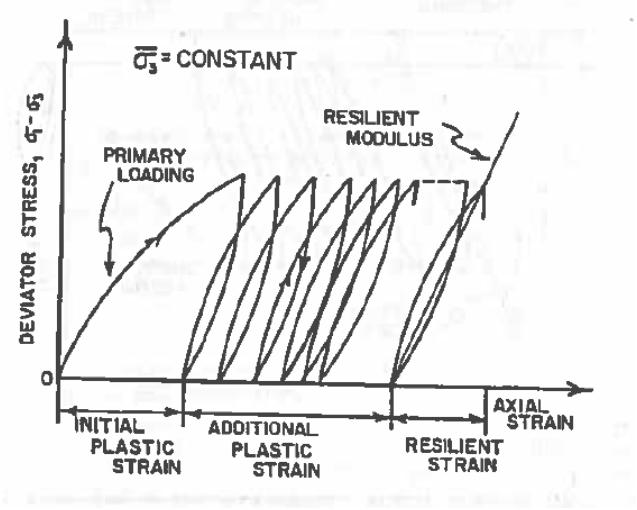

Figure 4.5. Stress-Strain Curve under Repeated Loading (Selig, 1982)

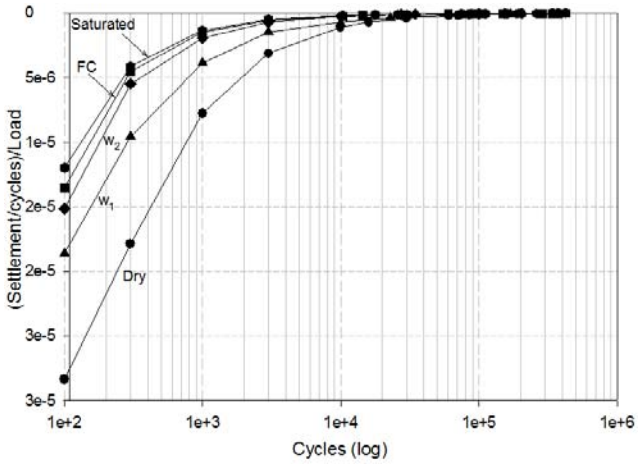

Figure 4.6. Settlement per Cycle in Moderately Fouled Ballast (F_{15}) for EWL of 60 kips

4.5.2 Plastic Settlement

Figure 4.7 presents the permanent strain changes versus cumulative traffic for fouled ballast. This figure shows that after adding moisture from dry to field capacity conditions, the highly fouled ballast (F_{30}) strengthens from the increase in traffic and shows less settlement than moderately fouled ballast (F_{15}). This strengthening is because of high capillary tension between the fine particles in highly fouled ballast and better compaction because of the ballast being more well-graded. By saturating the highly fouled ballast and eliminating the capillary tension, the settlement increases drastically in amount and rate by increase in amount of traffic. This behavior indicates the risk of a significant settlement for highly fouled ballast at a heavy rainfall and high traffic conditions. Moderately fouled ballast after saturation doesn't show a sudden change in the rate and amount of settlement. In saturated conditions, increase in amount of cyclic loading has a small effect on the amount and rate of settlement in both moderately and highly fouled ballast.

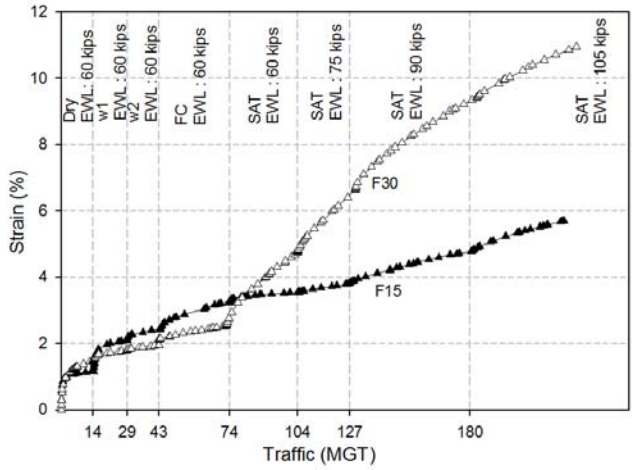

Figure 4.7. Plastic Strain vs. Traffic in Fouled Ballast

The amount of settlement over accumulation of traffic is related to the amount of settlement at 1 MGT and the amount of traffic after 1 MGT (Selig & Waters, 1994). Therefore,

evaluating the effects of geotechnical properties and load increase on the rate of settlement can be studied without considering the initial porosity and stress level of the ballast. Selig et al. in 1981 by conducting field tests reported that the best fit equation for evaluating the rate of settlement is power equation (Eq. (4.3)). To evaluate the effects of geotechnical properties and load increment on the rate of settlement, the power equation of strain changes versus traffic plots in log-log scale has been studied after 1 MGT traffic.

4.5.2.1 The Effect of Water Content

Figure 4.8 shows the changes of plastic strain versus traffic at different moisture conditions but at constant fouling conditions. Figure 4.9 presents the power of the best fitting equations of the log-log scale plots in Figure 4.8 versus water content from dry to field capacity conditions after 1 MGT traffic.

In clean ballast, the rate of settlement does not change significantly from dry to field capacity conditions (Figure 4.8a and 9). Saturation in clean ballast increases the rate of the settlement versus traffic (Figure 4.8a) although saturation might not happen for clean ballast in the real track.

In moderately fouled ballast the rate of settlement increases with increase in water content from dry to saturated conditions (Figure 4.8b and 9). In highly fouled ballast the rate of settlement increases with an increase in water content from dry to intermediary water content conditions (w_2). In the field capacity conditions of highly fouled ballast the rate of settlement decreases because of strengthening due to capillary tension as discussed in the previous sections (Figure 4.8c and 9). Saturation which eliminates the capillary tension, increases the rate of settlement drastically with an increase in the amount of traffic.

The rate of degradation of moderately fouled ballast by increase in moisture over increase in amount of traffic is higher than highly fouled ballast from dry to field capacity conditions (Figure 4.9).

In moderately and highly fouled ballast, about 3% increase in the amount of water content quadruples and doubles the rate of settlement versus traffic, respectively.

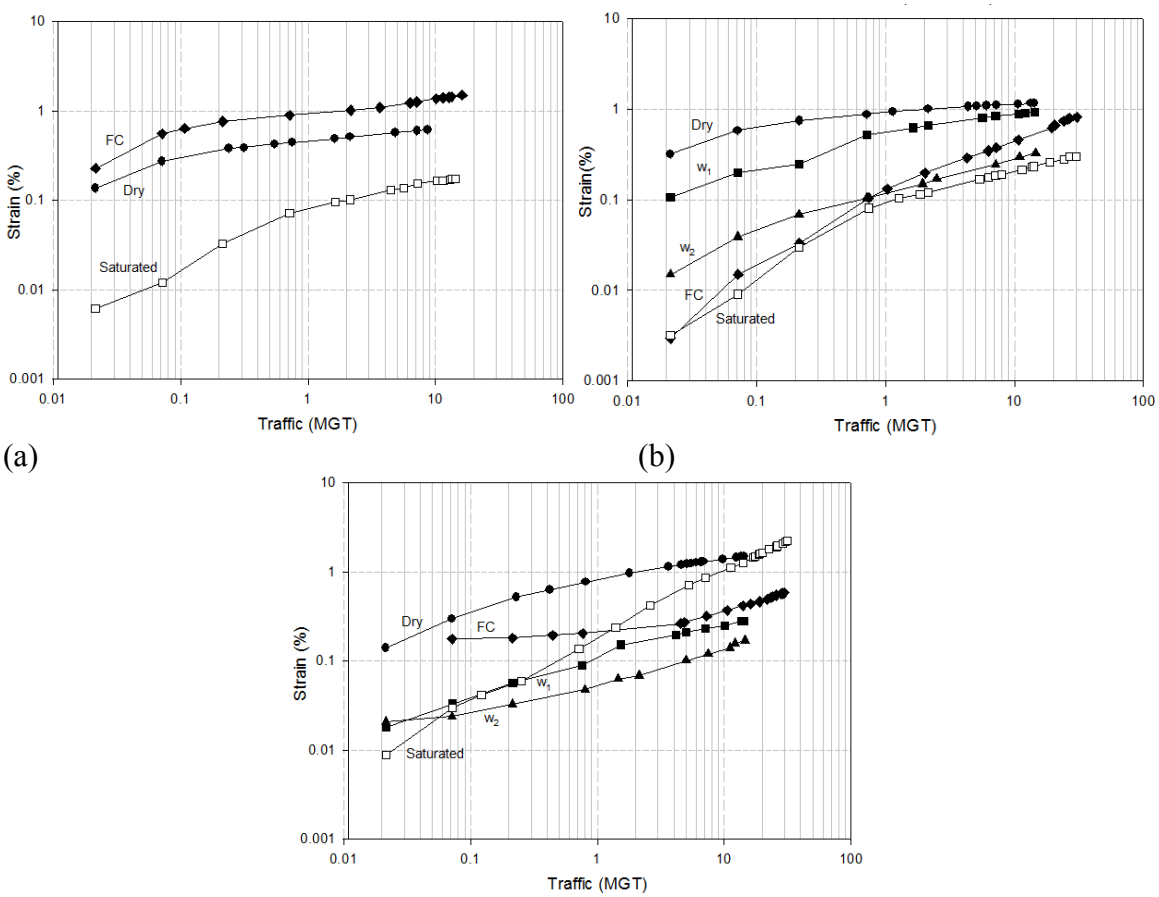

Figure 4.8. Plastic Strain vs. Traffic (Log-Log Scale) at Different Water Contents but Constant Equivalent Wheel Load of 60 kips (a) Clean Ballast (b) Moderately Fouled Ballast (F_{15}) (c) Highly Fouled Ballast (F_{30})

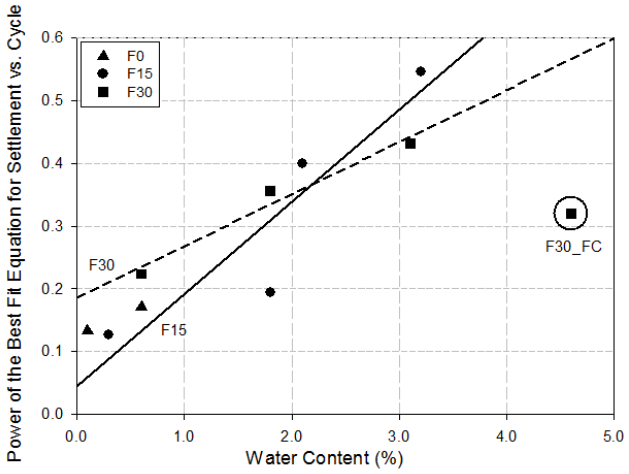

Figure 4.9. The Best Fit Equation Power of Plots in Figure 4.8 vs. Water Content

4.5.2.2 The Effect of Fouling Percentage

Figure 4.10 shows the changes of plastic strain versus traffic in log-log scale at different fouling conditions and constant moisture conditions. Figure 4.11 presents the power of the best fitting equations of the log-log scale plots in Figure 4.10 versus fouling percent after 1 MGT.

An increase in fouling from clean to moderately fouled ballast at dry conditions does not have a significant effect on the rate of settlement while the change in fouling has a significant effect on the rate of settlement for ballast at field capacity and saturated conditions (Figure 4.10 and 11).

An increase in fouling percentage from moderately fouled ballast (F_{15}) to highly fouled ballast (F_{30}) has a significant effect on the rate of settlement over traffic increase for all water content conditions except field capacity. This was discussed in previous sections (Figure 4.10 and 11).

The degradation of fresh ballast to moderately fouled ballast and from moderately fouled ballast to highly fouled ballast as a result of 15% increase in amount of fouling

results in an average of 70 to 80% increase in the rate of settlement versus traffic for all moisture conditions.

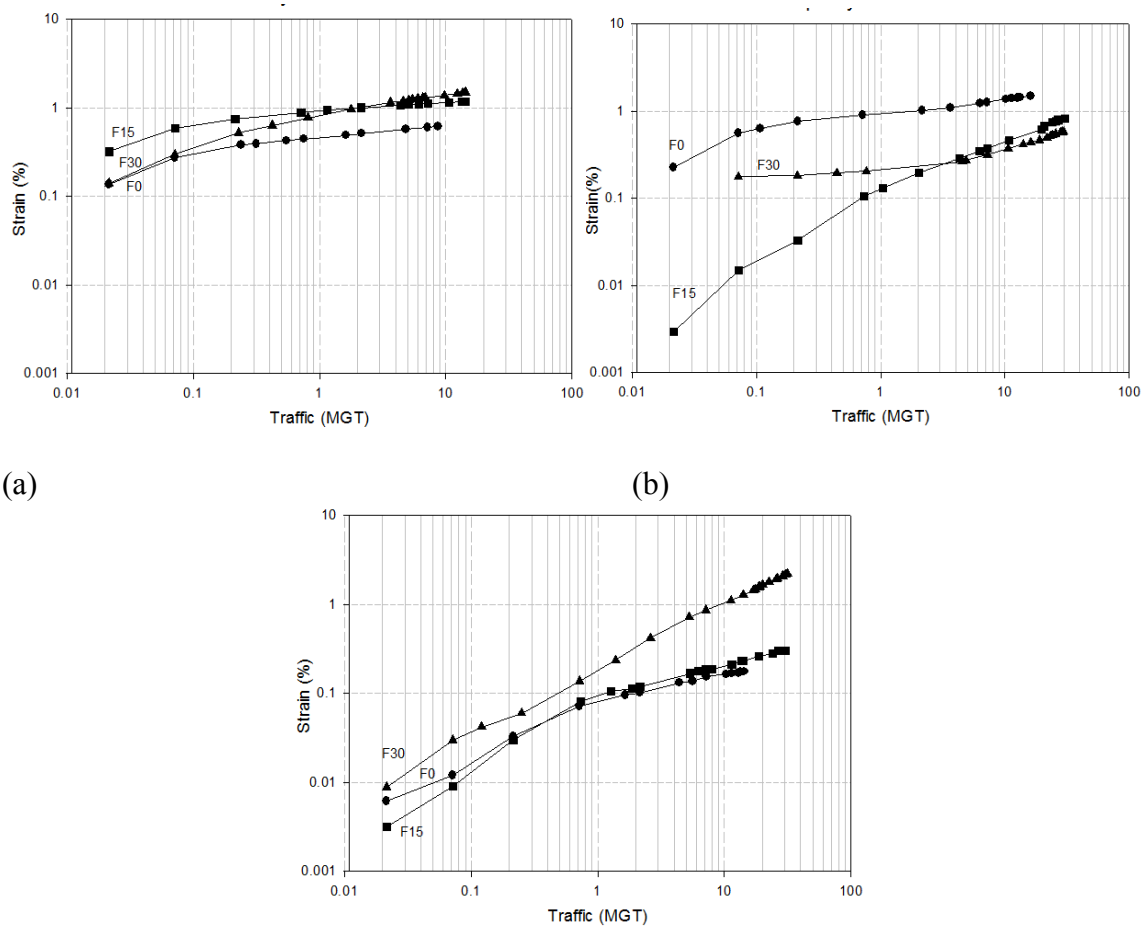

(a) (b)

(c)

Figure 4.10. Plastic Strain vs. Traffic (Log-Log Scale) at Different Fouling Percentages (a)Dry Conditions (b)Field Capacity Conditions (c)Saturated Conditions

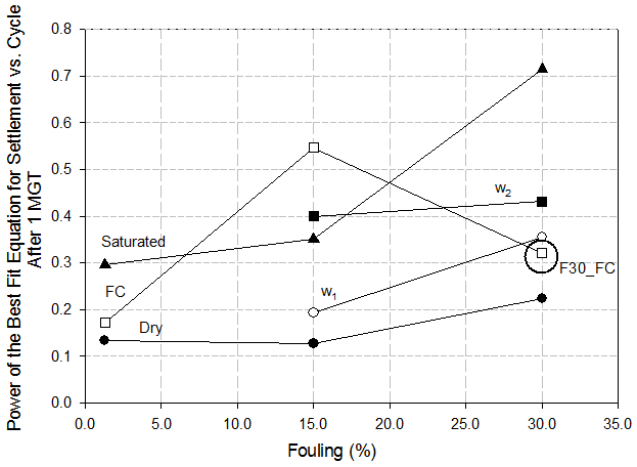

Figure 4.11. The Best Fit Equation Power of Plots in Figure 4.10 vs. Fouling Percentages

4.5.2.3 The Effect of Load increase

Figure 4.12 shows the changes of plastic strain versus traffic in log-log scale for different loading conditions and saturated moisture conditions. This figure illustrates that at moderately and highly fouled conditions a load increase up to 75% of dynamic load does not significantly affect the rate of settlement over traffic increase.

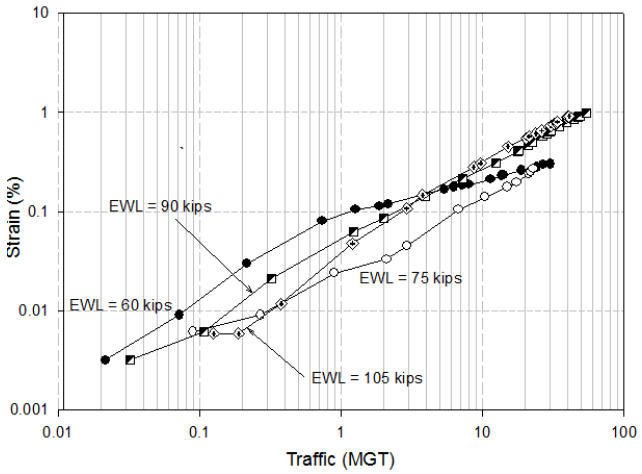

(a)

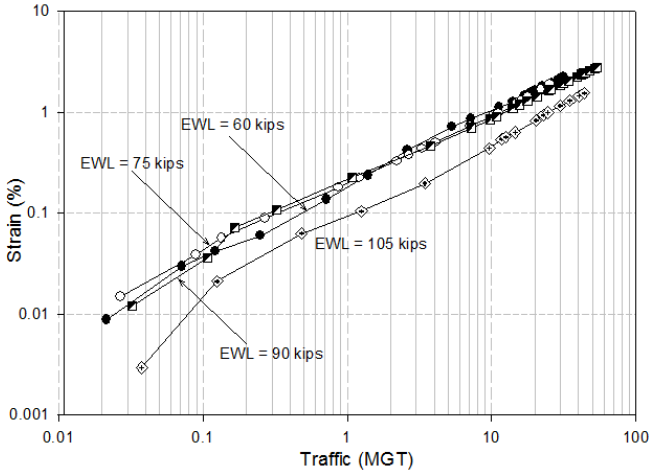

(b)

Figure 4.12. Plastic Strain vs. Traffic (Log-Log Scale) at Saturated Conditions and Different Loading Conditions (a) Moderately Fouled Ballast (F_{15}) (b) Highly Fouled Ballast (F_{30})

4.5.3 Resilient Behavior

4.5.3.1 Single Loading Cycle and the Effect of Indices Properties and Load Increase

To evaluate the effect of water content, fouling and loading on resilient behavior, the secant modulus of the loading hysteresis loop was normalized by the applied load. Figure 4.13 shows the normalized secant modulus of one cycle of loading and unloading at 100, 300, 1000, 10000, 30000, 100000, 200000 cycles and at different stages of the tests.

This figure illustrates that for clean ballast with an increase in traffic, the secant modulus of the loading hysteresis loop increases linearly. In addition, in clean ballast, increase in compaction from traffic has more significant effect on the ballast strength than changes in moisture from dry to saturated conditions.

In moderately and highly fouled ballast (F_{15} and F_{30}), although the moisture is increasing from dry to field capacity conditions, the secant modulus of the loading hysteresis loop

increases by increase in traffic loading. In other words, the effect of compaction from traffic is more significant than degradation by moisture increase. However, at saturated conditions, even with an increase in loading, the effect of moisture overcomes the effect of traffic loading in fouled ballast and the secant modulus significantly decreases by increase in MGT.

The rate of secant modulus increase as a function of MGT under highly fouled ballast conditions (F_{30}), is higher than moderately fouled ballast (F_{15}) from dry to field capacity conditions. This may be the result of better compaction of ballast with better graded ballast over increase in traffic.

In ballast with 15% and 30% fouling, with 3% and 4% increases in water content from dry to field capacity conditions, normalized secant modulus of hysteresis loop increases by 25% and 30%, respectively. The amount of normalized secant modulus in the first four stages of ballast test with different fouling percentages is in the order of clean, highly fouled ballast and moderately fouled ballast. Clean ballast has the higher modulus because of a strong contact between the angular particles. In fouled ballast which there is not much contact between angular particles, the highly fouled ballast has higher modulus. This is because most of the voids are filled with fouling and there is no room for ballast particles to move. Even breaking particles will make this situation worse. In moderately fouled ballast there is still enough air in the voids to get replaced by breaking particles and allow the ballast particles to move, so it is showing the lowest modulus.

After saturation the secant modulus of moderately fouled ballast becomes more than highly fouled ballast. This is as the result of insufficient permeability in highly fouled ballast to prevent pore water pressure created by repeated loading (Freeme & Servas, 1985).

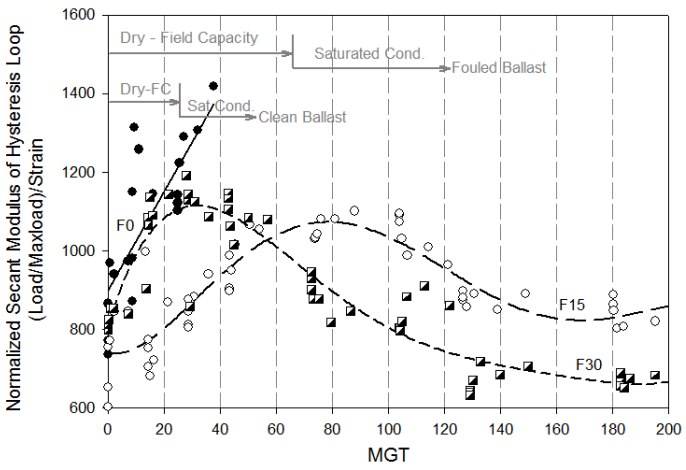

Figure 4.13. Normalized Secant Modulus of Hysteresis Loop after 100, 300, 1000, 10000, 30000, 100000, 200000 cycles vs. Traffic

4.5.3.2 Cumulative Loading and the Effect of Indices Properties and Load Increase

Figure 4.14 shows the cumulative permanent settlement and elastic deformation of moderately fouled and highly fouled ballast versus traffic. The solid lines indicate the plastic settlement which was discussed earlier and the dashed lines indicate elastic deformation.

This figure shows that in moderately and highly fouled ballast by increase in amount of traffic and increase in water content from dry to field capacity conditions, the elasticity of the ballast increases. This behavior is obvious by tracking the difference between plastic settlement and elastic deformation. This is as the result of degradation by moisture increase and accumulation of repeated loading. There is an exception in highly fouled ballast from w_2 to FC conditions that might be because of ballast strengthening by high capillary tension in fine particles.

Figure 4.14 also indicates that at saturated conditions, an increase in amount of loading results in an increase in the elasticity of fouled ballast by increase in accumulation of repeated loading. Figure 4.15 presents the same data shown in Figure 4.14 by showing the

average of difference between plastic settlement and elastic deformation at different stages of test. The amount and rate of increase in elasticity of fouled ballast over accumulation of traffic loading have been discussed in the following sections.

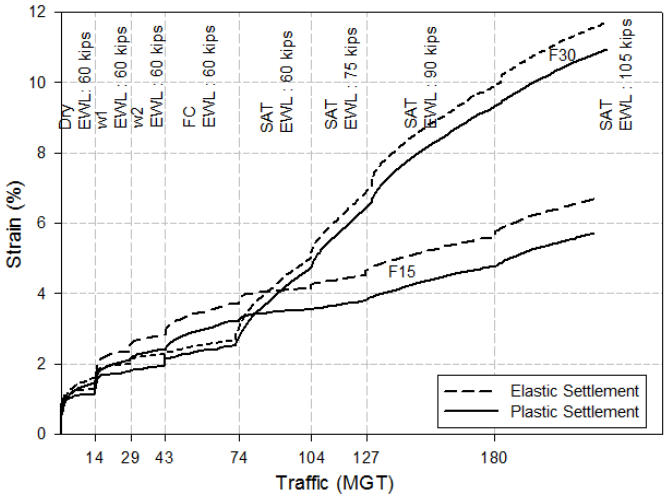

Figure 4.14. Elastic Deformation and Plastic Settlement vs. Traffic in Fouled Ballast

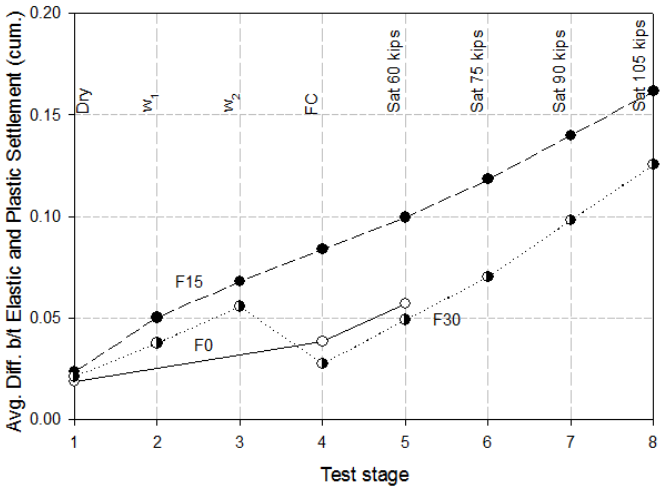

Figure 4.15. The Average Difference between Cumulative Plastic Settlement and Elastic Deformation (Elasticity) at Different Stages of the Tests

In order to quantitatively evaluate the effect of geotechnical properties and load increase on the elasticity of the fouled ballast, the average difference between plastic settle-

ment and elastic deformation was determined. Figure 4.16 shows the effect of water content on the difference between fouled ballast elastic deformation and plastic settlement. Based on this plot degradation of fouled ballast as the result of moisture, increases the elasticity linearly from dry to field capacity conditions over increase in traffic. The highly fouled ballast in field capacity conditions is an exception that shows low elasticity because of strengthening that has been discussed in the previous sections. In moderately and highly fouled ballast, about 3% increase in the amount of water content can triple the difference between elastic deformation and plastic settlement by traffic accumulation.

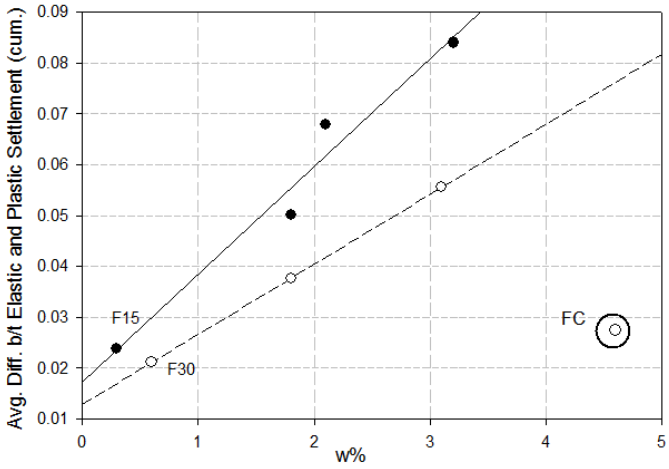

Figure 4.16. The Average Difference between Cumulative Elastic Deformation and Plastic Settlement vs. Water Content

Figure 4. 17 shows the effect of load increase on the difference between fouled ballast elastic deformation and plastic settlement at saturated conditions. This plot shows that elasticity has a linear correlation with traffic load increase. A 25% increase in dynamic load created by track defections can increase the elastic deformation from 20 to 35%.

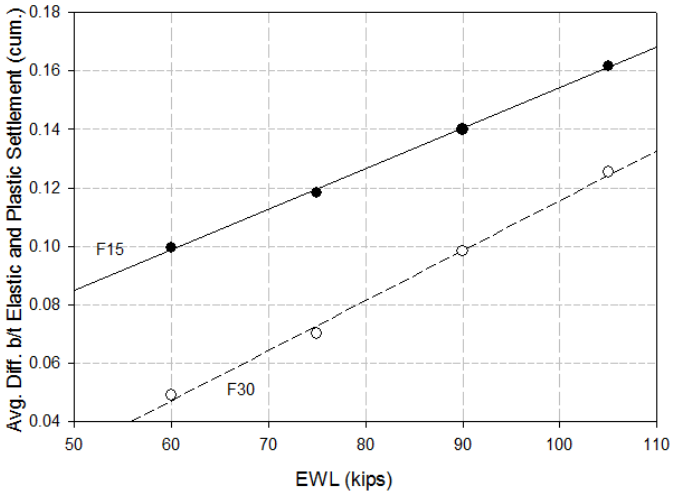

Figure 4.17. The Average Difference between Elastic Deformation and Plastic Settlement vs. Equivalent Wheel Load (EWL) at Saturated Conditions

4.6 Validity of the Box Test Results

In order to verify the applicability of the modified box test for predicting the settlement of ballast under heavy axle load (HAL), the box test results from this study were compared with real track settlement measured in FAST site in 1979 and 1981 (Selig *et al.*, 1981, Selig, 1981, Yoo, 1979) and predicted values of permanent strain by both stress paths and compaction states (Selig, 1982). Figure 4.18 shows the dynamic strain records from FAST test site in 1979 (Yoo, 1979), predicted values from a suggested equation (Selig, 1982), and non-compacted box test results of this study at different fouling conditions and at dry conditions. From the field measurements, each cycle of axle static load for the FAST car represents 65.8 tons which is higher than approximately 60 tons dynamic axle load in this study. The amount of vertical strain measured from the box test at moderately and highly fouled conditions are in good agreement with the lower range of the site measured data and predicted values for compacted samples. This is likely as the result of dry conditions of the box test results or lower load applied to the box. Comparing the box test results with the

predicted values of compaction states (Selig, 1982) shows that clean and fouled ballast box test results have a better agreement with compacted and uncompacted predictions, respectively. The friction angle values that have been used in the model (Selig, 1982) changes from 37.8 to 44.4 degrees from uncompacted to compacted samples and this value for the box test samples are between 39.0 to 40.6 from clean to highly fouled ballast. Therefore, predicted results also have a logical agreement with the box test results.

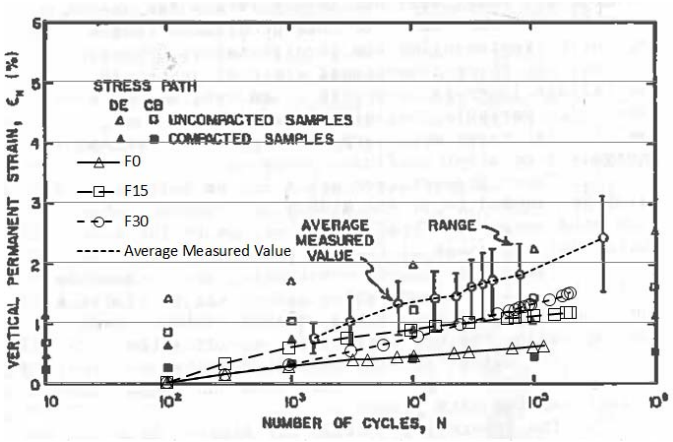

Figure 4.18. Comparison between Box Test Results with Recorded Data in FAST Site and Predicting Model (Selig, 1982)

The ballast strain after T traffic in MGT is related to the ballast strain after 1 MGT of traffic regarding to the following equation (Selig & Waters, 1994):

$$\varepsilon_T = \varepsilon_{T1} T^c \qquad \text{Eq. (4.3)}$$

where ε_T is ballast strain after T traffic, ε_{T1} is ballast strain after 1 MGT and c is a constant exponent. For measured data in the FAST test site with a 33 ton-axle load c = 0.21 was suggested (Selig *et al.*, 1981, Selig, 1981). As the FAST site field results were not evaluated base upon fouling content or water content, Figure 4.19 indicates a random selection of the comparison of box test results with FAST site measurements at different water content (dry

to field capacity) and fouling conditions. As can be seen in Figure 4.19, the results from the box test has a good compatibility with Eq. (4.3) and constant c parameter selected based on FAST site measurements. Figure 4.20 shows the range of difference between predicted values from Eq. (4.3) and box test results at different stages of the test and different recorded loading cycles. The positive values indicate an over prediction; the negative values show an under prediction.

It can be seen that in the four initial stages of the test with clean and fouled ballast and from dry to field capacity conditions, the error in strain values are less than 0.5%. In saturated conditions and increase in amount of load, the error between predicted values and box test results increases significantly. In addition, by increase in amount of moisture and load or increase in the number of test stages, Eq. (4.3) under predicts the strain values measured from the box test. Hence, data derived from Eq. (4.3) has a good agreement with box test results in water contents before saturation and the difference is not significant. Under saturated conditions and high loads, Eq. (4.3) under predicts the settlement in comparison with experimental results.

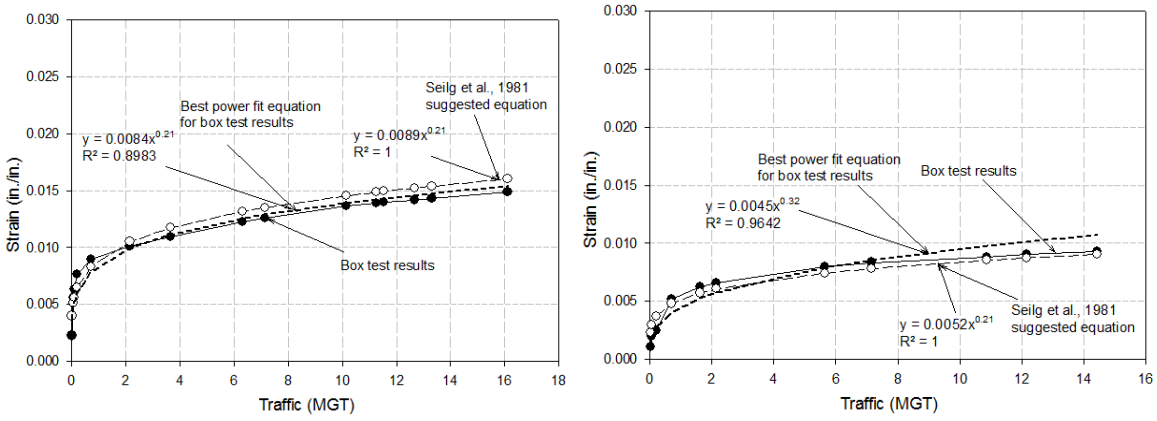

(a) (b)

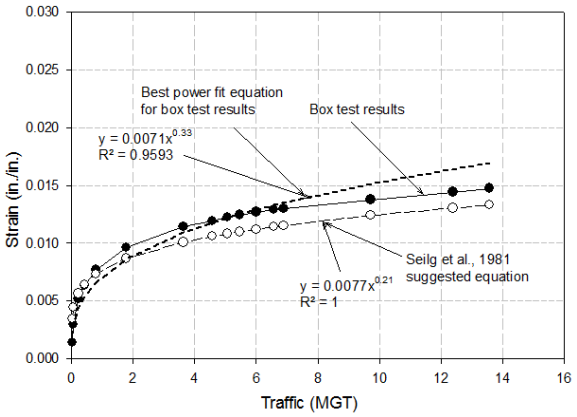

(c)

Figure 4.19. Comparison between Plastic Strain Measured from Box Test and Eq. (4.3) (a) F_0 at Field Capacity Conditions (b) F_{15} at Intermediate Water Content Conditions (c) F_{30} at Dry Conditions

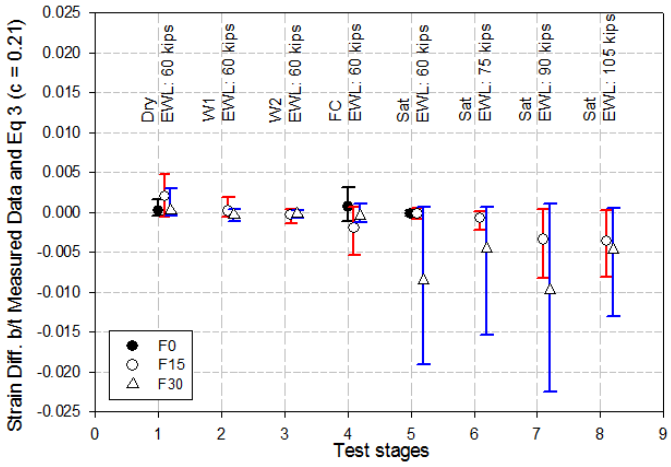

Figure 4.20. The Difference between Plastic Strain Measured from the Box Test and Predicted by Eq. (4.3) vs. Test Stages

4.7 Conclusions

Modified box test with cyclic equivalent Heavy Axle Load (HAL) were conducted on granite ballasted track with different fouling and moisture conditions at the University of Massachusetts, Amherst. The tests were continued up to 2,500,000 cycles to evaluate the effect of fouling percentage and water content on the dynamic behavior of ballast under heavy axle load and high traffic conditions. The dimension of the box test was modified

from its original version to decrease the effect of the boundary conditions and simulate the real conditions of the ballast under loading. The results were also verified with field measured data to evaluate the validity of the simulation. This can help the railroad industry to better understand the risk factors and maintenance needs of the track at different conditions. Based on the data analysis, the effect of these parameters were discussed and evaluated qualitatively and quantitatively on plastic settlement and elastic deformation of the ballasted track. Based on this study the following conclusions can be drawn:

- The results from this study have a good agreement in trend and value with field measured data in FAST test site. This validates the simulation of the modified box test with new dimensions.
- For ballast with the same material properties used in this study, Selig et al.'s equation (Eq. (4.3)) for predicting the ballast settlement is valid for clean and fouled ballast from dry to field capacity conditions. In addition, the results from this study shows that Selig et al.'s equation (Eq. (4.3)) is not appropriate for saturated conditions.
- Highly fouled ballast at heavy rainfall and high traffic conditions has the risk of significant settlement. In highly fouled ballast, the rate of settlement (inches/cycle) at saturated conditions can increase up to 50 times of field capacity conditions. This is because of the elimination of capillary tension formed at intermediary moisture conditions introducing a temporary strength.
- In clean ballast, the rate of settlement versus traffic does not change significantly from dry to field capacity conditions.

- The settlement rate of moderately fouled ballast (F_{15}), by increase in moisture over increase in amount of traffic, is higher than highly fouled ballast (F_{30}) from dry to field capacity conditions. Based on this study, a 3% increase in water content quadruples the rate of settlement versus traffic in moderately fouled ballast and doubles the rate of settlement versus traffic in highly fouled ballast.
- The effect of the fouling percentage increase from clean to moderately fouled ballast on the settlement rate is significant at field capacity and saturated conditions and negligible at dry conditions.
- The effect of the fouling percentage increase from moderately to highly fouled ballast on settlement rate is significant at all water contents.
- Regarding this study's results, an increase in load up to 75% does not significantly affect the rate of settlement versus traffic.
- At saturated conditions, an increase in amount of loading results in an increase in the elasticity of fouled ballast by increase in accumulation of repeated load
- In clean ballast, an increase in compaction from traffic has a more significant effect on the ballast strength than changes in moisture from dry to saturated conditions.
- In moderately and highly fouled ballast (F_{15} and F_{30}) at moisture contents ranging from dry to field capacity, the effect of compaction from traffic is more significant than the degradation by moisture increase on the ballast strength. However, at saturated conditions, the effect of moisture overcomes the effect of traffic compaction because of insufficient hydraulic conductivity to allow the dissipation of excess pore water pressure.

- In moderately and highly fouled ballast, about a 3% increase in the amount of water content can triple the elastic deformation by traffic accumulation.
- Elasticity has a linear relationship with traffic load increase.

CHAPTER 5

FOULING AND WATER CONTENT INFLUENCE ON THE BALLAST DEFORMATION AND ELECTROMAGNETIC PROPERTIES

5.1 Introduction

Infiltration of fines into ballast layer due to breakdown of granular particles, or breakdown fouled ballast creation, is a common track damage that leads a track to roughness problems and losing its acceptable ride quality and safety standards. Fouling and water held by fouling gradually deteriorates ballast by reducing hydraulic conductivity and strength properties (Fortunato *et al.*, 2010, Han & Selig, 1997, Indraratna & Salim, 2005, Selig & Waters, 1994). This situation leads a track to require maintenance. Increase in train traffic and load carrying capacity will result in more ballast breaking down and consequently higher maintenance costs. Railroads spend tens of millions of dollars for ballast and related maintenance in the U.S. (Railroad Facts, 2014). A considerable proportion of these costs are related to geotechnical problems of a track as the railroad foundation. Therefore, studying geotechnical deformation properties of ballast and understanding its performance at different situation will help to reduce these costs. Also numerical analysis and computer models used for predicting ballast behavior under different loading conditions need to be verified by deformation and indices properties through laboratory tests. Many static and dynamic triaxial lab tests have been performed on different type of fouled ballast with different grain size distributions (Alva-Hurtado, 1980, Brown, 1974, Ebrahimi, 2010, Indraratna *et al.*, 1998, Mishra *et al.*, 2013, Qian, 2016, Qian *et al.*, 2014, Suiker *et al.*, 2005b, Trinh, 2012, Tutumluer, 2015) but there are still need for evaluating the effect of

different breakdown fouling percentages at different moisture conditions on deformation properties of ballast. Accordingly, a large-scale laboratory testing program was performed on clean, moderately and highly fouled ballast contaminated by breakdown fouling. Each of these mixtures was tested under dry, field capacity and two points between the extremes, as intermediary water contents. The tests were also conducted under three confining pressures including 5, 10 and 15 psi. Material and experimental set up, specimen's preparation and results evaluating the effects of different fouling percentages, water contents and confining pressures have been discussed and presented.

Performing GPR surveys with different frequency antennas in places with different geologies represent that interpretation of GPR profiles can provide significant geotechnological information about soils, thickness of unconsolidated deposits, depth of bedrock, permafrost distribution and etc. in different deposits (Jol, 2009). Also some researchers explored relationship between dielectric properties of base course aggregates used in subgrade construction and evaluating existence of a correlation between dielectric properties and the strength and deformation characteristics of many types of soils and aggregates. They performed GPR surveys, geotechnical lab tests and in-situ tests for this assessment (Cosenza *et al.*, 2006, Fernandes *et al.*, 2008, Marschall *et al.*, 2007, Saarenketo & Scullion, 1996).

These evaluations clearly establish the basis for a possible relationship between GPR data and deformation characteristics of railroad ballast and need for evaluating this correlation for ballast at different conditions. Therefore, the results from the triaxial properties of fouled ballast from this study have been compared with the electromagnetic properties

of the same fouled ballast with the same indices properties to evaluate any existing correlation. The results have also been discussed and presented in this Chapter.

5.2 Material and Experimental Set up

5.2.1 Material

5.2.1.1 Ballast and Fouling

In this study ballast samples were granite crushed stones obtained from a designated quarry in Connecticut. The different sizes of crushed stone were mixed to meet American Railway Engineering and Maintenance-of-Way Association (AREMA) #4 gradation (*AREMA. Manual of Railway Engineering*, 2006). Breakdown fouling was abraded stone dust from the same quarry that was selected because it contributes to a large percentage of actual fouling (Selig & Waters, 1994). The tests were conducted on clean (<5% Fouling), moderately fouled ballast (15% fouling) and highly fouled ballast (30% fouling) to determine the effects of fouling and moisture held by fouling on deformation properties of ballast. F_0, F_{15} and F_{30} symbols have been used for ballast with <5%, 15% and 30 fouling, respectively. Percent fouling is the ratio of fine particles weight passing 3/8" sieve to the total weight of the fouled ballast (Selig & Waters, 1994). The particle size distribution plot has been presented in Figure 5.1 for all samples, where the clean sample is well meeting the AREMA#4 ballast and fouled samples exclude from the AREMA #4 gradation. Table 5.1 summarizes gradation characteristics of the clean and fouled ballast including D_{10}, D_{30}, D_{50}, D_{60}, C_u and C_c that are the diameters of the grains at 10%, 30%, 50%, 60% sieve passing, coefficients of uniformity and curvature of tested ballast, respectively. The Grain Size

Distribution tests were performed in general accordance with ASTM D6913-04 (American Society for Testing and Materials.).

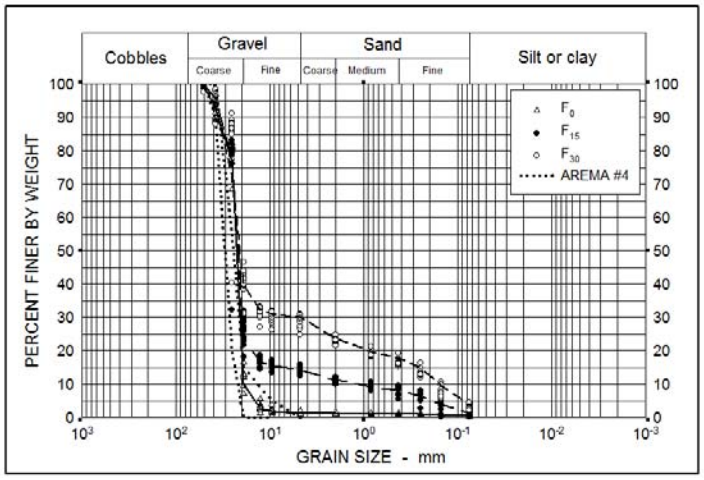

Figure 5.1: Grain Size Distribution Plot

5.2.1.2 Water Content

In order to evaluate the effect of water content on deformation properties of ballast, four stages of water content were tested including dry, field capacity and two points between the extremes. Field capacity is defined as the water content level of ballast immediately after saturation which the surface of the material is saturated but the voids are not. This simulates a heavy rainfall condition that ballast surface is soaked in water but the voids are not saturated. To define the amount of water needed to be added to the ballast triaxial samples, reconstituted samples with the same grain size distributions were built at the same room temperature. The reconstituted samples were saturated and drained immediately followed by water content sampling to find the field capacity water content. The ⅓ and ⅔ portions of distance between zero (dry) and field capacity were defined as intermediate water contents (w_1 and w_2). To verify the actual water content of the triaxial samples

in accordance with the defined water contents, water contents of whole samples were measured after breaking down. Water content sampling was conducted in general accordance with ASTM D2216-05 standard (American Society for Testing and Materials.).

For intermediate water contents, water was introduced to the samples from the top and for field capacity conditions water was added from the bottom and drained immediately. The water in all moist samples was added after building the samples and applying 2 psi (13.8 kPa) confining pressure. To allow for water equilibrium, the intermediate water content samples sat for 16 hours prior to the start of the test regarding to ASTM D7181-11 (American Society for Testing and Materials.). The samples with field capacity water content were loaded immediately after complete drainage. Table 5.1 shows the average of defined and actual water content for clean and fouled ballast.

Note that for clean ballast only one intermediate water content (w_1) was tested. This was because there was not enough fouling to hold water. Also, the field capacity water content was less than 1% which was hard to distinguish between intermediate water contents in such a small range.

5.2.2 Specimen Preparation and Experimental Set Up

The test specimen used for ballast triaxial test had a nominal diameter of 10 inches (25.4 cm) and nominal diameter of 20 inches (50.8 cm) corresponding to an aspect ratio of H/D = 2. In accordance with Figure 5.1, more than 98% of particles are smaller than 40 mm (1.57 in.), therefore the sample size ratio, defined as the diameter of the triaxial specimen divided by the maximum particle dimensions, is equal to 6.35. This number is more

than 6 which means that the sample size effects can be eliminated on the test results in accordance with the ASTM D7181-11 standard (3).

The triaxial apparatus used in this study is illustrated in Figure 5.2. Specimens were prepared by compacting ballast in 8 layers with equal thickness using a steel rod and a hand tamper. Layers were compacted in a mold with densities close to the measured densities in the real track (Selig, 1989) by careful control on thickness and weight of material in each layer. This indicates that the compaction characteristics in this study are representative for in- situ ballast layers. In the fouled specimens the needed amount of fouling was spread over each layer followed by compaction. The specimen was enclosed by a double-latex membrane with total thickness of 1.68 mm Table 5.1 shows the average of the specimen densities for clean and fouled ballast.

The circumferential displacement was measured by three string potentiometers mounted at ¼, ½ and ¾ of specimen height. In order to minimize friction between the membrane and the potentiometer cable, the cable was surrounded by small pieces of Teflon tubing.

The triaxial chamber was located in a load frame and loaded statically by using a MTS servo-controlled hydraulic system with a 110 kN (24 kips) capacity actuator. Isotropically consolidated drained triaxial compression tests were performed (CIDC) on clean and fouled ballast with 5psi (34.5 kPa), 10 psi (68.9 kPa) and 15psi (103.4 kPa) confining pressures with an axial strain rate of 0.04 in/min (Aursudkij *et al.*, 2009).

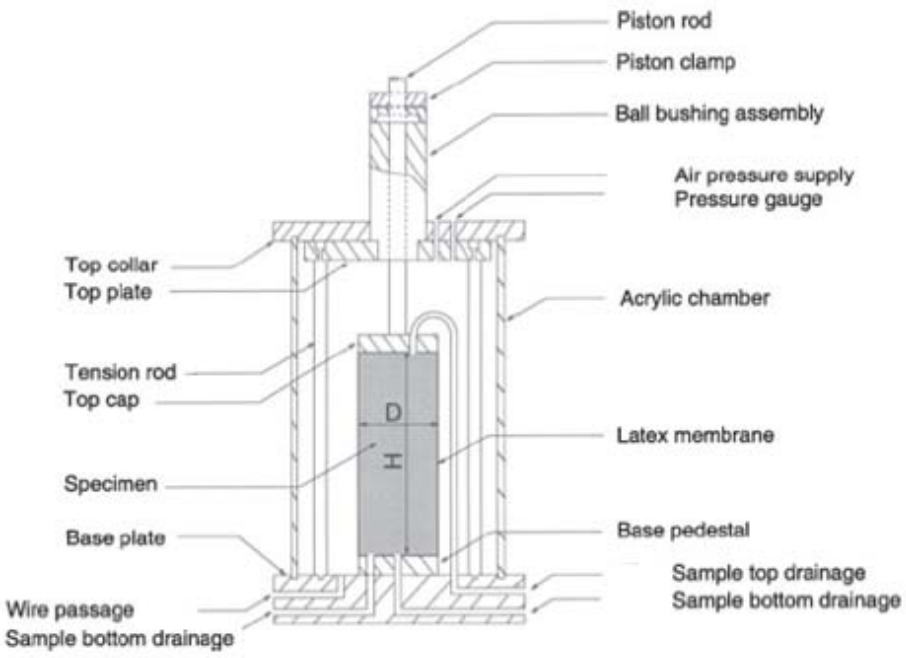

Figure 5.2: Components of Triaxial Load Apparatus

Table 5.1: Grain Size Distribution (GSD) Test Results, Density Values, Targeted and Average Measured Water Contents of the Samples

Parameters		F_0	F_{15}	F_{30}
Average Fouling (%)		2.0	15.7	30.0
D_{10}(mm)		16.7	1.2	0.2
D_{30}(mm)		21.2	19.5	13.0
D_{50}(mm)		24.0	22.7	21.0
D_{60}(mm)		25.2	24.2	23.0
Cu		1.5	20.2	100.0
Cc		1.1	13.1	31.9
Dry density (kg/m3)		1561	1958	2133
Targeted Water Content from reconstituted sample (%)	Dry	0.0	0.0	0.0
	w_1	0.3	1.1	1.6
	w_2	0.5	2.1	3.2
	Field Capacity	0.8	3.2	4.8
Measured Water Content from Model Track (%)	Dry	0.1	0.3	0.6
	w_1	0.5	1.7	1.7
	w_2	---	2.4	3.0
	Field Capacity	0.8	3.2	4.5

5.3 Results Presentation and Discussion

5.3.1 Stress and Strain Behavior

The deviator stress changes versus axial strain of CIDC triaxial tests on samples with different fouling percentages, water contents and confining pressures are shown in Figure 5.3 and 5.4. The peak deviator stress $(\sigma_1-\sigma_3)_P$ increases with increase in confining pressure as expected.

It can be seen in Figure 5.3 that by increasing the water content at constant fouling percentage and confining pressure, the peak deviator stress decreases. Although there is some scatter at intermediate water contents, which might be as the result of imperfect water distribution in whole sample, the total trend is clear.

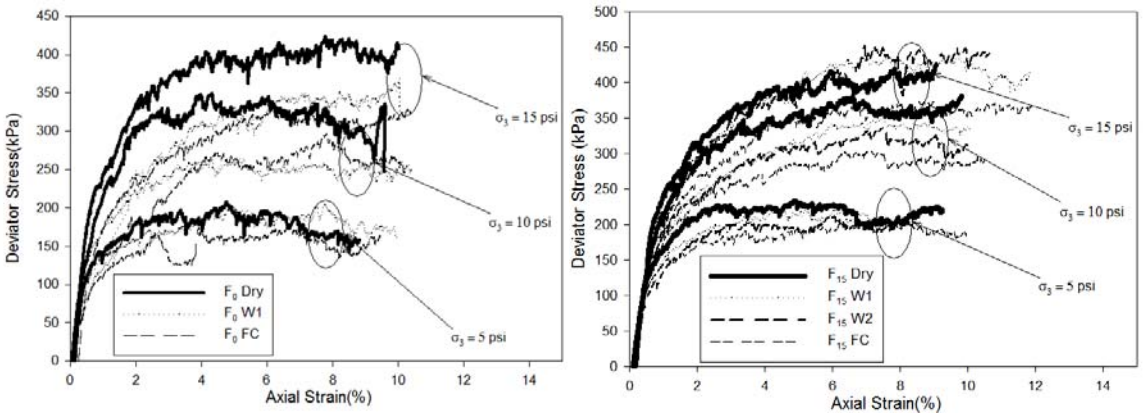

(a) (b)

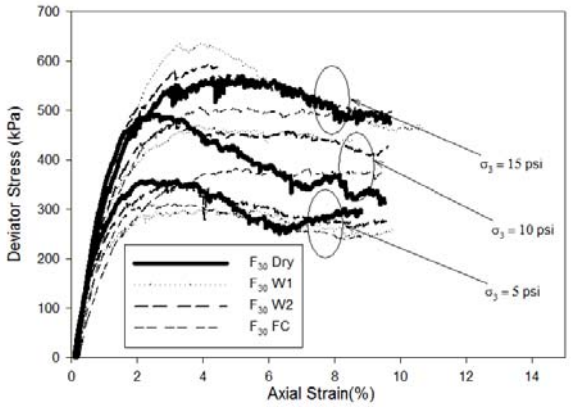

(c)

Figure 5.3: Stress-Strain Behavior During CIDC Triaxial Tests at Different Confining Pressures and Water Contents (a) Clean Ballast (b) Moderately Fouled Ballast (F_{15}) (c) Highly Fouled Ballast (F_{30})

Figure 5.4 also indicates that an increase in fouling percentage at constant confining pressure and water content increases the peak deviator stress. This is as the result of better gradation of fouled ballast in comparison with clean ballast in the same moisture and confining pressure conditions. Fouling fine particles within fouled ballast matrix will help to gain a higher density and better packing. (Tutumluer, 2015).

The changes of stress-strain behavior parameters in magnitude and rate versus water content and fouling percentage are quantitatively evaluated in the following sections.

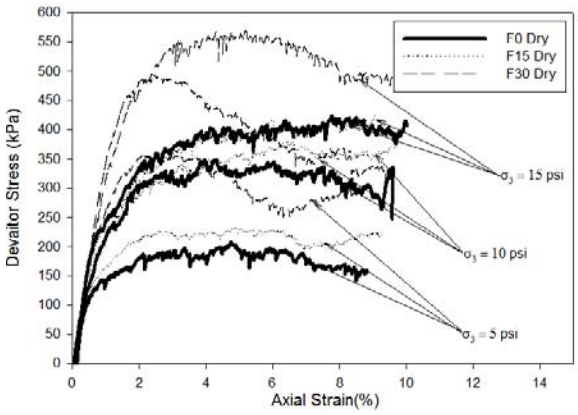

(a)

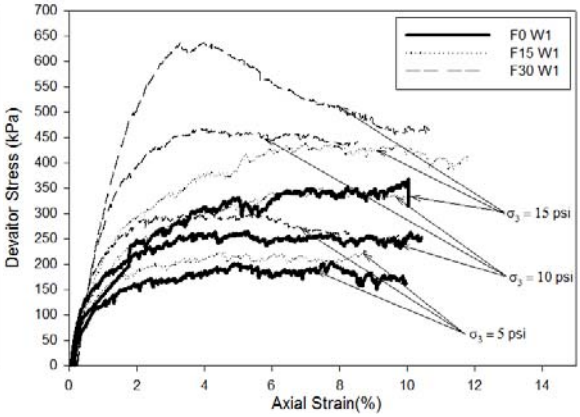

(b)

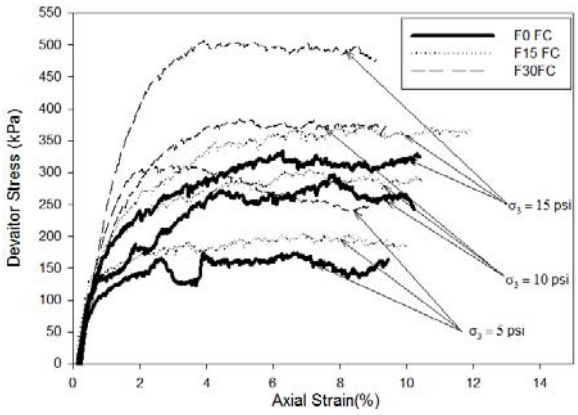

(c)

5.4: Stress-Strain Behavior During CIDC Triaxial Tests at Different Confining Pressures and Fouling Percentages (a) Dry Condition (b) Intermediate Water Content Condition (c) Field Capacity Water Content Condition

5.3.2 Shear Strength

5.3.2.1 Effect of Water Content and Confining Pressure

Figure 5.5 and 5.6 show the effect of water content on the maximum shear strength at different fouling percentages and confining pressures. These figures show that by increase in water content the maximum shear strength decreases linearly and the rate of this decrease is affected by confining pressures and Fouling percentages.

Figure 5.5 indicates that the rate of this reduction decreases from clean to fouled ballast although, fouling percentages do not have a significant effect on the rate of this reduction from moderately to highly fouled ballast. This can be as the result of capillary tension among wet fine particles in fouled ballast and lesser effect of water on contact area of ballast aggregates. Regarding to the results of this study, a 1% increase in water content, results in a 25%, 6% and 4% decrease in maximum shear strength of clean, moderately and highly fouled ballast, respectively. In a constant confining pressure, 15% increase in fouling will result in about 75% decrease in the rate of shear strength reduction versus water

content from clean to moderately fouled ballast and it is negligible from moderately to highly fouled ballast.

The reduction rate of maximum shear strength versus water content, increases with the increase in confining pressure (Figure 5.6). This behavior indicates that the greater contact area between particles attributed to higher confining pressure, the more effect of moisture on decreasing shear strength of ballast. Based on this study results, increase in confining pressure from 5 to 10 psi can double or triple the rate of shear strength reduction versus water content and from 10 to 15 psi can increase this rate by approximately 45% at a constant fouling condition.

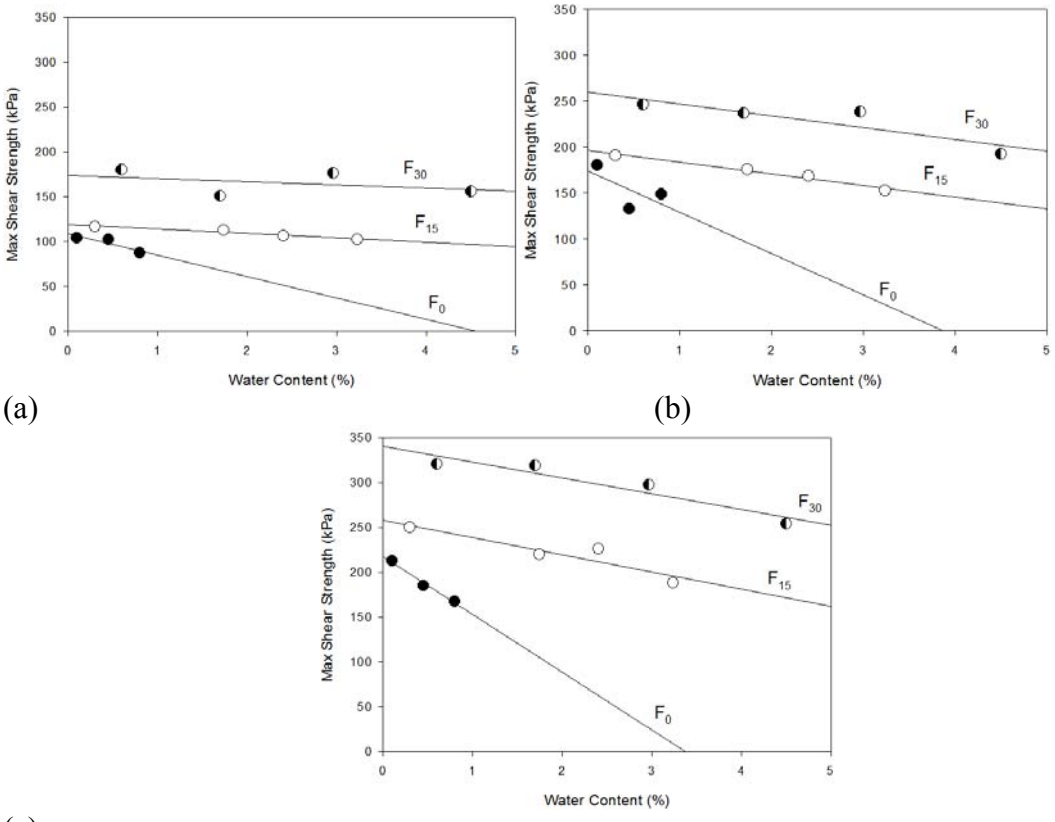

Figure 5.5: Changes of Max Shear Strength vs. Water Content at Different Fouling Conditions (a) 5 psi Confining Pressure (b) 10 psi Confining Pressure (c) 15 psi Confining Pressure

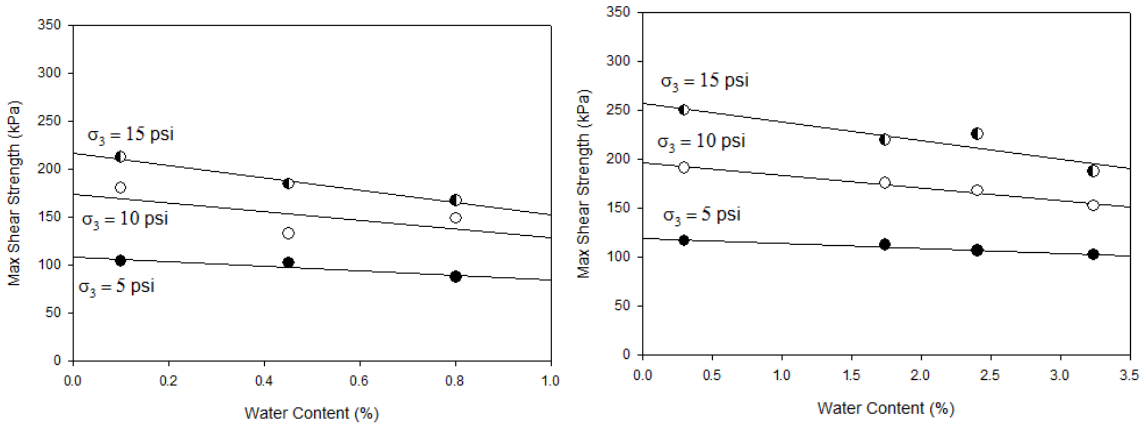

(a) (b)

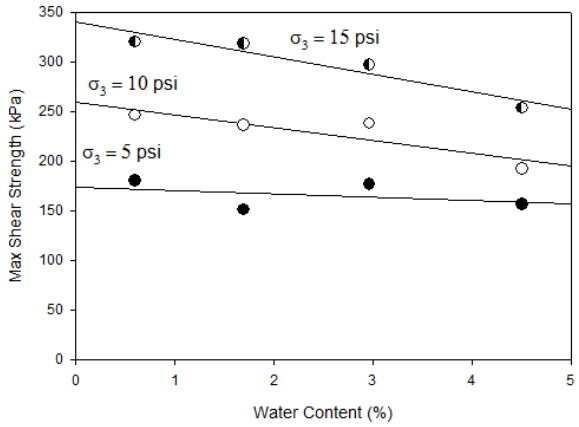

(c)

Figure 5.6: Changes of Max Shear Strength vs. Water Content at Different Confining Pressures (a) Clean Ballast (F_0) (b) Moderately Fouled Ballast (F_{15}) (c) Highly Fouled Ballast (F_{30})

5.3.2.2 Effect of Fouling Percentages and Confining Pressure

Figure 5.7 is a three-dimensional view showing the effect of confining pressure and fouling on the maximum shear strength of ballast. This figure generally shows that regardless to the amount of moisture, by increase in fouling and confining pressure the maximum shear strength of ballast increases.

In order to evaluate this behavior more precisely, the effect of individual variables of Figure 5.7 have been assessed in two dimensional views in Figures 5.8 and 5.9.

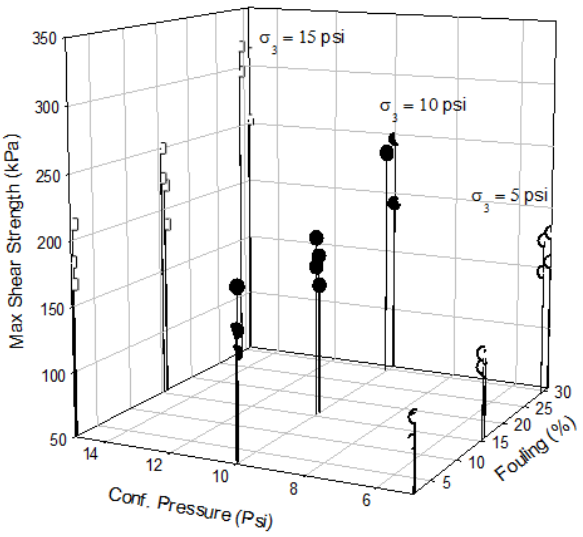

Figure 5.7: Effect of Fouling and Confining Pressure on the Maximum Shear Strength of Clean and Fouled Ballast

Interestingly, the increase in breakdown fouling does not result in strength loss in constant water content and water held by fouling is the main reason for ballast degradation that was discussed in the previous section (Figure 5.8). Increase in shear strength of ballast with an increase in breakdown fouling is the result of a better gradation, higher density and compaction that helps ballast matrix to achieve higher shear strength (Charles & Watts, 1980, Indraratna *et al.*, 1998, Tutumluer, 2015).

Figure 5.8 also indicates that shear strength increase as the result of fouling increase is a non-linear behavior and increase in confining pressure increases the maximum shear strength as expected (Indraratna *et al.*, 1998, Suiker *et al.*, 2005a).

Figure 5.9 is another view of Figure 5.7 that highlights the effect of water content. This figure also shows a non-linear behavior of increase in maximum shear strength as the result of increase in breakdown fouling percentage. The confining pressure and fouling do

not have a significant effect on the rate of shear strength changes versus breakdown fouling (Figures 5.8 and 5.9).

In average 15% increase in fouling percentage will result in 10% increase in max shear strength from clean to moderately fouled ballast while this value is 40 % from moderately to highly fouled ballast in a constant confining pressure.

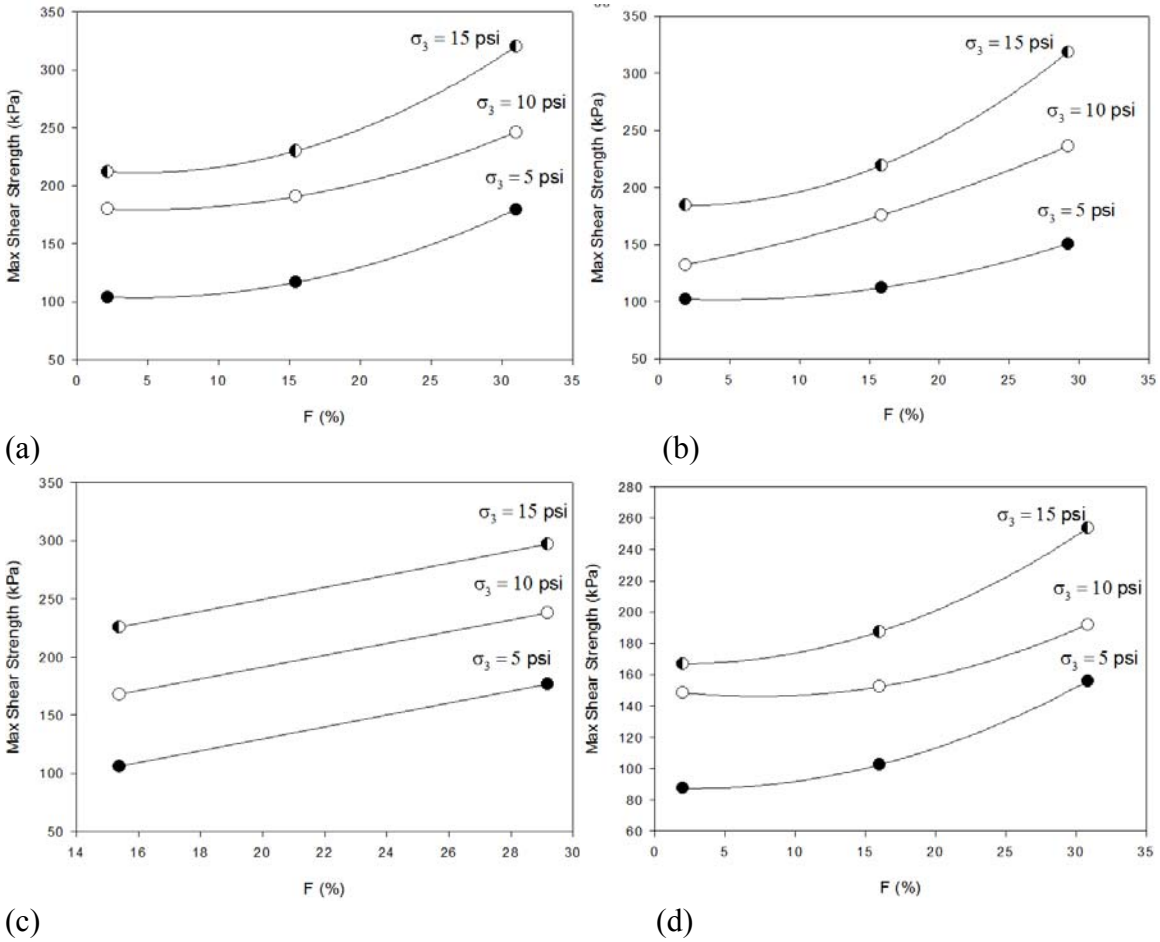

Figure 5.8: Effect of Fouling on the Maximum Shear Strength of Ballast at Different Confining Pressures and Constant Water Content (a) Dry (b) w_1 (c) w_2 (d) Field Capacity. Note: w_2 has two studied points in moderately and highly fouled ballast

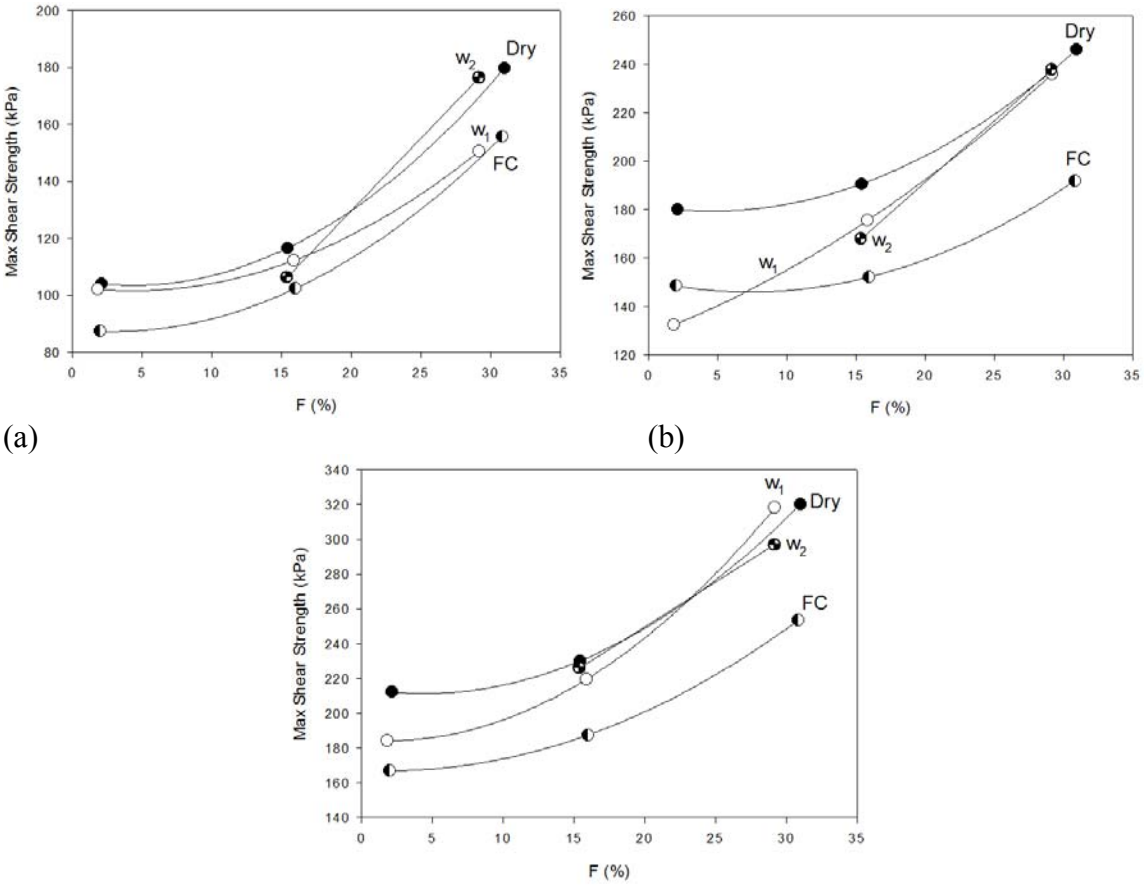

Figure 5.9: Effect of Fouling on the Maximum Shear Strength of Ballast at Constant Confining Pressure and Different Water Contents (a) 5 psi Confining Pressure (b) 10 psi Confining Pressure (c) 15 psi Confining Pressure. Note: w_2 has two studied points in moderately and highly fouled ballast

5.3.3 Friction Angle

In the field of granular mechanics, the deviatoric stress invariant, q, and the hydrostatic stress invariant, p, parameters are more appropriate for describing frictional failure of granular materials under three dimensional stress conditions, stress path analyses have been used in this study instead of principal stresses (Suiker *et al.*, 2005, Sulem, 2004). The effect of water content and fouling percentage on friction angles of fouled ballast are discussed in following sections.

5.3.3.1 Effect of Water Content

In order to study the effect of water content on the frictional failure of ballast, the stress paths for clean ballast at different water contents are presented in Figure 5.10. Clearly, the friction angle decreases with the increase in water content. This is as the result of better ballast interlocking at dry conditions than moist conditions. Figure 5.11 shows friction angle changes versus water content in all samples of this study. In clean ballast reduction of friction angle by increase in water content is clear from dry to field capacity water contents. In fouled ballast, the friction angle is decreasing from dry to field capacity conditions by a small amount. Scatters in friction angle in fouled ballast can be as the result of an error because of strengthening by capillary tension at intermediary moistures. The reduction rate of friction angle versus water content decreases from clean to fouled ballast although, this rate is not changing significantly in fouled ballast with different fouling percentages. Approximately 1% increase in water content results in 12% reduction of friction angle in clean ballast and less than 2% in fouled ballast from dry to field capacity water contents.

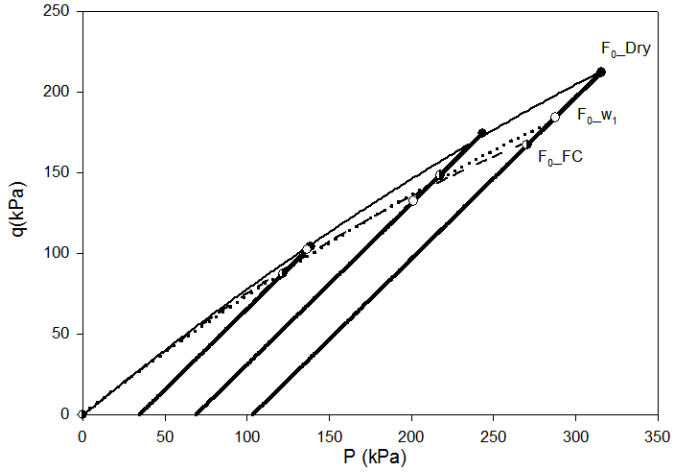

Figure 5.10: Stress Paths for Clean Ballast at Different Water Content Conditions

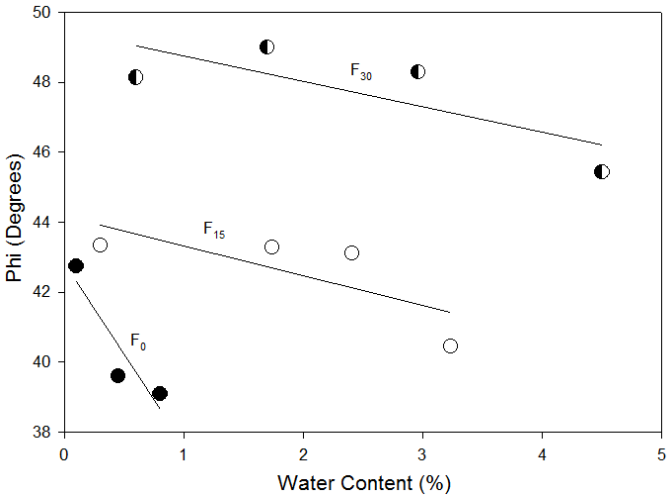

Figure 5.11: Changes of Friction Angle vs. Water Content at Different Fouling Conditions

5.3.3.2 Effect of Fouling

Figure 5.12 indicates the effect of breakdown fouling on friction angle and stress conditions at failure and at constant water content conditions. This figure clearly shows that increase in breakdown fouling results in an increase in friction angle and shear strength of ballast. Although fouling is one of the main reasons for degradation of ballast, in constant water content the friction angle increases by increase in breakdown fouling percentages non-linearly (Figure 5.13). In accordance with the effect of water content on strength properties of ballast, discussed in previous sections, it becomes more clear that the main decay of fouled ballast is moisture that fouling increases its effect by holding it in ballast layer. Water content does not have a defined effect on the rate of friction angle changes versus fouling percentages regarding to this study results. Approximately, 15% increase in fouling from clean to moderately fouled ballast increases the friction angle by 5% and from moderately fouled ballast to highly fouled ballast by 15% in constant moisture conditions.

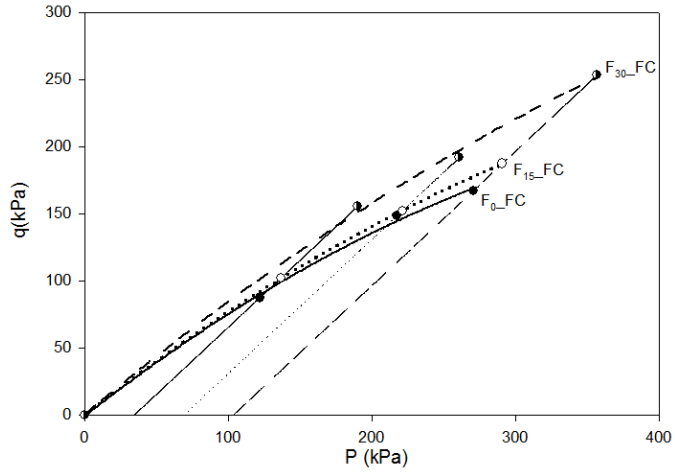

Figure 5.12: Stress Paths for Different Fouling Conditions at Field Capacity Water Contents

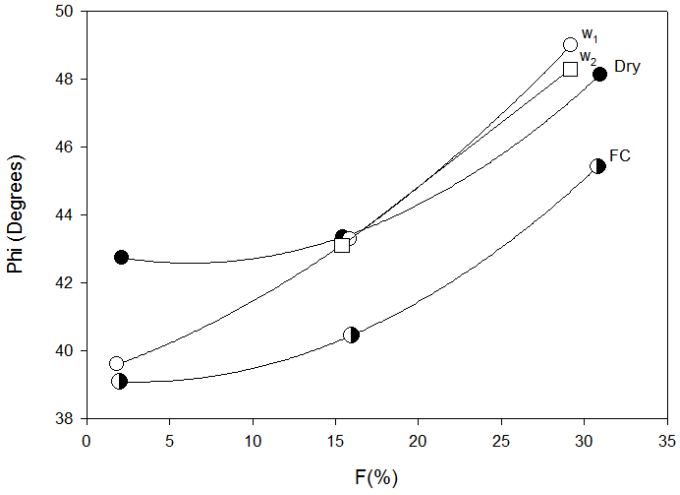

Figure 5.13: Changes of Friction Angle vs. Fouling Percentages at Different Water Contents

5.3.4 Elastic Modulus

In order to look at the effect of breakdown fouling and water content on secant modulus of clean and fouled ballast, the secant modulus of elasticity at 50% of drained shear strength (E50) was evaluated. The effect of water content, confining pressure and fouling percentage on E50 of fouled ballast are discussed in following sections.

5.3.4.1 Effect of Fouling and Confining Pressure

Indraratna et al. (1998), conducted CIDC triaxial tests on coarse and fine particles. They reported that coarser particles result in a considerably higher axial strain upon loading, attributed to larger void ratios and resulting in smaller deformation modulus (Indraratna *et al.*, 1998). They also reported that an increase in confining pressure results in the initial elastic modulus increasing and after 180 kPa (26.1 psi) confining pressure the changes in elastic modulus is insignificant.

A three-dimensional view plot of the effect of confining pressure and fouling on E50 is shown in Figure 5.14. Regardless to moisture condition of ballast, by increase in breakdown fouling, elastic modulus increases. This figure does not show a defined effect of confining pressure on the elastic modulus. Figure 5.15 shows a two-dimensional view of Figure 5.14 at constant water content. This figure indicates that the effect of confining pressure on the elastic modulus in the range used in this study is not significant although the effect of breakdown fouling is significant and clear.

With the assumption of a linear relationship between E50 modulus and fouling percentage, with a 15% increase in breakdown fouling percentage, the modulus increases by 30% regardless of the confining pressure and water content conditions.

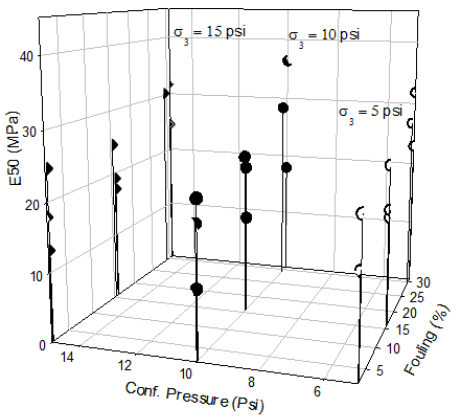

Figure 5.14: Effect of Fouling and Confining Pressure on the Elastic Modulus of Clean and Fouled Ballast

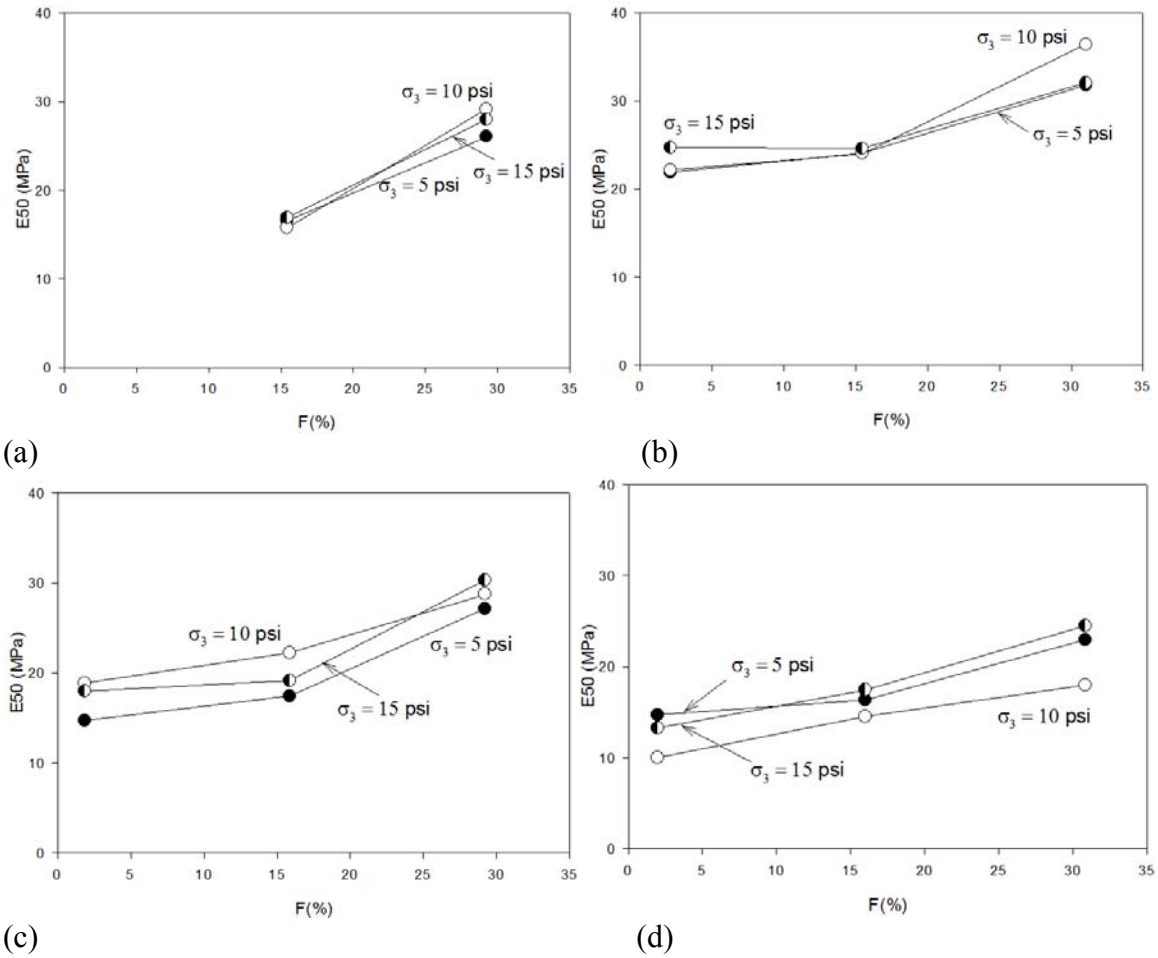

Figure 5.15: Effect of Fouling on E50 Modulus of Ballast at Different Confining Pressures and Constant Water Content (a) Dry (b) w_1 (c) w_2 (d) Field Capacity. Note: w_2 has two studied points in moderately and highly fouled ballast

5.3.4.2 Effect of Water Content

In the last section it was shown that the effect of confining pressure on E50 modulus is not significant, therefore the effect of water content has been shown at constant confining pressure in Figure 5.16. Elastic modulus decreases linearly with the increase in water content (Figure 5.16). This is as the result of greater strain upon loading in moist ballast in comparison with dry ballast. The rate of this reduction is higher in clean ballast in comparison with fouled ballast while it is hard to distinguish between the degradation rate of moderately fouled ballast (F_{15}) from highly fouled ballast (F_{30}). This can be as the result of capillary tension among wet fine particles in fouled ballast and a lesser effect of water on contact area of ballast aggregates.

Regarding to the results of this study, with a 1% increase in water content, E50 decreases 60%, 12% and 8% in clean, moderately and highly fouled ballast, respectively. In a constant confining pressure, 15% increase in fouling will result in approximately an 80% decrease in the rate of E50 reduction versus water content from clean to moderately fouled ballast and a 25% decrease in that rate for moderately to highly fouled ballast.

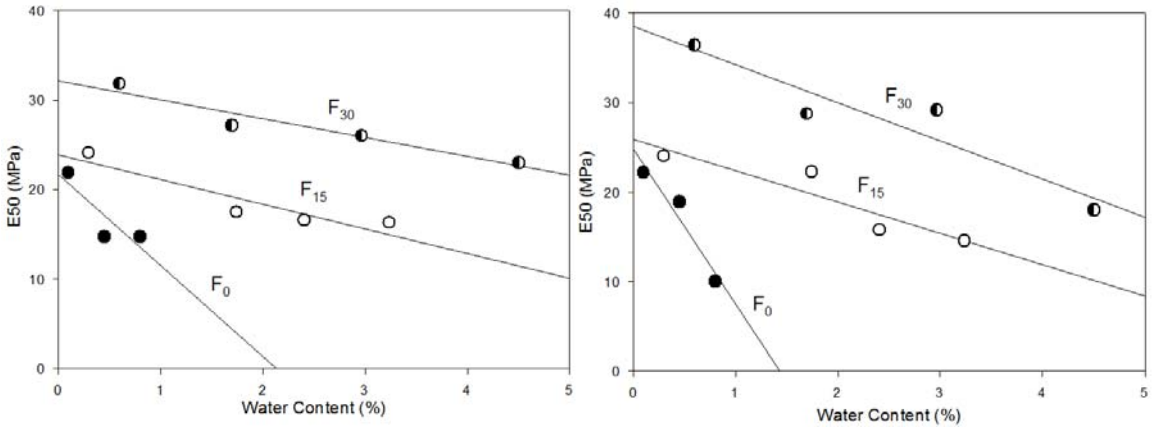

(a) (b)

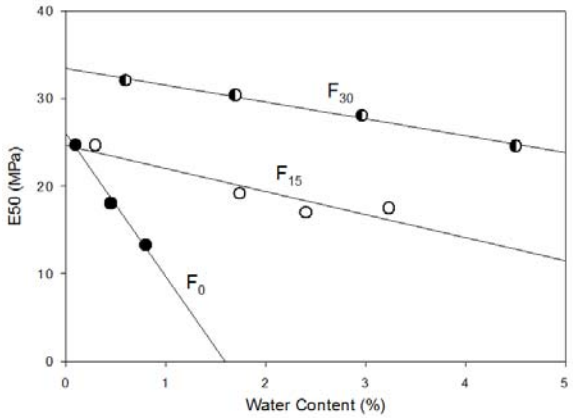

(c)

Figure 5.16: Changes of E50 Modulus vs. Water Content at Different Fouling Conditions (a) 5 psi Confining Pressure (b) 10 psi Confining Pressure (c) 15 psi Confining Pressure

5.3.5 Dilatancy

Previous studies have shown that the rate of volume change at failure decreases with an increase in cell pressure (Billam, 1971). Figure 5.17 shows a typical plot of volume strain changes versus axial strain for the clean ballast of this study at different water content and confining pressures. This figure clearly shows that regardless of the moisture and fouling conditions, an increase in confining pressure the rate of volume strain versus axial strain decreases as expected. In order to study the effect of breakdown fouling and water content quantitatively on the rate of dilation, on volume strain versus axial strain plots (Figure 5.17) slope of the line starting from the peak volume strain and ending at axial strain corresponding to failure has been evaluated.

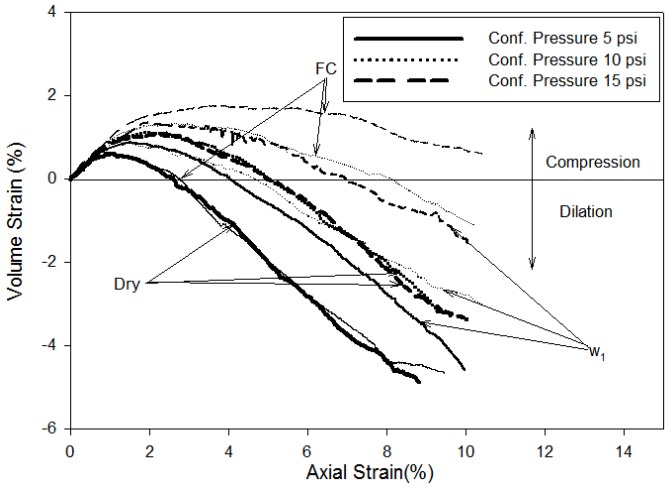

Figure 5.17: Changes of Volume Strain versus Axial Strain for Clean Ballast

5.3.5.1 Effect of Water Content

Charles and Watts (1980), reported that the larger dilation rate of granular materials are associated with the maximum principal stress ratios (Charles & Watts, 1980). Also Indraratna et al. (1998) used a hyperbolic fit to describe the relationship between the ballast dilatancy factor defined as $D_p = 1 - (^{d\varepsilon_v}/_{d\varepsilon_a})$ (Rowe, 1962) and the maximum principal stress ratio (Indraratna *et al.*, 1998). Although the dilatancy rate used in this study, is increasing non-linearly with an increase in maximum principal stress ratio, it is difficult to distinguish between different water contents from this view (Figure 5.18).

Figure 5.19 clearly shows the effect of the confining pressure increase on the volume strain rate reduction, which agrees with literature (Billam, 1971), and presents a better view of the effect of water content on the volume strain rate at constant fouling conditions. In clean ballast by increase in water content the dilatancy volumetric strain rate decreases clearly and the effect of confining pressure on the volumetric strain rate becomes stronger

in samples with higher water contents (Figures 5.17 and 5.19a). Water decreases the interlocking friction of ballast thereby affecting the dilatancy strain rate. In fouled ballast, the increase in water content from dry to field capacity conditions decreases the dilatancy volumetric strain rate with some scatter in intermediate water content conditions (Figures 5.19b and 5.19c). There is no evidence of a defined effect of water content on the volume strain rate-confining pressure relationship based on the results of this study (Figure 5.19).

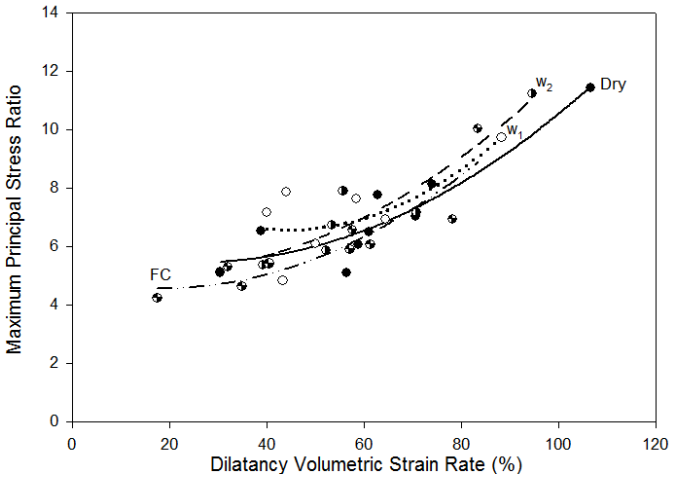

Figure 5.18: Maximum Principal Stress Ratio versus Dilatancy Volumetric Strain Rate at Different Water Contents

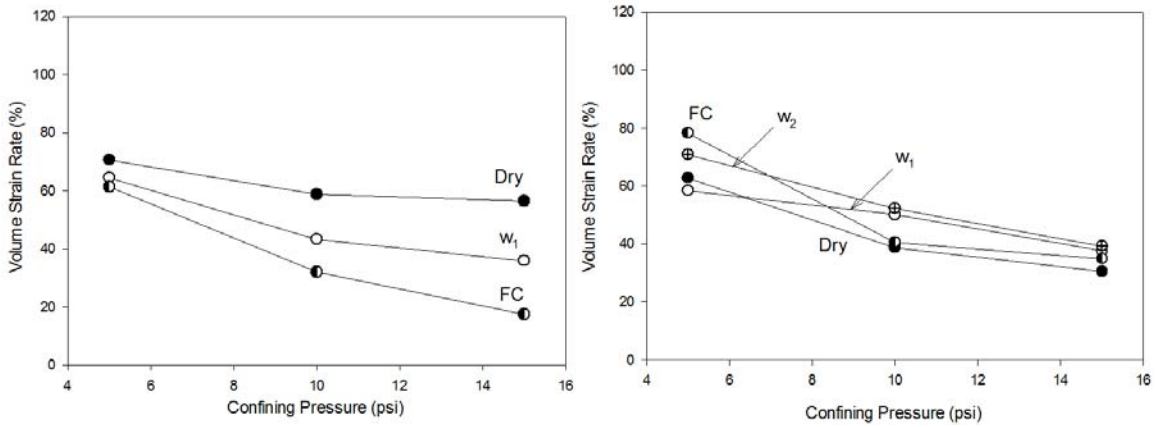

(a) (b)

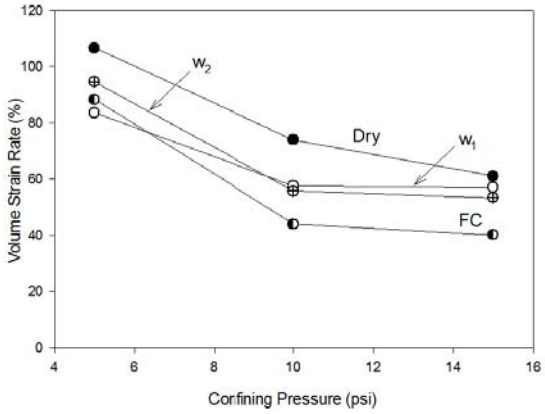

(c)

Figure 5.19: The Dilatancy Volumetric Strain Rate versus Confining Pressure at Different Water Contents and Constant Fouling Conditions (a) Clean Ballast (b) Moderately Fouled Ballast (F_{15}) (c) Highly Fouled Ballast (F_{30})

5.3.5.2 Effect of Fouling

Figure 5.20 presents the change of maximum principal stress ratio versus dilatancy volumetric strain rate (%) for different fouling condition regardless to water content conditions. Unlike water content (Figure 5.18), fouling is significantly affecting the strength-dilatancy relationship. The best hyperbolic fit in Figure 5.20, presents a higher dilatancy volumetric strain rate associated with higher maximum principal stress ratio as the result of higher fouling conditions. Note that this relationship is independent of water content conditions. In comparison with Figure 5.18 it can be concluded that the effect of fouling is more significant on the strength-dilatancy relationship than water content in ballast.

Regarding to Figure 5.21, dilatancy volumetric strain rate increases by increase in breakdown fouling percentages. This is as the result of smaller void ratio of fouled ballast in comparison with clean ballast that leads the sample to higher rate of dilation after the initial compression. There is not a defined effect of breakdown fouling percentage on the volume strain rate -confining pressure relationship based on the results of this study (Figure 5.21).

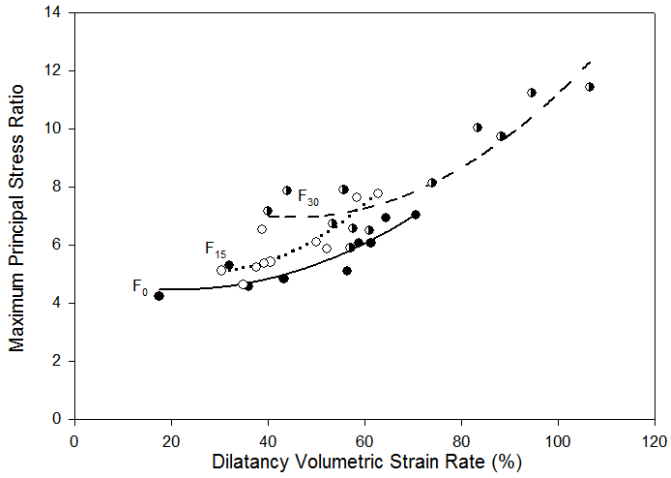

Figure 5.20: Maximum Principal Stress Ratio versus Dilatancy Volumetric Strain Rate at Different Fouling Conditions

5.3.6 Breakage Degree

There have been different methods used for quantifying ballast particles breakage degree using percent passing a single sieve size or changes in grain size distribution (Indraratna *et al.*, 1998, Indraratna *et al.*, 2005, Miura, 1979). In this study in order to evaluate the effect of water content, fouling percentage and confining pressure on breakage degree of ballast particles, both grain size distribution and passing a single sieve size methods are used.

It is obvious that the greater the breakage, the more shift of grain size distribution curve toward smaller particle sizes. Figure 5.22 shows the effect of confining pressure on the shift of grain size distribution for clean and fouled ballast. Qualitatively, this figure shows that under a constant fouling condition, an increase in confining pressure will increase the shift in the grain size distribution curve toward smaller particle sizes, as expected (Indraratna *et al.*, 2005, Salim & Indraratna, 2004). These plots also indicate that by increase in breakdown fouling percentages the grain size distribution shift increases. This is

as the result of higher density and more particle-to-particle contact area in ballast with higher fouling percentages that results in more particle split and corner degradation.

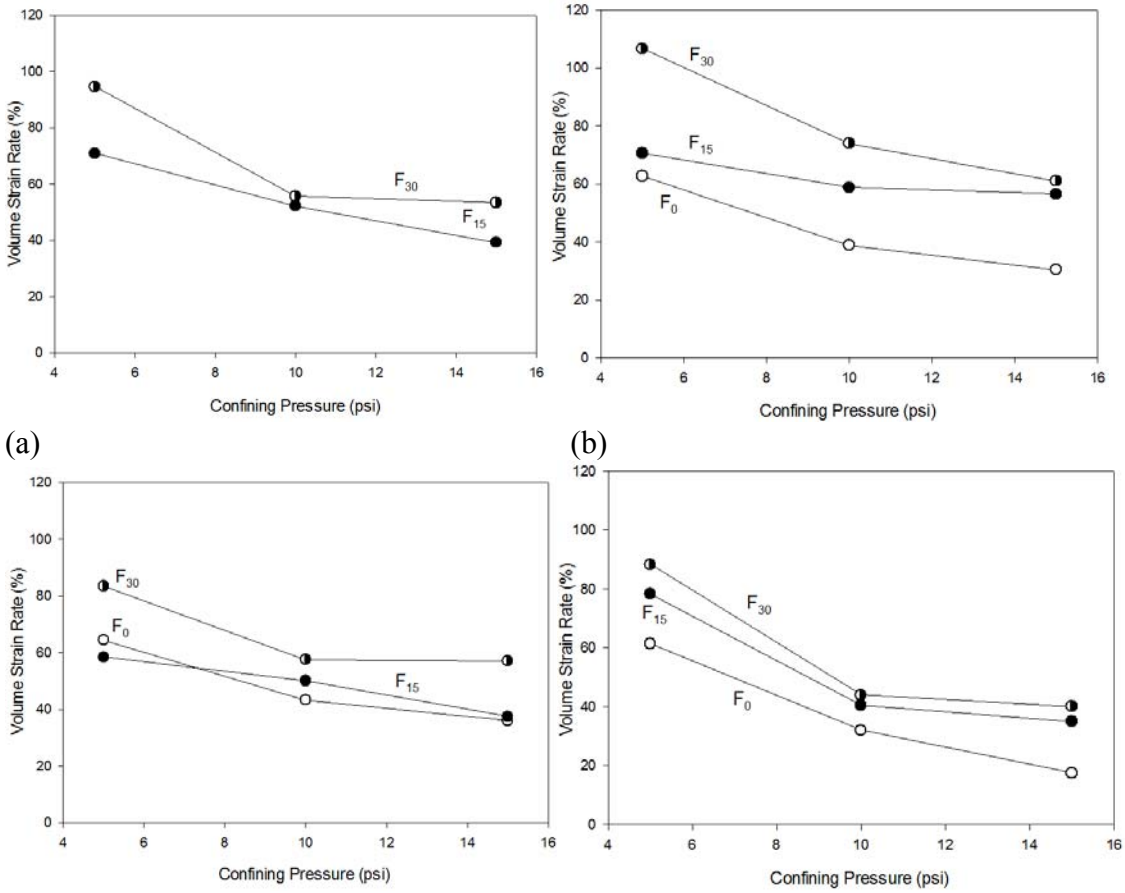

Figure 5.21: The Dilatancy Volumetric Strain Rate versus Confining Pressure at Different Fouling Conditions and Constant Water Content (a) Dry (b) w_1(c) w_2 (d) Field Capacity. Note: w_2 has two studied points in moderately and highly fouled ballast

It can also be seen that most of the breakage in grain size distribution in this study is taking place at grain size range between 1 to 20 millimeters (Figures 22b and 22c). This is outside of the scope of this research but might have agreement with the concept of studies correlating breakage to shape and sizes of particles (McDowell *et al.*, 1996).

The grain size distribution plots of moderately fouled ballast and highly fouled ballast also show that confining pressure changes between 5psi (34.5 kPa) to 10psi (68.9 kPa) has more effect on breakage degree than 10psi (68.9 kPa) to 15psi (103.4 kPa) in this study.

The ranges of confining pressure showing increase in breakage degree in this study also is in agreement with the confining pressure ranges for Optimum Degradation Zone (ODZ) and Compressive, Stable Degradation Zone (CSDZ) defined by Indraratna et al. (2005) (Indraratna *et al.*, 2005).

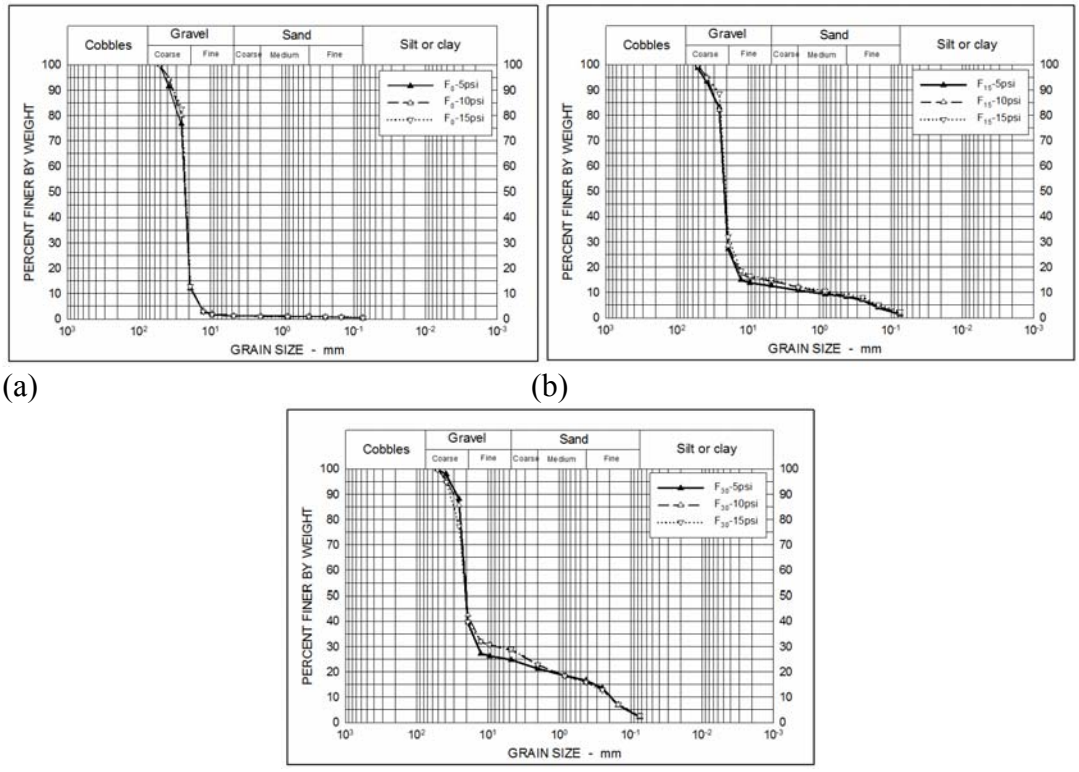

(a) (b)

(c)

Figure 5.22: Effect of Confining Pressure on the Particle Degradation Curve at Different Fouling Conditions (a) Clean Ballast (b) Moderately Fouled Ballast (F_{15}) (c) Highly Fouled Ballast (F_{30})

In order to study the effect of water content on the rate of particle breakage, percent passing 3/8" sieve versus confining pressure at different water contents and constant fouling conditions was plotted (Figure 5.23). The 3/8 inch sieve size was selected because of

separating fouling from ballast based on the fouling percentage definition (Selig & Waters, 1994).

Figure 5.23 indicates that by increase in water content the rate of breakage versus confining pressure decreases. This is as the result of reduction in particle-to-particle contact stress and frictional interlock by increase in water content. Note that Figure 5.23 only has plots for fouled ballast samples. That is because clean ballast samples cannot hold enough water on the particles surface to affect the particle-to-particle contact area. By 1% increase in water content the rate of breakage versus confining pressure decreases in an average of 25-30% in moderately and highly fouled ballast.

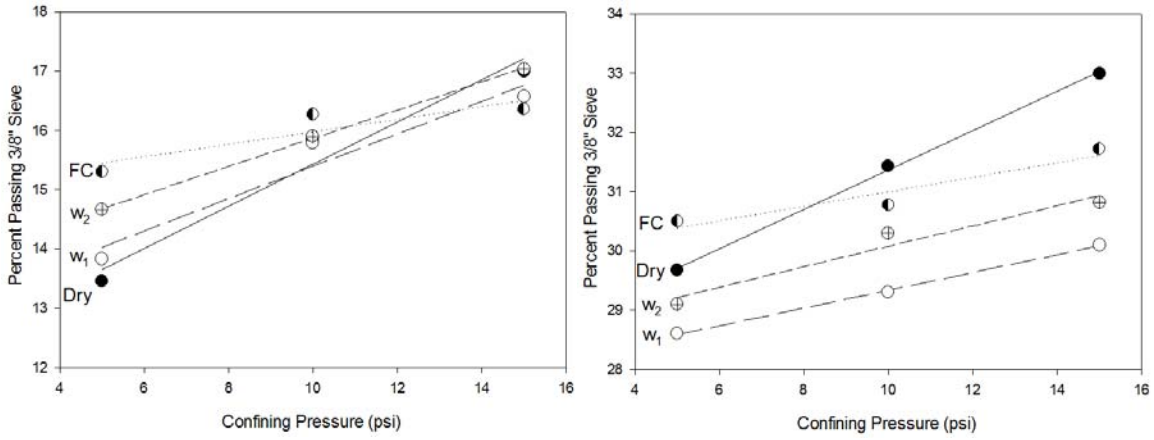

(a) (b)

Figure 5.23: Percent Passing 3/8" Sieve versus Confining Pressure at Different Water Contents and Constant Fouling Conditions (a) Moderately Fouled Ballast (F_{15}) (b) Highly Fouled Ballast (F_{30})

5.3.7 Results Verification with Literature

At low confining pressure, high principal stress ratios have been observed in granular materials. This behavior has been attributed to greater frictional interlock of particles at lower confining pressure (Charles & Watts, 1980, Indraratna *et al.*, 1998, Marachi *et al.*, 1900, Marsal, 1967).

Indraratna et al. (1998) presented the following non-linear equation for the relationship between principal stress ratio and confining pressure:

$$R_p = a(\sigma_3)^b \quad \text{Eq. (5.1)}$$

where R_p is the maximum principal stress ratio, a is the maximum principal ratio at $\sigma_3 = 1$, and b is a constant ratio related to degree of particle degradation.

The changes of maximum principal stress ratio versus confining pressure of this study have been compared with the results from the other researches on granular materials for verification (Figure 5.24). The trend of the stress ratio changes versus confining pressure is in good agreement with the literature and shows a high R squared fitting Eq. (5.1) regardless to the moisture conditions.

Figure 5.24 also indicates that by increase in breakdown fouling, regardless to water content from dry to field capacity condition, the maximum principal stress ratio increases. This is as the result of better packing of particles and was discussed in the *Shear Strength* section.

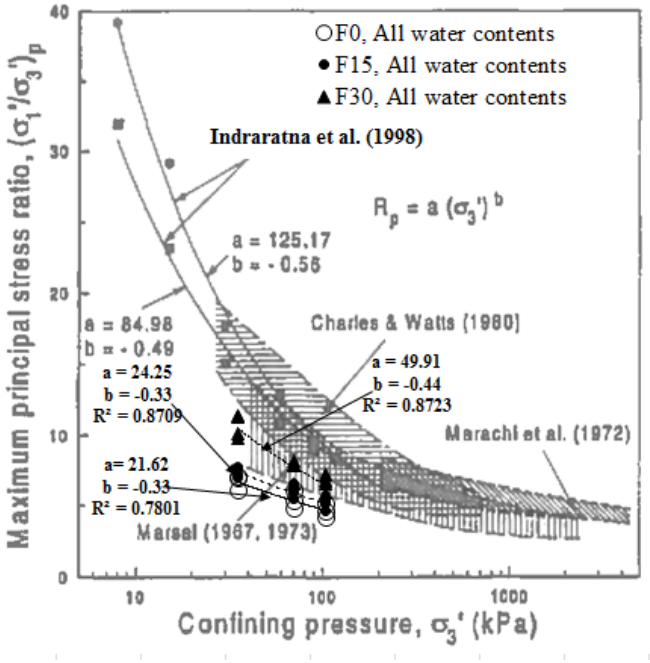

Figure 5.24: Effect of Confining Pressure on the Maximum Principal Stress Ratio for Various Granular Materials and this Study (Indraratna *et al.*, 1998). Note: The upper band is representing values obtained from tests on Basalt

The changes of peak friction angle versus confining pressure for this study and other studies have been presented in Figure 5.25. This plot clearly shows that by increase in confining pressure, the peak friction angle decreases. The results from this study is in good agreement in trend and magnitude with other studies.

Fouling percentage doesn't have a significant effect on the reduction rate of friction angle by increase in confining pressure. The higher values of friction angle at lower

confining pressure is because of interparticle contact stresses which are much below the crushing strenght of granular materials (Indraratna *et al.*, 1998).

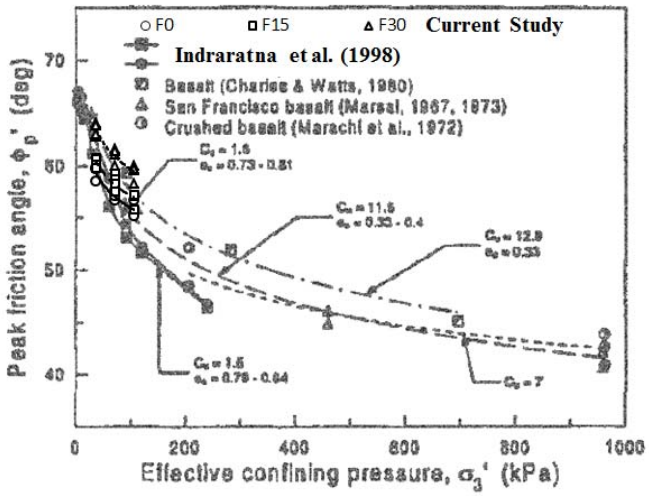

Figure 5.25: Effect of Confining Pressure on the Peak Friction Angle for Various Granular Materials and this Study (Indraratna *et al.*, 1998)

5.4 Ground Penetrating Radar and Deformation Properties

In order to study any existing correlation between deformation properties and electromagnetic properties of fouled ballast, the results from this study were compared with ground penetrating radar (GPR) analysis on fouled ballast with the same grain size distribution and indices properties conducted by Kashani et al. (Kashani *et al.*, 2016) explained in Chapter 3. Kashani et al. (2016) assessed the effect of water content and fouling on time and frequency domain analysis of GPR data by the help of full scale laboratory models. GPR data were collected by using a ground coupled antenna with 450 MHz and 2 GHz frequency antennas. Three models with different breakdown fouling percentages were constructed. Each model was surveyed by GPR at different water contents. The models had all

railroad track components such as sub-ballast, ballast, timber ties and rail to simulate a real track situation.

The index properties of ballast from this study and Kashani et al. (Kashani *et al.*, 2016) study, presented in Chapter 3, are shown in Table 5.2. As it can be seen in Table 5.2 the index properties from these two studies are in a good agreement. This validates the comparison of electromagnetic and deformation properties of the fouled ballast from these two studies. Note that the changes in density in both studies is mostly related to the fouling percentage by keeping the clean ballast in all mixtures constant and adding different percentages of fouling. And also, using any correlation presented in this section for engineering purposes is limited to granite ballast with breakdown fouling and compactness in the same range of density in this study.

Table 5.2: Comparison between the Indices Geotechnical Properties of this Study and Kashani et al. (2016)

Parameters		This Study			Kashani et al. (2016)		
		F_0	F_{15}	F_{30}	Model 1	Model 2	Model 3
Average Fouling (%)		2.0	15.7	30.0	1.3	14.9	27.1
Dry density (kg/m^3)		1561	1958	2133	1555	1921	2117
Measured Water Content from Model Track (%)	Dry	0.1	0.3	0.6	0.1	0.3	0.6
	w_1	0.5	1.7	1.7	0.5	1.6	3.5
	w_2	---	2.4	3.0	0.5	2.1	4.0
	Field Capacity	0.8	3.2	4.5	0.6	3.4	4.6

5.4.1 GPR Wave Propagation and Deformation Properties of Ballast

For this section the GPR data collected with 450 MHz antenna by Kashani et al. (2016) have been used and compared with the results from this study.

5.4.1.1 Dielectric Permittivity and E50 Modulus

Figure 5.26 shows the dielectric permittivity and E50 modulus changes versus water content from Kashani et al. (2016) study, presented in Chapter 3, and this study. As expected, the increase in water content results in an increase in dielectric permittivity (Kashani *et al.*, 2016) and a decrease in E50 modulus (Section 5.3.4). Plots in Figure 26 show the ranges of water content in both studies and the opposite correlation of dielectric permittivity and E50 with water content.

Figure 5.27 shows the correlation between the dependent variables of plots in Figure 5.26. This figure shows that there is a linear correlation between E50 modulus as a deformation property and dielectric permittivity as an electromagnetic property of fouled ballast. In clean ballast because of low water content (<1%) the dielectric permittivity does not change significantly, therefor there is not a defined correlation between E50 and permittivity. By increase in amount of fouling and water held by fouling a linear correlation can be seen between E50 and dielectric permittivity. By increase in dielectric permittivity, E50 modulus decreases and the rate of this reduction increases by increase in amount of fouling. This plot can be used to predict the approximate amount of ballast modulus from known dielectric permittivity, which can be measured by GPR trace travel time, and known fouling percentages, which can be well predicted by GPR data analysis.

Regarding to the results of this study, in breakdown fouled ballast at moist conditions (not dry or saturated) 1 unit increase in the amount of dielectric permittivity results in 9 to 12% decrease in E50 modulus.

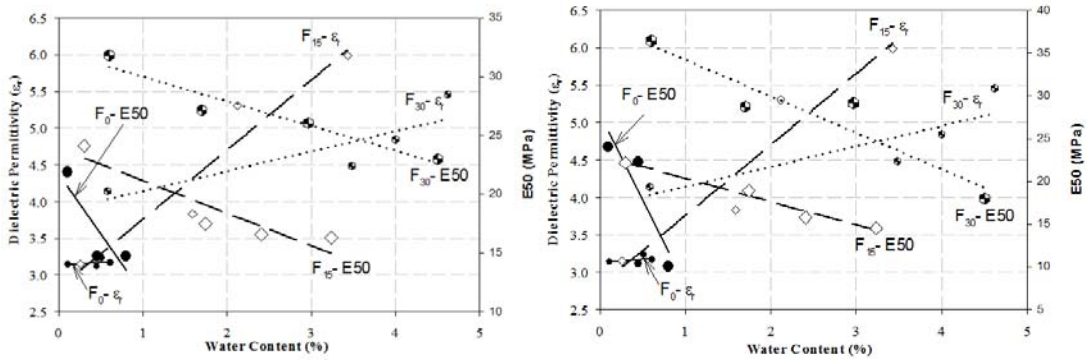

(a) (b)

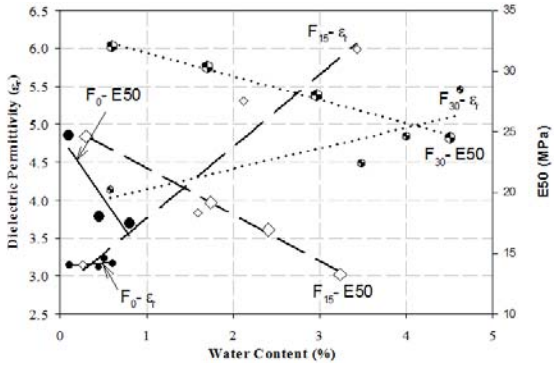

(c)

Figure 5.26: Changes of Dielectric Permittivity and E50 Modulus versus Water Content Changes at different Fouling Conditions and Confining Pressures (a) 5 psi Confining Pressure (b) 10 psi Confining Pressure (c) 15 psi Confining Pressure Note: Larger Markers Show E50 and Smaller Markers Show Dielectric Permittivity

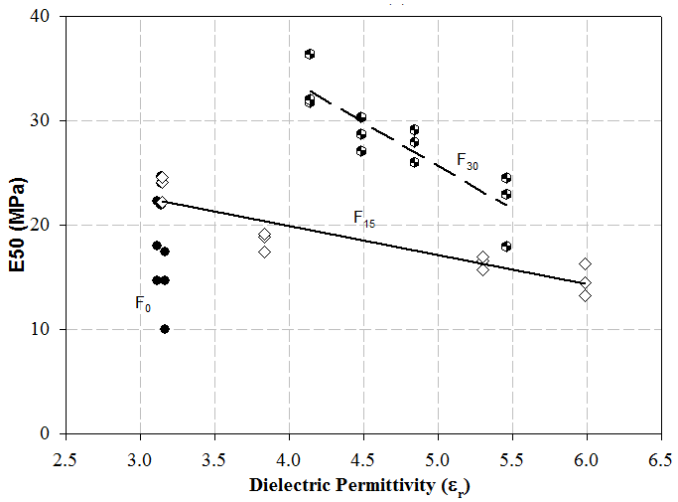

Figure 5.27: Changes of E50 Modulus versus Dielectric Permittivity at Different Fouling Conditions

5.4.1.2 Wave Propagation Velocity and E50 Modulus

Regarding to the Maxwell's equation, dielectric permittivity is oppositely related to propagation velocity of an electromagnetic wave with a constant factor of the speed of light. Therefore, the relationship between E50 modulus and propagation velocity is expected to be the opposite of E50 and dielectric permittivity.

Figure 5.28 is showing the changes of electromagnetic signal propagation velocity and E50 modulus versus water content changes from this study and Chapter 3 (Kashani *et al.*, 2016).

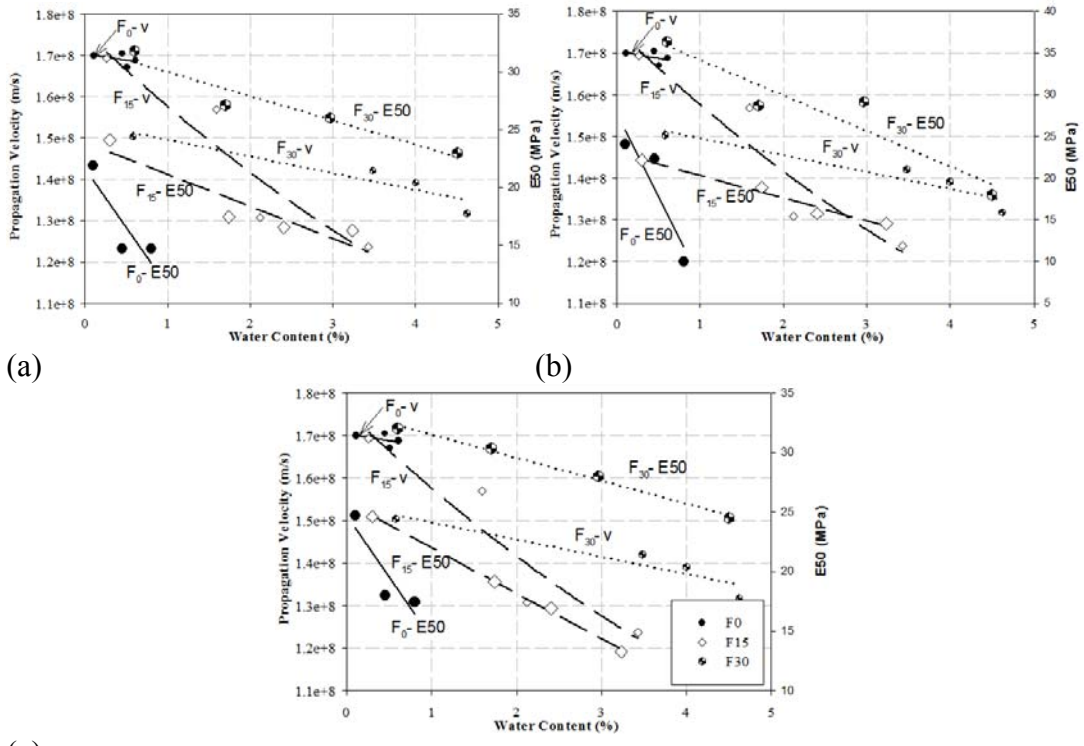

Figure 5.28: Changes of Propagation Velocity and E50 Modulus versus Water Content Changes at different Fouling Conditions and Confining Pressures (a) 5 psi Confining Pressure (b) 10 psi Confining Pressure (c) 15 psi Confining Pressure Note: Larger Markers Show E50 and Smaller Markers Show Propagation Velocity

Figure 5.29 shows the correlations of the dependent variables of plots in Figure 5.28. This figure shows a linear relationship between E50 modulus as a deformation property and electromagnetic wave propagation velocity as an electromagnetic property of fouled ballast. Note that there is not a defined correlation at clean ballast condition. That is because of less water held by clean ballast (<1%) and insignificant changes of wave propagation velocity by increase in fouling at dry conditions. As it was also discussed in the previous section, this plot might be used for predicting the E50 modulus of fouled ballast by measuring the ballast dielectric permittivity (or propagation velocity) and fouling percentage. These parameters can easily be measured by GPR as a non-destructive testing tool.

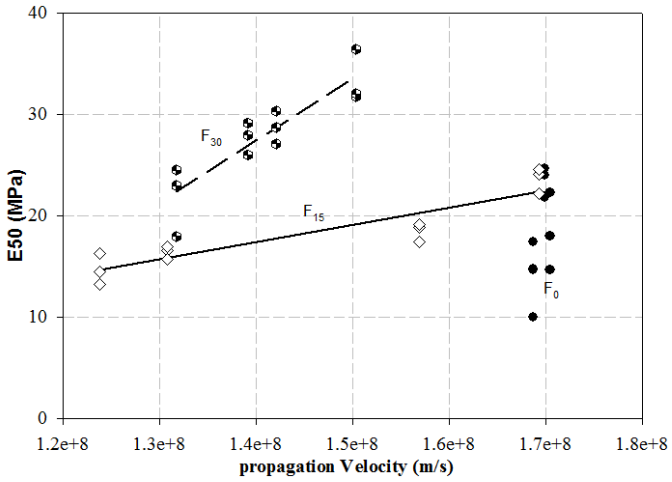

Figure 5.29: Changes of E50 Modulus versus Propagation Velocity at Different Fouling Conditions

5.4.2 GPR Frequency Spectrum Analysis and Deformation Properties of Ballast

5.4.2.1 Fast Fourier Transform and E50 Modulus at Dry Conditions

Studies conducted by Clark et al. (2004), Silvast et al. (2006), Al-Qadi et al. (2010) and Kashani et al. (2016) provided valuable information evaluating the effect of fouling and water content on frequency spectrum analysis (Al-Qadi *et al.*, 2010, Clark *et al.*, 2004,

Kashani *et al.*, 2016, Silvast *et al.*, 2006). In accordance with the frequency analysis on GPR traces using 2 GHz antenna by Kashani et al. (2016) on the same samples of this study, and the triaxial test results of this study some correlations has been evaluated and discussed as following.

Increase in amount of fouling at dry conditions (or increase in density) doesn't have a significant effect on time domain analysis (Kashani *et al.*, 2016). Figure 5.30a shows how increase in dry density, as the result of more fouling, will increase the modulus of ballast (Section 5.3.4) and will decrease the normalized area under Fast Fourier Transform (FFT) plot from GPR analysis. The correlation between average E50 modulus from this study and average normalized area under FFT plot from GPR data analysis is presented in Figure 5.30b. This figure shows that by increase in modulus at dry condition, the normalized area under FFT plot decreases. This is as the result of more energy of GPR signal absorbed by an increase in the amount of fouling filling the voids that significantly affects the area under FFT plot from clean to fouled ballast.

This behavior is not linear. The reduction amount of normalized area under FFT plot from clean to moderately fouled ballast (F_{15}) is much higher than moderately fouled ballast (F_{15}) to highly fouled ballast (F_{30}). It seems that replacing air voids with fouling material from clean to F_{15} has a much more significant effect on the signal energy absorption than adding more fouling to voids from F_{15} to F_{30}.

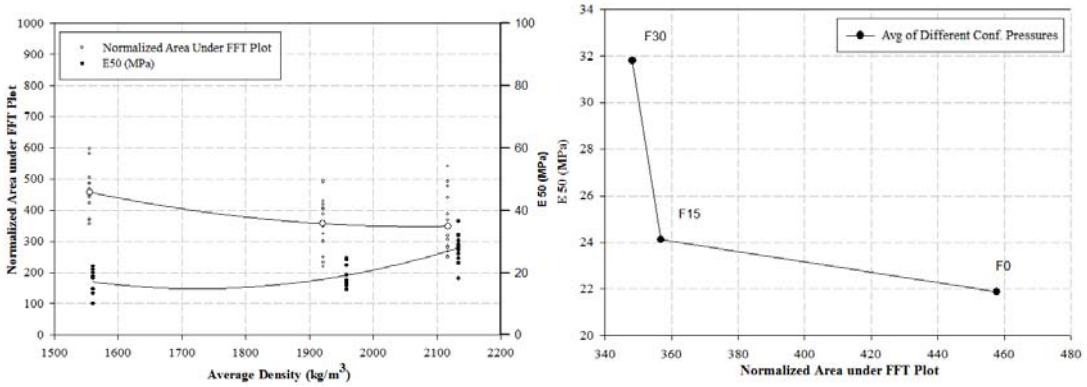

(a) (b)

Figure 5.30: (a) Effect of Density on Normalized Area under FFT Plot from GPR Analysis and E50 Modulus from Triaxial Tests at Dry Conditions (b) The Correlation between E50 Modulus from Triaxial Tests and Normalized Area under FFT Plot from GPR at Dry Condition

5.4.2.2 Fast Fourier Transform and E50 Modulus at Constant Fouling Conditions

An increase in amount of water content might change the correlation trend between E50 modulus and area under FFT plot (Figures 5.30b and 5.32). This is because both water and fouling decrease the energy of the GPR signal by filling air voids volumetrically but, fouling and water content affect ballast strength properties oppositely.

Although by comparing the small markers in Figure 5.31 with Figures 5.26 and 5.28 indicates that the effect of water content on GPR signal time domain analysis is significantly more evident than frequency domain analysis (Kashani *et al.*, 2016), using frequency spectrum analysis for evaluating deformation properties of ballast is strongly related to water content conditions.

Figure 5.31 shows the effect of water content on both the area under FFT plot from GPR tests and the E50 modulus from triaxial tests at different confining pressure conditions. Figure 5.32 shows an increase in normalized area under FFT plot versus increase in E50 modulus at different water content conditions and constant fouling conditions. The

rate of E50 modulus changes versus area under FFT plot increases by increase in Fouling percentage.

Note that careful control needed in using these correlations because of significant effect of both fouling and moisture on electromagnetic and deformation properties of ballast. One of these index properties (moisture or density) should be kept constant to evaluate the correlation between E50 and area under FFT plot.

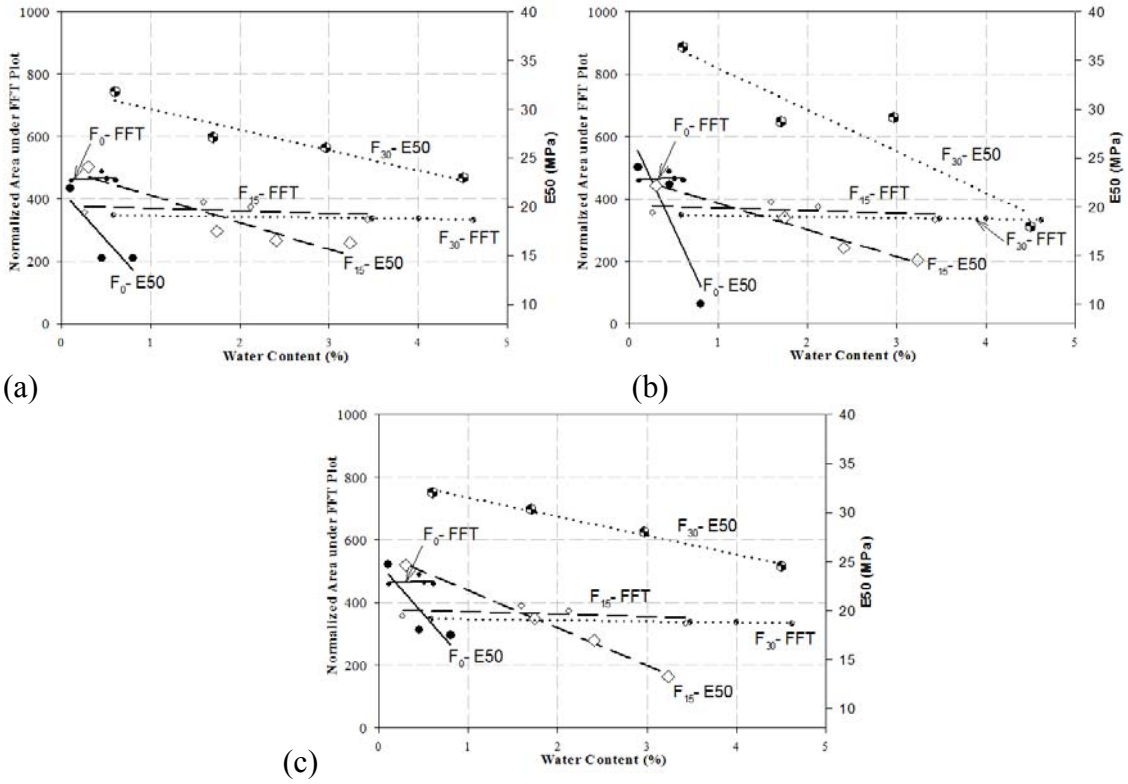

Figure 5.31: Changes of Normalized Area under FFT Plot and E50 Modulus versus Water Content Changes at different Fouling Conditions and Confining Pressures (a) 5 psi Confining Pressure (b) 10 psi Confining Pressure (c) 15 psi Confining Pressure Note: Larger Markers Show E50 and Smaller Markers Show Area under FFT Plot

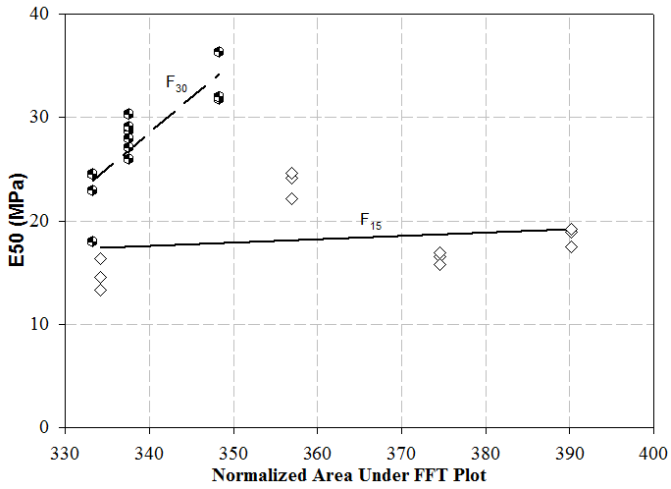

Figure 5.32: The Correlation between E50 Modulus from Triaxial Tests and Normalized Area under FFT Plot from GPR at Constant Fouling Conditions

5.4.3 GPR Time Domain Analysis and Deformation Properties of Ballast

5.4.3.1 The GPR trace and E50 Modulus at Constant Dry Conditions

Ballast under different fouling and water content conditions generates different electromagnetic scattering patterns (Al-Qadi *et al.*, 2008, Kashani *et al.*, 2016). Using the time domain analysis of GPR traces using 2 GHz antenna by Kashani et al. (2016)(Kashani *et al.*, 2016) on the same samples of this study, and the triaxial test results some correlations has been evaluated and discussed as following.

Figure 5.33a shows that an increase in dry density (increase in fouling percentage), decreases the area under squared amplitude of GPR traces and increases the E50 modulus from triaxial tests (Section 5.3.4). This is expected because less air voids in ballast results in less scatter in GPR traces, and better grain size distribution results in higher modulus in traixial test results. Figure 5.33b indicates that there is a correlation between dependent

variables of Figure 5.33a. An increase in E50 modulus results in scatter reduction of GPR traces under constant water content conditions.

Regarding to the results of this study, a 50% increase in the amount of area under squared amplitude of GPR traces results in a 15% decrease in E50 modulus of ballast at dry conditions (Water content <1%). This is valid when the changes in area under squared amplitude of GPR traces is only attributed to an increase in breakdown fouling at dry conditions.

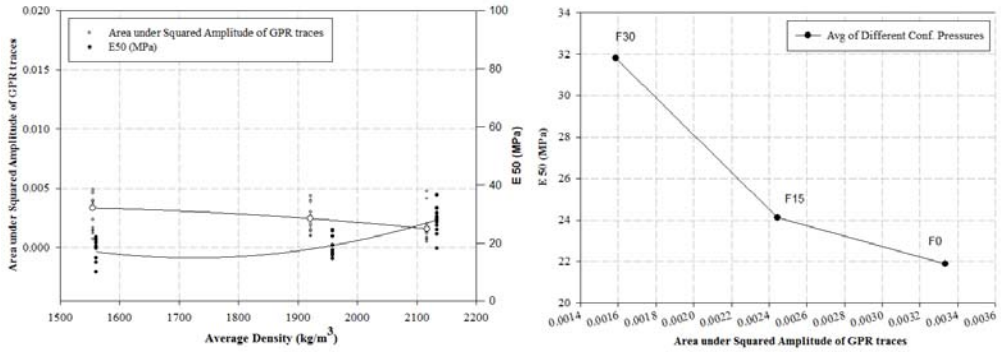

(a) (b)

Figure 5.33: (a) Effect of Density on the Area under Squared Amplitude of GPR traces and E50 Modulus from Triaxial Tests at Dry Conditions (b) The Correlation between E50 Modulus from Triaxial Tests and Area under Squared Amplitude of GPR traces at Dry Conditions

5.4.3.2 The GPR trace and E50 Modulus at Constant Fouling Conditions

Figures 5.34 and 5.35 show that the trend presented in Figure 5.33b is only valuable for constant water content conditions. Because an increase in the amount of water content will still keep reducing the area under squared amplitude of GPR traces while the modulus of fouled ballast tends to decrease with the increase in moisture. Figure 5.35 can be used to evaluate the correlation between GPR traces and ballast modulus at constant fouling conditions and different moisture conditions.

As mentioned in the last section, careful control is needed in using these correlations because of significant effect of both fouling and moisture on electromagnetic and deformation properties of ballast. One of these index properties (moisture or density) should be kept constant to evaluate the correlation between E50 and area under squared amplitude of GPR traces.

Regarding to the results of this study, a 50% increase in the amount of area under squared amplitude of GPR traces results in a 30-60% increase in E50 modulus of ballast under wet conditions (not dry or saturated). This is valid for the condition that changes in the area under squared amplitude of GPR traces is only attributed to an increase in water content at constant fouling conditions.

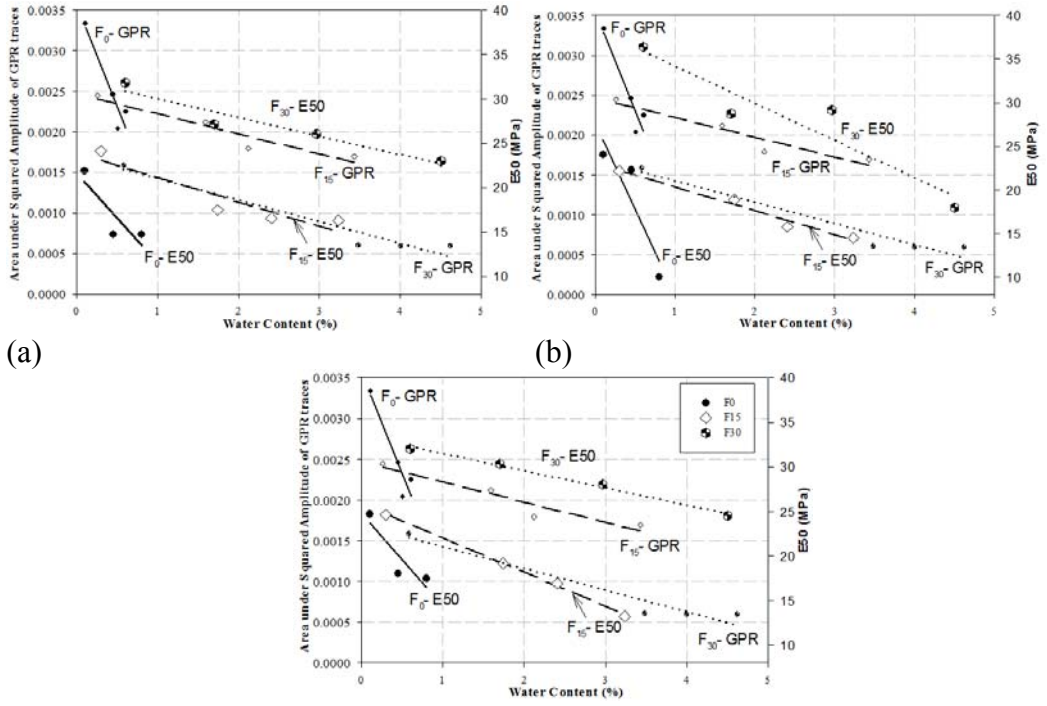

(a) (b)

(c)

Figure 5.34: Changes of Area under Squared Amplitude of GPR traces and E50 Modulus versus Water Content Changes at different Fouling Conditions and Confining Pressures (a) 5 psi Confining Pressure (b) 10 psi Confining Pressure (c) 15 psi Confining Pressure Note: Larger Markers Show E50 and Smaller Markers Show the Area under Squared Amplitude of GPR traces

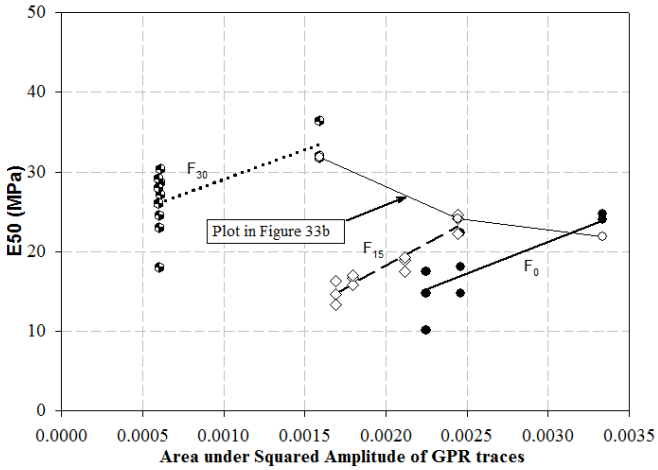

Figure 5.35: The Correlation between E50 Modulus from Triaxial Tests and Area under Squared Amplitude of GPR traces at Constant Fouling Conditions

5.4.4 Max Shear Strength of Ballast and GPR analyses

In order to be able to predict the approximate maximum shear strength of clean and fouled ballast from GPR data analysis and this study, the relationship between E50 modulus and maximum shear strength of all tested samples is presented in Figure 5.36. The dashed line shows the average trend; the solid lines show the prediction intervals of 95% of the data.

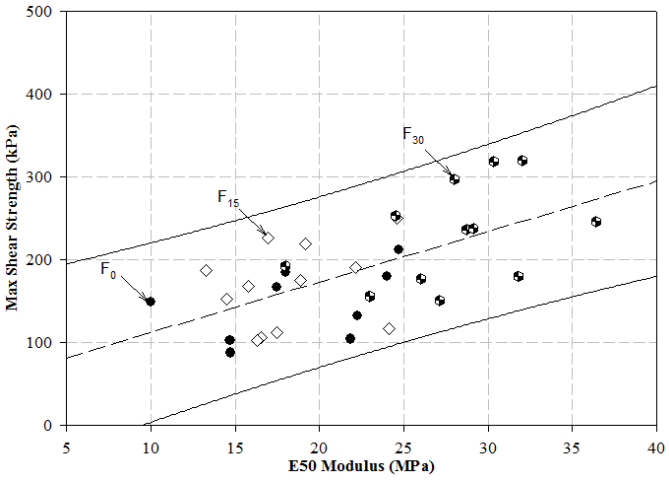

Figure 5.36: Relationship between E50 Modulus and Max Shear Strength of Clean and Fouled Ballast by Traiaxial Tests at all Moistures

5.5 Conclusion

Large scale static drained triaxial tests were performed on clean and breakdown fouled ballast at different water content conditions to evaluate the effect of these two parameters on deformation properties of ballast. Based on the triaxial test results, the effects of water content, fouling percentage and confining pressure on ballast deformation properties were discussed and evaluated qualitatively and quantitatively.

Also, analyses on Ground Penetrating Radar (GPR) data acquired from surveys on full-scale laboratory models with the geotechnical indices properties same as this study were used to evaluate any existing correlation between electromagnetic and deformation properties of ballast. This assessment was also discussed in this study and some correlations have been suggested for estimating ballast's elastic modulus and maximum shear strength by GPR data analysis. In regards to this study the following conclusions can be drawn:

- By increasing water content the maximum shear strength of ballast decreases linearly and the rate of this decrease is affected by confining pressures and Fouling percentages.
- Interestingly, increase in breakdown fouling is not resulting in strength loss in constant water content and water held by fouling is the main reason for ballast degradation.
- Regardless to confining pressure and water content conditions, approximately a 15% increase in breakdown fouling percentage might result in 30% increase in elastic modulus of ballast.

- By increasing breakdown fouling friction degree increases non-linearly and water content does not have a significant effect on the rate of this behavior.
- By increasing water content friction angle decreases and the rate of this reduction decreases by increase in breakdown fouling.
- Elastic modulus decreases linearly by increase in water content and the rate of this reduction is higher in clean ballast in comparison with fouled ballast.
- The effect of fouling on the relationship between ballast strength and volumetric strain rate during dilation is more significant than water content.
- An increase in confining pressure results in an increase in ballast breakage. The more the water content the less the rate of breakage versus confining pressure.
- There is a linear correlation between E50 modulus (and maximum shear strength) and dielectric permittivity (and wave propagation velocity) of fouled ballast at wet conditions.
- With an increase in dielectric permittivity, E50 modulus (and maximum shear strength) decreases and the rate of this reduction is higher in highly fouled ballast than moderately fouled ballast.
- With an increase in wave propagation velocity, E50 modulus (and maximum shear strength) increases and the rate of this change is higher in highly fouled ballast than moderately fouled ballast.
- There are correlations between E50 modulus (and maximum shear strength) of fouled ballast and time domain and frequency spectrum analyses of GPR data. However, using these correlations needs awareness of indices properties of ballast.

CHAPTER 6

CONCLUSIONS AND FUTURE WORK

6.1 Conclusions

This research was conducted to investigate the effects of water content and breakdown fouling percentage on the electromagnetic and static and dynamic mechanical properties of ballast. The study also involved evaluating any existing correlation between electromagnetic and deformation properties of ballast that can be used to predict the mechanical behavior of ballast by Ground Penetrating Radar (GPR). The principal results from this research work are as follows:

1. An increase in breakdown fouling will increase the field capacity water content. This behavior is a linear behavior. Based on experiments in this study a plot (Figure 3.4) has been presented for estimating field capacity water content based on fouling percentages.
2. Comparing the attenuated GPR signal energy in dry samples shows that the effect of density on the frequency spectrum analysis is significantly more evident than in time domain analysis of GPR data.
3. Moisture and density affect the magnitude of the frequency spectrum amplitude of GPR data analysis. A few percentage points increase in water content has more effect on peak magnitude than about 36% change in density in dry condition.
4. Standard deviation of GPR wave amplitude and area trapped by scattered wavelets are both showing a promising trend by changes in density and moisture.

These parameters can be used for water and fouling quantification in GPR time domain analyses.

5. For ballast with the same material properties used in this study, Selig et al.'s equation for predicting the ballast settlement (Eq. (4.3)) is valid for clean and fouled ballast from dry to field capacity conditions. In addition, the results show that Selig et al.'s equation is not appropriate for saturated conditions.
6. Highly fouled ballast at heavy rainfall and high traffic conditions has the risk of significant settlement. In highly fouled ballast, the rate of settlement (in./cycles) at saturated conditions can increase up to 50 times of field capacity conditions.
7. In moderately and highly fouled ballast at moisture contents ranging from dry to field capacity, the effect of compaction from traffic is more significant than degradation by moisture increase on the ballast strength. However, at saturated conditions, the effect of moisture overcomes the effect of traffic compaction and this is because of insufficient hydraulic conductivity to allow the dissipation of excess pore water pressure.
8. In moderately and highly fouled ballast, about a 3% increase in the amount of water content can triple the elastic deformation by traffic accumulation.
9. Interestingly, increase in breakdown fouling is not resulting in strength loss in constant water content and water held by fouling is the main reason for ballast degradation.

10. There is a linear correlation between E50 modulus (and maximum shear strength) and dielectric permittivity (and wave propagation velocity) of fouled ballast at wet conditions.
11. By an increase in dielectric permittivity or decrease in GPR wave propagation velocity, E50 modulus (and maximum shear strength) decreases and the rate of this reduction is higher in highly fouled ballast than moderately fouled ballast.
12. There are correlations between E50 modulus (and maximum shear strength) of fouled ballast and time domain and frequency spectrum analyses of GPR data. However, using these correlations needs awareness of indices properties of ballast.

6.2 Anticipated Contribution to the Railroad Geotechnical Community

The results of this study can be used in the railroad geotechnics in the aspects of the following:

- Performance of both GPR survey and geotechnical tests on the same clean, medium fouled and highly fouled ballast can help developing correlations between mechanical and electrical properties of ballast
- Collection of data and development of a complete static and dynamic geotechnical testing program on ballast samples with different breakdown fouling percentages and water contents can be used to improve the understanding of ballasted railroad track risk factors
- Determination of deformation and strength characteristics of fouled track ballast will result in better assessment of the train risk when fouling is observed

- Collection of GPR and geotechnical data in different fouling percentages can help developing standards for detecting the railroad high risk areas by GPR survey
- Data collection by static and dynamic tests in different water contents will simulate loading from heavy rainfall condition to dry condition
- Investigation of the effect of cycles of load on the track settlement rate in different fouling percentages can be used in train passing simulations
- Measurement of deformation properties of ballast with different fouling percentages and moisture contents can be used in ballasted track computer models

6.3 Future work

The full-scale laboratory models for GPR survey with trapezoidal section area and defined boundary conditions were tested, refined and showed promising results. Also the results from dynamic loading of new ballast box test with modified dimensions represent a good agreement with the actual field measurements. In addition, there are correlations between electromagnetic and mechanical properties of ballast that can be used to predict the ballast behavior by performing Non-Destructive Tests (NDT) such as GPR. However, more tests are needed to be performed to obtain more points for defining strong correlations and GPR calibration in different conditions. The following are some suggestions for future research:

1. Perform GPR surveys on the full-scale laboratory models with different types of ballast and fouling and with higher amount of water content;
2. Build a stronger full-scale box test with materials that do not reflects GPR signals such as concrete and a large load frame for performing dynamic load immediately

after GPR survey. This will minimize the correlation errors between electromagnetic and mechanical properties of ballast;

3. Perform the dynamic box test on different types of ballast and fouling;
4. Modify the box by adding transducers on the internal walls for measuring the confining pressures while loading. And also using Matrix Based Tactile Surface Sensors (MBTSS) under the tie section to assure the application of designed equivalent load;
5. Perform trixial tests on different types of ballast and fouling. Comparing their results with GPR data analyses on the same material and conditions.

BIBLIOGRAPHY

Al-Qadi, I. L., Xie, W., & Roberts, R. (2008). Time-Frequency Approach for Ground Penetrating Radar Data Analysis to Assess Railroad Ballast Condition. Research in Nondestructive Evaluation, 19(4), 219-237.

Al-Qadi, I. L., Xie, W., Roberts, R., & Leng, Z. (2010). Data Analysis Techniques for GPR Used for Assessing Railroad Ballast in High Radio-Frequency Environment. Journal of Transportation Engineering, 136(4), 392-399.

Alva-Hurtado, J. E. D. (1980). A Methodology To Predict The Elastic and Inelastic Behavior of Railroad Ballast. Ph D Dissertation, University of Massachusetts.

ASTM. (2008) Annual Book of Standards, Volume 04.08, Soil and Rock (II): D5714 - Latest. ASTM, Philadelphia, PA.

Anbazhagan, P., Bharatha, T., & Amarajeevi, G. (2012). Study of Ballast Fouling in Railway Track Formations. Indian Geotechnical Journal, 42(2), 87-99.

Anbazhagan, P., Indraratna, B., Rujikiatkamjorn, C., & Su, L. (2010). Using a Seismic Survey to Measure the Shear Modulus of Clean and Fouled Ballast. Geomechanics and Geoengineering: An International Journal, 5(2), 117-126.

Anbazhagan, P., Lijun, S., Buddhima, I., & Cholachat, R. (2011). Model Track Studies on Fouled Ballast Using Ground Penetrating Radar and Multichannel Analysis of Surface Wave. Journal of Applied Geophysics, 74(4), 175-184.

AREMA. (2010). Manual for Railway Engineering. American Railway Engineering & Maintenance-of-way Assoc.

Aursudkij, B., McDowell, G. R., & Collop, A. C. (2009). Cyclic Loading of Railway Ballast Under Triaxial Conditions and in a Railway Test Facility. Granular Matter, 11(6), 391-401. doi: 10.1007/s10035-009-0144-4

Balanis, C. A. (1989). Advanced Engineering Electromagnetics (Vol. 20): Wiley New York.

Bednarczyk, Z. (2008). Application of GPR Scanning for Landslide Investigations in Polish Carpathians. Paper presented at the 14th European Meeting of Environmental and Engineering Geophysics.

Benedetto, A., Benedetto, F., & Tosti, F. (2012). Gpr Applications for Geotechnical Stability of Transportation Infrastructures. Nondestructive Testing and Evaluation, 27(3), 253-262.

Bennett, K. C., Ho, C. L., & Nguyen, H. Q. (2011). Verification of Box Test Model and Calibration of Finite Element Model Evaluation of Railroad Ballast Performance. Transportation Research Record(2261), 171-177. doi: 10.3141/2261-20

Billam, J. (1971). Some Aspects of the Behaviour of Granular Materials at High Pressures. Paper Presented at The Proceeding Of The Roscoe Memorial Symposium, Cambridge.

Brown, S. F. (1974). Repeated Load Testing of a Granular Material. Journal of the Geotechnical Engineering Division, 100(GT7), 825-841.

Budiono, D., McSweeney, T., Dhanasekar, M., & Gurung, N. (2004). The Effect of Coal Dust Fouling on The Cyclic Behaviour of Railtrack Ballast. Cyclic Behaviour of Soils and Liquefaction Phenomena. Taylor & Francis Group, London.

Chang, C., and Selig, E. T. (1980). GEOTRACK Model for Railroad Truck Performance. Journal of Geotechnical Engineering Division, 106(11), 1201-1218.

Charles, J. A., & Watts, K. (1980). The Influence of Confining Pressure on the Shear Strength of Compacted Rockfill. Geotechnique, 30(4), 353-367.

Chen, L.S. (1948). An Investigation Of Stress-Strain and Strength Characteristics of Cohesionless Soils by Triaxial Compression Tests. Proceeding of 2nd ICSMFE, Rotterdam, 5, 35-43.

Chrismer, S. M. (1986). Considerations of Factors Affecting Ballast Performance. American Railway Engineering Association, 87.

Clark, M., Gillespie, R., Kemp, T., McCann, D., & Forde, M. (2001). Electromagnetic Properties of Railway Ballast. NDT & E International, 34(5), 305-311.

Clark, M., Gordon, M., & Forde, M. C. (2004). Issues Over High-Speed Non-Invasive Monitoring of Railway Trackbed. NDT & E International, 37(2), 131-139.

Colla, C., Burnside, C., Clark, M., Broughton, K., & Forde, M. (1998). Comparison of Laboratory and Simulated Data for Radar Image Interpretation. NDT & E International, 31(6), 439-444.

Collingwood, B. (1988). An Investigation of the Cause of Railroad Ballast Fouling. Master of Science Degree Project Report No. AAR88-350P. University of Massachusetts.

Conyers, L. B., & Goodman, D. (1997). Ground-Penetrating Radar: AltaMira Press.

Cosenza, P., Marmet, E., Rejiba, F., Cui, Y. J., Tabbagh, A., & Charlery, Y. (2006). Correlations between Geotechnical and Electrical Data: A Case Study at Garchy in France. Journal of Applied Geophysics, 60(3), 165-178.

Costa, A. (2006). Permeability-Porosity Relationship: A Reexamination of the Kozeny-Carman Equation Based on a Fractal Pore-Space Geometry Assumption. Geophysical Research Letters, 33(2).

Courcelles, B., Modaressi-Farahmand-Razavi, A., Gouvenot, D., & Esnault-Filet, A. (2010). Influence of Precipitates on Hydraulic Performance of Permeable Reactive Barrier Filters. International Journal of Geomechanics, 11(2), 142-151.

Coutinho, R. Q., & Mayne, P. W. (2012). Geotechnical and Geophysical Site Characterization 4: CRC Press.

Daniels, D. J. (1996). Surface-penetrating radar. Electronics & Communication Engineering Journal, 8(4), 165-182.

Daniels, D. J. (2005). Ground penetrating radar. Wiley Online Library.

Diyaljee, V. A. (1987). Effects of Stress History on Ballast Deformation. Journal of Geotechnical Engineering, 113(8), 909-914.

Dombrow, W., Huang, H., & Tutumluer, E. (2009). Comparison of Coal Dust Fouled Railroad Ballast Behavior—Granite vs. Limestone. Paper Presented at the Bearing Capacity of Roads, Railways and Airfields. 8th International Conference (BCR2A'09).

Ebrahimi, A., Tinjum, J. M., and Edil, T. B. (2010). Large-Scale Cyclic Triaxial Testing of Rail Ballast. Paper presented at the Proceedings of the AREMA Annual Conference, Orlando, Florida.

Feldman, F., & Nissen, D. (2002). Alternative Testing Method for the Measurement of Ballast Fouling: Percentage Void Contamination. Conference on Railway Engineering, Nov 10-13, Australia, 101-111.

Fernandes, F. M., Pereira, M., Correia, A. G., Caldeira, L., & Lourenço, P. B. (2008). Assessment of Layer Thickness and Uniformity in Railway Embankments with Ground Penetrating Radar, 1st International Conference on Transportation Geotechnics, 786-790.

Fortunato, E., Pinelo, A., & Fernandes, M. M. (2010). Characterization of the Fouled Ballast Layer in the Substructure of a 19th Century Railway Track under Renewal. Soils and foundations, 50(1), 55-62.

Freeme, C., & Servas, V. (1985). Advances in Pavement Design and Rehabilitation. Accelerated Testing of Pavements, CSIR–Pretoria.

Gallagher, G., Leiper, Q., Williamson, R., Clark, M., & Forde, M. (1999). The Application of Time Domain Ground Penetrating Radar to Evaluate Railway Track Ballast. NDT & E International, 32(8), 463-468.

Giannakos, K. (2010). Loads On Track, Ballast Fouling, and Life Cycle under Dynamic Loading in Railways. Journal of Transportation Engineering, 136(12), 1075-1084.

Gräbe, P., & Clayton, C. (2009). Effects of Principal Stress Rotation on Permanent Deformation in Rail Track Foundations. Journal of Geotechnical and Geoenvironmental Engineering, 135(4), 555-565.

Halabe, U. B., Sotoodehnia, A., & Kenneth, R. (1993). Modeling Of the Electromagnetic Properties of Concrete. ACI Materials Journal, 90(6).

Han, X., & Selig, E. (1997). Effects of Fouling on Ballast Settlement. Paper Presented at the Proceedings of the 6th International Heavy Haul Railway Conference.

Hicks, R. G., & Monismith, C. L. (1971). Factors Influencing the Resilient Response of Granular Materials. Highway research record (345).

Holtz, W., & Gibbs, H. J. (1956). Triaxial Shear Tests on Pervious Gravelly Soils. Journal of Soil Mechanics and Foundation Engineering Division, 82(1), 1-22.

Huang, H., & Tutumluer, E. (2011). Discrete Element Modeling for Fouled Railroad Ballast. Construction and Building Materials, 25(8), 3306-3312. doi: 10.1016/j.conbuildmat.2011.03.019

Huang, H., Tutumluer, E., & Dombrow, W. (2009). Laboratory Characterization of Fouled Railroad Ballast Behavior. Transportation Research Record: Journal of the Transportation Research Board, 2117(1), 93-101.

Hugenschmidt, J. (2000). Railway Track Inspection Using GPR. Journal of Applied Geophysics, 43(2), 147-155.

Hyslip, J. P., Olhoeft, G. R., Selig, E. T., & Smith, S. S. (2005). Ground Penetrating Radar for Railroad Track Substructure Evaluation. FRA Report No. DOT/FRA/ORD-05/04.

Hyslip, J. P., Smith, S. S., Olhoeft, G. R., & Selig, E. T. (2003). Assessment of Railway Track Substructure Condition Using Ground Penetrating Radar. Paper presented at the AREMA (American Railway Engineering and Maintenance-of-Way Association) International Conference.

Indraratna, B., Ionescu, D., & Christie, H. (1998). Shear Behavior of Railway Ballast based on Large-Scale Triaxial Tests. Journal of Geotechnical and Geoenvironmental Engineering, 124(5), 439-449.

Indraratna, B., Lackenby J, Christie D. (2005). Effect of Confining Pressure on the Degradation of Ballast under Cyclic Loading. Geotechnique, 55(4), 325-328.

Indraratna, B., & Salim, W. (2005). Mechanics of Ballasted Rail Tracks: A Geotechnical Perspective: CRC Press.

Indraratna, B., Su, L.-j., & Rujikiatkamjorn, C. (2011). A New Parameter for Classification and Evaluation of Railway Ballast Fouling. Canadian Geotechnical Journal, 48(2), 322-326.

Indraratna, B., Tennakoon, N. C., Nimbalkar, S. S., & Rujikiatkamjorn, C. (2013). Behaviour of Clay-Fouled Ballast under Drained Triaxial Testing. Geotechnique,63(5), 410-419.

Ionescu, D. (2004). Evaluation of the Engineering Behaviour of Railway Ballast. University of Wollongong Thesis Collection, 421.

Jack, R., & Jackson, P. (1999). Imaging Attributes of Railway Track Formation and Ballast Using Ground Probing Radar. NDT & E International, 32(8), 457-462.

Jain, V., & Keshav, K. (1999). Stress Distribution in Railway Formation–A Simulated Study. Paper presented at the Proceedings of the 2nd International Symposium on Pre-Failure Deformation Characteristics of Geomaterials–IS Torino.

Janardhanam, R., & Desai, C. (1983). Three-Dimensional Testing and Modeling of Ballast. Journal of Geotechnical Engineering, 109(6), 783-796.

Jol, H. M. (2008). Ground penetrating radar theory and applications: Elsevier.

Kalcheff, I., & Hicks, R. (1973). Test Procedure for Determining the Resilient Properties of Granular Materials. Journal of Testing and Materials, 1(6).

Kashani, H. F., Ho, C. L., Clement, W. P., & Oden, C. P. (2016). Evaluating the Correlation Between the Geotechnical Index and the Electromagnetic Properties of Fouled Ballasted Track by a Full-Scale Laboratory Model. Transportation Research Record(2545), 66-78. doi: 10.3141/2545-08

Kashani, H. F., Ho, C. L., Oden, C. P., & Smith, S. S. (2015). Model Track Studies by Ground Penetrating Radar (GPR) on Ballast With Different Fouling and Geotechnical Properties Paper presented at the Proceeding of 2015 Joint Rail Conference, San Francisco.

Klugar, K. (2014). A Contribution to Ballast Mechanics. Paper presented at the Railroad Track Mechanics and Technology: Proceedings of a Symposium Held at Princeton University, April 21-23, 1975.

Koerner, R. M. (1970). Effect of Particle Characteristics on Soil Strength. Journal of Soil Mechanics & Foundations Div.

Kolbuszewski, J., & Frederick, M. (1963). The Significance of Particle Shape and Size on the Mechanical Behaviour of Granular Materials. Paper presented at the Proceedings of European conference on the soil mechanics and foundation engineering.

Kolisoja, P. (1997). Resilient Deformation Characteristics of Granular Materials: Tampere University of Technology.

Koltermann, C. E., & Gorelick, S. M. (1995). Fractional Packing Model for Hydraulic Conductivity Derived from Sediment Mixtures. Water Resources Research, 31(12), 3283-3297.

Leng, Z., & Al-Qadi, I. L. (2010). Railroad Ballast Evaluation Using Ground-Penetrating Radar. Transportation Research Record: Journal of the Transportation Research Board, 2159(1), 110-117.

Leslie, D. (1963). Large-Scale Triaxial Tests on Gravelly Soils. Paper presented at the Proceeding of the second panamerican Conference on Soil Mechanics and Foundation Engineering, Rio de Janeiro.

Li, D., Hyslip, J., Sussmann, T. and Chrismer, S. (2016). Railway Geotechnics: CRC Press.

Li, D., & Selig, E. T. (1998). Method for Railroad Track Foundation Design. Development. Journal of Geotechnical and Geoenvironmental Engineering, 124(4), 316-322.

Liu, X., Saat, M. R., & Barkan, C. P. L. (2012). Analysis of Causes of Major Train Derailment and Their Effect on Accident Rates. Transportation Research Record(2289), 154-163. doi: 10.3141/2289-20

Marachi, N. D., Chan, C. K., & Seed, H. B. (1900). Evaluation of Properties of Rockfill Materials. Journal of Soil Mechanics & Foundations Div, 97(SM1).

Marsal, R. J. (1967). Large-Scale Testing of Rockfill Materials. Journal of the Soil Mechanics and Foundations Division, 93(2), 27-43.

Marschall, K., Werban, U., Reboulet, E., Linder, S., Hirsch, M., Paasche, H., & Dietrich, P. (2007). Combination of Near Surface Geophysical and Geotechnical Methods for Exploring Construction Sites. Paper presented at the Near Surface 2007-13th EAGE European Meeting of Environmental and Engineering Geophysics.

McDowell, G. R., Bolton, M. D., & Robertson, D. (1996). The Fractal Crushing of Granular Materials. Journal of the Mechanics and Physics of Solids, 44(12), 2079-&. doi: Doi 10.1016/S0022-5096(96)00058-0

McHenry, M., Brown, M., LoPresti, J. (2014). In-Track Measurement of Ballast-Tie Interface Pressure Using Matrix Based Tactile Surface Sensors. Technology Digest, 1-4.

Skolnik, M. I. (1980). Introduction to RADAR systems: Mac-Graw Hill Book Company, New-York.

Mishra, D., Kazmee, H., Tutumluer, E., Pforr, J., Read, D., & Gehringer, E. (2013). Characterization of Railroad Ballast Behavior Under Repeated Loading Results from New Large Triaxial Test Setup. Transportation Research Record(2374), 169-179. doi: 10.3141/2374-20

Mitchell, J. K., & Soga, K. (1976). Fundamentals of Soil Behavior: Wiley New York.

Miura, N., and O. Hara, S. (1979). Particle-Crushing of a Decomposed Granite Soil under Shear Stresses. Soils and Foundations, 19(3), 1-14.

Morgan, J. (1966). The Response of Granular Materials to Repeated Loading. Australian Road Research Board Proceedings.

Narayanan, R., Kumke, C. J., & Li, D. (2001). Railroad Track Substructure Monitoring Using Ground Penetrating Radar (GPR). Rail International, 32.

Narayanan, R. M., Jakub, J. W., Li, D., & Elias, S. E. (2004). Railroad Track Modulus Estimation Using Ground Penetrating Radar Measurements. NDT & E International, 37(2), 141-151.

Norman, G. M., & Selig, E. T. (1983). Ballast Performance Evaluation with Box Tests. Area Bulletin, 692(84), 207-239.

Parsons, B. K. (1990). Hydraulic Conductivity of Railroad Ballast and Track Substructure Drainage: Department of Civil Engineering, University of Massachusetts.

Pell, P., & Brown, S. (1972). The Characteristics of Materials for the Design of Flexible Pavement Structures. Paper presented at the Third International Conference on the Structural Design of Asphalt Pavements, Grosvenor House, Park Lane, London, England, Sept. 11-15, 1972.

Pilon, J., Allard, M., & Levesque, R. (1992). Geotechnical Investigations of Permafrost in Ungava With Ground Penetrating Radar. Innovation and Rehabilitation. Paper presented at the Proceedings of the 45th Canadian Geotechnical Conference. Canadian Geotechnical Society.

Qian, Y., Mishra, D., Tutumluer, E., Hashash, Y. M., and Ghaboussi, J. (2016). Moisture Effects on Degraded Ballast Shear Strength Behavior. Paper presented at the Joint Rail Conference, Columbia, SC.

Qian, Y., Tutumluer, E., Hashash, Y. M. A., & Ghaboussi, J. (2014). Effects of Ballast Degradation on Permanent Deformation Behavior from Large-Scale Triaxial Tests. Proceedings of the Asme Joint Rail Conference, 2014.

Qian, Y., Tutumluer, E., Hashash, Y. M. A., Ghaboussi, J., & Davis, D. D. (2015). Ballast Settlement Ramp to Mitigate Differential Settlement in a Bridge Transition Zone. Transportation Research Record(2476), 45-52. doi: 10.3141/2476-07

Railroad Fact (2014). The Association of American Railroads (AAR), Washington, D.C.

Raymond, G. P. (1985). Research on Railroad Ballast Specification and Evaluation. Handbook of Transportation Engineering, 3rd Edition. McGraw-Hill, London.

Raymond, G. P., & Diyaljee, V. A. (1979). Railroad Ballast Load Ranking Classification. Journal of the Geotechnical Engineering Division, 105(10), 1133-1153.

Redden, J., Selig, E., & Zarembski, A. (2002). Stiff Track Modulus Considerations. Railway Track and Structures, 98(2).

Reynolds, J. M. (2011). An Introduction to Applied and Environmental Geophysics: John Wiley & Sons.

Roberts, R., Rudy, J., Al-Qadi, I., Tutumluer, E., & Boyle, J. (2006). Railroad Ballast Fouling Detection Using Ground Penetrating Radar: A New Approach Based on Scattering from Voids. ECNDT 2006–Th. 4.5, 1.

Rowe, P. W. (1962). The Stress-Dilatancy Relation for Static Equilibrium of an Assembly of Particles in Contact. Paper presented at the Proceedings of the Royal Society of London A: Mathematical, Physical and Engineering Sciences.

Saarenketo, T., & Scullion, T. (1996). Laboratory andt GPR Tests to Evaluate Electrical and Mechanical Properties of Texas and Finnish Base Course Aggregates. Paper presented at the Proceedings of the 6th International Conference on Ground Penetrating Radar, Sendai, Japan.

Salim, W., & Indraratna, B. (2004). A New Elastoplastic Constitutive Model for Coarse Granular Aggregates Incorporating Particle Breakage. Canadian Geotechnical Journal, 41(4), 657-671. doi: 10.1139/T04-025

Santamarina, J. C., Klein, K., & Fam, M. (2001). Soils and Waves: Particulate Materials Behavior, Characterization and Process Monitoring: John Wiley and Sons Ltd.

Selig, E. (1989). Compilation of Field Mearsurements on Ballast State of Compactness. American Railway Engineering Association, 90 (Bulletin No. 723), 382-391.

Selig, E. (2002). Ground Penetrating Radar Evaluation of Railway Track Substructure Conditions. Paper presented at the Proceedings of the SPIE.

Selig, E., Yoo, T., Adegoke, C., & Stewart, H. (1981). Status Report-Ballast Experiments, Intermediate (175 MGT), Substructure Stress and Strain Data: Technical Report FAST/TTC/TM-81/03, University of Massachusetts, for US DOT Transportation Systems Center, Cambridge, MA, USA.

Selig, E. T. (1981). FAST Substructure Static Strain and Deflection Measurements from 175 To 422 Mgt. Cambridge, MA: Transportation System Center

Selig ET, A.-H. J. (1982). Predicting Effects of Repeated Wheel Loading on Track Settlement. Paper presented at the International Heavy Haul Conference, Colorado Spring.

Selig, E. T., & Russo, V. D. (1991). Causes of Ballast Fouling. Area Bulletin, 731, 145-157.

Selig, E. T., & Waters, J. M. (1994). Track Geotechnology and Substructure Management: T. Telford.

Shangguan, P., Al-Qadi, I. L., & Leng, Z. (2012). Development of Wavelet Technique to Interpret Ground-Penetrating Radar Data for Quantifying Railroad Ballast Conditions. Transportation Research Record: Journal of the Transportation Research Board, 2289(1), 95-102.

Shao, W., Bouzerdoum, A., Phung, S. L., Su, L., Indraratna, B., & Rujikiatkamjorn, C. (2011). Automatic Classification of Ground-Penetrating-Radar Signals for Railway-Ballast Assessment. Geoscience and Remote Sensing, IEEE Transactions on, 49(10), 3961-3972.

Shenton, M. J. (1975). Deformation of Railway Ballast under Repeated Loading Conditions. Extracted from Symposium on Railroad Track Mechanics, RRIS 01 130826, Publication 7602.

Silvast, M., Levomäki, M., Nurmikolu, A., & Noukka, J. (2006). NDT Techniques in Railway Structure Analysis. Paper presented at the Proceedings of the 7th World Congress on Railway Research, Montreal, Canada, June 4-8, 2006.

Silvast, M., Nurmikolu, A., Wiljanen, B., & Levomaki, M. (2010). An Inspection of Railway Ballast Quality Using Ground Penetrating Radar in Finland. Proceedings of the Institution of Mechanical Engineers, Part F: Journal of Rail and Rapid Transit, 224(5), 345-351.

Smith, S. S. (1995). Detecting Pavement Deterioration with Subsurface Interface Radar. Sensors-the Journal of Applied Sensing Technology, 12(9), 29-41.

Stewart, H., Selig E. T. (1982). Predictions of Track Settlement under Traffic Loading. Paper presented at the International Heavy Haul Conference, Colorado Spring.

Su, L. J., Rujikiatkamjorn, C., & Indraratna, B. (2010). An Evaluation of Fouled Ballast in a Laboratory Model Track Using Ground Penetrating Radar. ASTM Geotechnical Testing Journal, 33(5), 343-350.

Suiker, A. S., Selig, E. T., & Frenkel, R. (2005). Static and Cyclic Triaxial Testing of Ballast and Subballast. Journal of Geotechnical and Geoenvironmental Engineering, 131(6), 771-782.

Suiker, A. S. J., Selig, E. T., & Frenkel, R. (2005). Static and Cyclic Triaxial Testing of Ballast and Subballast. Journal of Geotechnical and Geoenvironmental Engineering, 131(6), 771-782. doi: 10.1061/(Asce)1090-0241(2005)131:6(771)

Sulem, J., and Vardoulakis, I. G. . (2004). Bifurcation Analysis in Geomechanics: CRC Press.

Sussmann Jr, T. R. (1999). Application of Ground-Penetrating Radar to Railway Track Substructure Maintenance Management, PhD Dissertation, University of Massachusetts.

Sussmann, T. R., O'Hara, K. R., & Selig, E. T. (2002). Development of Material Properties for Railway Application of Ground-Penetrating Radar. Paper presented at the Ninth International Conference on Ground Penetrating Radar (GPR2002).

Sussmann, T. R., Selig, E. T., & Hyslip, J. P. (2003). Railway Track Condition Indicators from Ground Penetrating Radar. NDT & E International, 36(3), 157-167.

Taylor, J. D. (2000). Ultra-wideband radar technology: CRC press.

Tennakoon, N., Indraratna, B., Rujikiatkamjorn, C., Nimbalkar, S., & Neville, T. (2012). The Role of Ballast Fouling Characteristics on the Drainage Capacity of Rail Substructure. Geotechnical Testing Journal, 35(4), 1-4.

Tillard, S., Dubois, J. C. (1995). Analysis of GPR Data: Wave Propagation Velocity Determination. Journal of Applied Geophysics, 33(1), 77-91.

Trinh, V. N., Tang, A. M., Cui, Y.-J., Dupla, J.-C., Canou, J., Calon, N., Schoen, O. (2012). Mechanical Characterisation of the Fouled Ballast in Ancient Railway Track Substructure by Large-Scale Triaxial Tests. Soils and foundations, 52(3), 511-523.

Trinh, V. N., Tang, A. M., Cui, Y. J., Dupla, J., Canou, J., Calon, N, Lambert, L., Robinet, A., and Schoen, O. (2012). Mechanical Characterization of the Fouled Ballast in Ancient Railway Track Substructure by Large-scale Triaxial Test. Soils and foundations, 52(3), 511-523.

Tung, K. W. (1989). An investigation of the causes of railroad ballast fouling: Department of Civil Engineering, University of Massachusetts.

Tutumluer, E., Qian, Y., Li, D., Basye, C. (2015). Ballast Degradation Characterization Through Trixial Testing. Technology Digest, 1-4.

Uzarski, D., & McNeil, S. (1994). Technologies for planning railroad track maintenance and renewal. Journal of Transportation Engineering, 120(5), 807-820.

Whiteley, R. J., & Siggins, A. (2000). Geotechnical and NDT Applications of Ground Penetrating Radar in Australia. Paper presented at the 8th International Conference on Ground Penetrating Radar.

Yin, J. H. (2009). Influence of Relative Compaction on The Hydraulic Conductivity of Completely Decomposed Granite in Hong Kong. Canadian Geotechnical Journal, 46(10), 1229-1235.

Yoo, T., Chen, H., & Selig, E. (1978). Railroad Ballast Density Measurement. ASTM Geotechnical Testing Journal, 1(1).

Yoo, T. S., Selig E. T. (1979). Field Observations of Ballast and Subgrade Deformations in Track. Transportation Research Record, 733.

Zhang, S. X., Chan, L. S., & Xia, J. (2004). The Selection of Field Acquisition Parameters for Dispersion Images from Multichannel Surface Wave Data. Pure and Applied Geophysics, 161(1), 185-201.